AD-A092 419    AIR FORCE INST OF TECH WRIGHT-PATTERSON AFB OH      F/G 7/4
FLAMELESS ATOMIC ABSORPTION SPECTROSCOPY: EFFECTS OF NITRATES A--ETC(U)
MAY 80    N AKERLIND
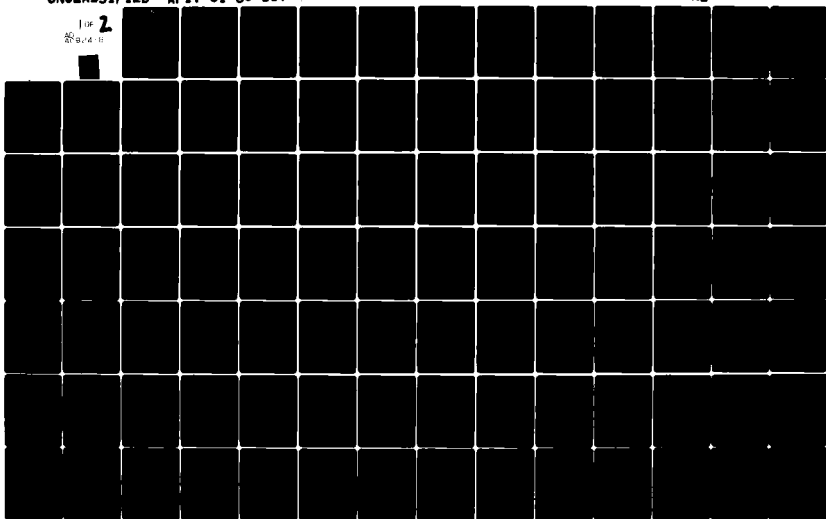UNCLASSIFIED    AFIT-CI-80-15T                    NL

1 OF 2
AD
A092419

LEVEL II

# REPORT DOCUMENTATION PAGE

READ INSTRUCTIONS
BEFORE COMPLETING FORM

| 1. REPORT NUMBER | 2. GOVT ACCESSION NO. | 3. RECIPIENT'S CATALOG NUMBER |
|---|---|---|
| CI-80-15T | AD-A092 449 | |

| 4. TITLE (and Subtitle) | 5. TYPE OF REPORT & PERIOD COVERED |
|---|---|
| Flameless Atomic Absorption Spectroscopy: Effects of Nitrates and Sulfates. | THESIS/DISSERTATION |
| | 6. PERFORMING ORG. REPORT NUMBER |

| 7. AUTHOR(s) | 8. CONTRACT OR GRANT NUMBER(s) |
|---|---|
| Capt Nils Akerlind, Jr | |

| 9. PERFORMING ORGANIZATION NAME AND ADDRESS | 10. PROGRAM ELEMENT, PROJECT, TASK AREA & WORK UNIT NUMBERS |
|---|---|
| AFIT STUDENT AT: University of Texas at Austin | |

| 11. CONTROLLING OFFICE NAME AND ADDRESS | 12. REPORT DATE |
|---|---|
| AFIT/NR | May 1980 |
| WPAFB OH 45433 | 13. NUMBER OF PAGES |
| | 138 |

| 14. MONITORING AGENCY NAME & ADDRESS(If different from Controlling Office) | 15. SECURITY CLASS (of this report) |
|---|---|
| | UNCLASS |
| | 15a. DECLASSIFICATION DOWNGRADING SCHEDULE |

16. DISTRIBUTION STATEMENT (of this Report)

APPROVED FOR PUBLIC RELEASE; DISTRIBUTION UNLIMITED

DTIC
ELECTE
DEC 0 4 1980

E

17. DISTRIBUTION STATEMENT (of the abstract entered in Block 20, if different from Report)

18. SUPPLEMENTARY NOTES

19. KEY WORDS (Continue on reverse side if necessary and identify by block number)

20. ABSTRACT (Continue on reverse side if necessary and identify by block number)

ATTACHED

AD A092419

BDC FILE COPY

DD FORM 1473   EDITION OF 1 NOV 65 IS OBSOLETE
1 JAN 73

8011 24 063

Flameless Atomic Absorption Spectroscopy:

Effects of Nitrates and Sulfates

by

Nils Akerlind, Jr., B.S.

Captain

United States Air Force

1980

138 pages

Master of Arts

The University of Texas at Austin

Like other analytical techniques, flameless atomic absorption is subject to matrix or interference effects. Upon heating, nitrate and sulfate salts decompose to generate oxidizing species such as nitrogen dioxide or sulfur trioxide. These concomitant oxidants are capable of gas phase reactions with the analyte atoms, thereby reducing the analyte free atom concentration and thus decreasing the analyte absorbance signal. The effects of sodium nitrate, potassium nitrate, sodium sulfate or potassium sulfate on the absorbance signal of iron, nickel, tin, chromium, silver, and copper was studied utilizing both the graphite filament atomizer and the graphite furnace atomizer.

Thermodynamic calculations were employed to explain/predict the effects of oxygen on the analyte free atom concentration. An optical system was developed which allows the simultaneous measurement of the transient absorbance signal at various spatial zones with the commercial furnace atomizer.

Bibliography

S.G. Salmon and J.A. Holcombe, Anal Chem, 51, 648 (1979)

J.A. Holcombe, R.H. Eklund and J.E. Smith, Anal Chem, 51, 1205 (1979)

R.H. Eklund and J.A. Holcombe, Anal Chim. Acta, 109, 97 (1979)

FLAMELESS ATOMIC ABSORPTION SPECTROSCOPY:

EFFECTS OF NITRATES AND SULFATES

BY

NILS AKERLIND, JR., B.S.

THESIS

Presented to the Faculty of the Graduate School of

The University of Texas at Austin

in Partial Fulfillment

of the Requirements

for the Degree of

MASTER OF ARTS

THE UNIVERSITY OF TEXAS AT AUSTIN

May, 1980

The purpose of this questionnaire is to ascertain the value and/or contribution of research accomplished by students or faculty of the Air Force Institute of Technology (ATC). It would be greatly appreciated if you would complete the following questionnaire and return it to:

AFIT/NR
Wright-Patterson AFB OH 45433

Research Title:  Flameless Atomic Absorption Spectroscopy:

Effects of Nitrates and Sulfates

Author:  Capt Nils Akerlind, Jr.

Research Assessment Questions:

1. Did this research contribute to a current Air Force project?

   a.    Yes                          b.    No

2. Do you believe this research topic is significant enough that it would have been researched (or contracted) by your organization or another agency if AFIT had not?

   a.    Yes                          b.    No

3. The benefits of AFIT research can often be expressed by the equivalent value that your agency achieved/received by virtue of AFIT performing the research. Can you estimate what this research would have cost if it had been accomplished under contract or if it had been done in-house in terms of manpower and/or dollars?

   a.    Man-years _____.        b.    $_____

4. Often it is not possible to attach equivalent dollar values to research, although the results of the research may, in fact, be important. Whether or not you were able to establish an equivalent value for this research (3 above), what is your estimate of its significance?

   a. Highly          b. Significant     c. Slightly       d. Of No
      Significant                           Significant        Significance

5. AFIT welcomes any further comments you may have on the above questions, or any additional details concerning the current application, future potential, or other value of this research. Please use the back of this questionnaire for your statement(s).

---

NAME        GRADE        POSITION

---

ORGANIZATION            LOCATION                                    USAF SCN 75-20B

FLAMELESS ATOMIC ABSORPTION SPECTROSCOPY:
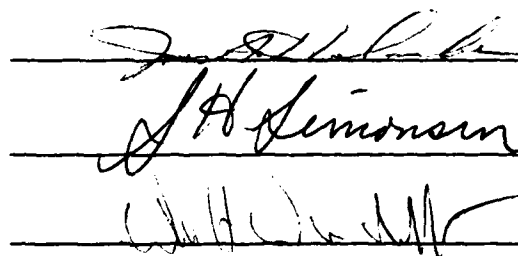
EFFECTS OF NITRATES AND SULFATES

APPROVED:

# TABLE OF CONTENTS

# CHAPTER I.   INTRODUCTION

Since its introduction by Walsh in 1955,[1] atomic absorption spectroscopy has evolved into the analytical method of choice for trace and ultratrace elemental analysis.  This technique enjoys widespread applicability (60-70 elements) coupled with limited sample preparation, but is hindered by its nonadaptability to simultaneous multielemental analysis.

Flameless atomic absorption spectroscopy, pioneered by L'vov,[2] employs an electrothermally heated atomizer instead of a flame to produce the free atoms required for analysis.  Because of efficiency of sample introduction and atomization, together with lower background noise, it is more sensitive than flame atomic absorption by a factor of 20-500.[3]  Flameless atomic absorption permits the direct analysis of both solid and liquid samples and is ideally suited to microsample analysis.  It is possible to detect $10^{-12}$-$10^{-14}$g. of the analyte and consequently is often the method of choice for ultratrace analysis.

There are two basic types of atomizer designs; the filament, and the furnace.  The

filament atomizer is an open system in which the analyte is atomized into the space above the atomizer. The West-type filament atomizer[4] consists of a rod clamped between two water-cooled support electrodes. The filament is usually made of graphite, but may be a Ta ribbon[5] or graphite coated with various refractory materials such as Ta, W[6] or pyrolytic graphite.[7] In almost all atomizer designs an inert sheath gas, usually Ar or $N_2$, is used to minimize the entrainment of air and subsequent oxidation of the atomizer.

In the furnace atomizer the analyte sample is contained within the volume of the furnace. This allows for increased heating of the gas phase and for interactions with the furnace walls. Generally the transient analyte absorbance signal persists longer in the furnace atomizer than the filament atomizer and observed interferences are minimized. There are several furnace designs. The L'vov furnace[8] has evolved into a hollow graphite tube approximately 40 mm in length with an inner diameter from 3 to 5 mm. This furnace is preheated up to 2500°C and the sample is then introduced and atomized by means of a secondary electrode plug in the bottom of the furnace. The light from the source,

typically a hollow cathode lamp, an electrodeless discharge lamp, or a continum source, passes longitudinally through the furnace.

The Massmann furnace[9] is composed of a long (approximately 50 mm) graphite cylinder mounted between two electrodes. The sample, in liquid form, is introduced onto the furnace wall through a small hole in the top of the furnace. A modified Mini-Massmann furnace (9 mm long, 3 mm inside diameter) has been adapted by Varian Techtron for commercial manufacture. Atomization of the sample from the furnace wall occurs as the entire furnace is rapidly heated to a prese-lected final temperature. This is in contrast to the L'vov furnace where the sample is atomized into a nearly isothermal environment. There are many other atomizer designs including Ta boats,[10] wire loops,[11] graphite crucibles,[12] graphite braids,[13] etc., which were developed for specific studies but are not in widespread use.

Once the liquid sample has been introduced, the subsequent heating cycle generally is composed of three stages; the dry, the ash, and the atomize. During the dry step, the solvent is gently evaporated by increasing the temperature of the atomizer to near

the boiling point of the solvent. The ash stage allows for the pyrolysis of the sample matrix by increasing the atomizer temperature to a value intermediate between the drying temperature and the appearance temperature of the analyte. The ash is routinely employed for samples with organic matrices. The atomization step produces the free analyte atoms by quickly raising the atomizer temperature to a preset final temperature (1500-3000°C) and maintaining that temperature until the transient analyte signal has disappeared. Hydrogen gas is sometimes mixed with the inert sheath gas to create an enhanced reducing environment for the analyte and thereby minimize some matrix problems.[14]

The theoretical and mathematical approaches to free atom formation and the transient analyte signal have been attempted and are documented in the literature.[15-22] Johnson and West[21] developed a simplified model to explain atomization from a graphite filament atomizer. This model has been expanded and enhanced by the work of Torsi and Tessari.[17, 19, 20] Their mathematical model agrees well with empirical observations of the absorbance signal of Ni and Pb vaporized from a filament atomizer under carefully controlled conditions.

L'vov has studied the atomization process in the
furnace atomizer and has developed a simplified
model for the general shape of the absorbance signal.
In this model the vaporization rate of analyte is
assumed constant and the analyte loss from the
observation zone is governed solely by diffusion.
Two fundamental parameters developed by L'vov
have become widely used in the characterization
of the absorbance signal.  Tau one $(T_1)$ is the time
required for the absorbance signal to rise from
the appearance time to the maximum peak height,
while tau two $(T_2)$ is the time required for the
absorbance signal to fall from the maximum peak
height to a value of 1/e of the maximum.  Faulk[22]
has treated appearance and diffusive loss of
the analyte for both the filament and furnace
atomizer.  Empirical studies aimed at elucidating
the mechanistic pathway to the formation of free
atoms in the furnace atomizer have been addressed
by Sturgeon and Chakrabarti.[16]  Utilizing early
time absorbance data, they calculate approximate
activation energies for various processes which
lead to free analyte atom formation.  They conclude
that the appearance of the free metal is preceded
by such species as the metal dimer, metal oxide, or

metal chloride.

As with most analytical techniques, flameless atomic absorption spectroscopy is subject to matrix or interference effects. Due to longer residence times within the analytical volume, higher local concentrations of analyte and interferent, and somewhat lower temperatures, many interferences are more pronounced when flameless atomization is employed in place of flames. While the exact cause of many matrix effects is not fully understood, some interferences are thought to arise from alterations in the graphite surface by the matrix. Similarly, a matrix with a high salt content may change the contact between the graphite and the analyte thereby altering the analyte release mechanism. Some analytes form refractory carbides[23] and are particularly difficult to vaporize. Prevolatilization and loss of the analyte as a molecular species is known to occur and is best documented for halides.[24,25] Gas phase reactions which deplete the analyte free atom concentration, thereby reducing the analyte absorbance signal, have been studied in this laboratory.[26,27]

The original goal of this thesis research was to determine the effect of nitrates and sulfates

on the analyte signal in the commercial graphite
furnace atomizer and to relate this data to the
graphite filament. During the course of this
research, the reactions of the thermal decomposition
products of the added nitrate and sulfate anions
with the analyte above a graphite filament atomizer
were reexamined, and an optical system for gathering
simultaneous time and spatial absorbance data within
the graphite furnace atomizer was developed. The
latter development was used to provide additional
insight into reactions occurring within the
tube-type atomizer that is not normally available
using the spatially integrating optics of the
commercial instrument.

## References for Chapter I

1. A. Walsh, Spectrochim. Acta, 7, 108 (1955).

2. B.V. L'vov, Spectrochim. Acta, 17, 761 (1961).

3. B.R. Culver, Analytical Methods for Carbon Rod Atomizers, Varian Techtron Pty., Ltd., Spring-vale, Australia, 1975, p. 1.

4. K.W. Jackson, T.S. West, and L. Balchin, Anal. Chem., 45, 249 (1973).

5. T. Takeuchi, M. Yanagisawa, and M. Suzuki, Talanta, 19, 465 (1972).

6. H. Fritzsche, W. Wegscheider, G. K:  ˄p, and H.M. Ortner, Talanta, 26, 219 (1979).

7. G. Hall, M.P. Bratzel, Jr., and C.L. Chakrabarti, Talanta, 20, 755 (1973).

8. B.V. L'vov, Spectrochim. Acta, 24B, 53 (1969).

9. H. Massmann, Spectrochim. Acta, 23B, 215 (1968).

10. H.M. Donega and T.E. Burgess, Anal. Chem., 42, 1521 (1970).

11. M.D. Bratzel, Jr., R.M. Dagnall, and J.D. Winefordner, Appl. Spectrosc., 24, 518 (1970).

12. Y.I. Belyaev, T.A. Koveshnikoua, and B.I. Kostin, Zh. Anal. Khim, 28, 2111 (1973).

13. A. Montaser, S.R. Goode, and S.R. Crouch, Anal. Chem., 46, 599 (1974).

14. M.D. Amos, P.A. Bennett, K.G. Brodie, P.W. Lung,

and J.P. Matdusek, Anal. Chem., 43, 211 (1971).

15. B.V. L'vov, Spectrochim. Acta, 33B, 153 (1978).

16. R.E. Sturgeon and C.L. Chakrabarti, Progress in Analytical Atomic Spectroscopy, 1, 5 (1978).

17. G. Torsi and G. Tessari, Anal. Chem., 47, 842 (1975).

18. S.L. Paveri-Fontana, G. Tessari, and G. Torsi, Anal. Chem., 46, 1032 (1974).

19. G. Torsi and G. Tessari, Anal. Chem., 47, 839 (1975).

20. S.L. Paveri-Fontana, G. Tessari, and G. Torsi, Anal. Chem., 46, 1032 (1974).

21. D.J. Johnson, B.L. Sharp, T.S. West, and R.M. Dagnall, Anal. Chem., 47, 1234 (1975).

22. H. Falk, Spectrochim. Acta, 33B, 695 (1978).

23. G. Baudin, M. Chaput, and L. Feve, Spectrochim. Acta, 26B, 425 (1971).

24. W.C. Campbell and J.M. Ottaway, Talanta, 22 729 (1975).

25. S. Yasuda and H. Kakiyama, Anal. Chim. Acta, 89, 369 (1977).

26. R.H. Eklund and J.A. Holcombe, Anal. Chim. Acta, 108, 53 (1979).

27. R.H. Eklund and J.A. Holcombe, Anal. Chim. Acta, 109, 97 (1979).

28.  J.A. Holcombe, R.H. Eklund, and J.E. Smith,
     Anal. Chem., $\underline{51}$, 1205 (1979).

CHAPTER II. GAS PHASE INTERFERENT REACTIONS

## 2.1  Effects of Nitrate and Sulfate Concomitants

Most samples and standards for analysis by
flameless atomic absorption spectroscopy are
routinely dissolved and stored in dilute nitric
or sulfuric acid.  In addition, many samples
contain significant amounts of dissolved nitrate
and sulfate salts.  Thus, during the desolvation
stage of the atomization cycle there is a signi-
ficant probability of formation of nitrate or
sulfate salts.

Previous work in this laboratory[1] has
demonstrated that nitrate and sulfate salts can
cause significant analyte signal depressions
above a graphite filament atomizer.  Upon heating,
the nitrate salts generally decompose in the
following manner:[2,3]

$$2MNO_{3(s)} \rightarrow M_2O_{(s)} + 2NO_{2(g)} + \tfrac{1}{2}O_{2(g)}$$
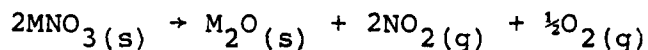
Similarly, the thermal decomposition of sulfate
salts generally proceeds as follows:[2,4]

$$MSO_{4(s)} \rightarrow MO_{(s)} + SO_{3(g)} \rightarrow MO_{(s)} + SO_{2(g)} + \tfrac{1}{2}O_{2(g)}$$
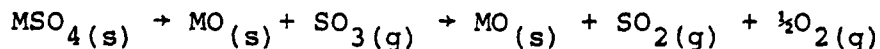
The species $NO_2$, $SO_3$, $O_2$, and to some extent $SO_2$ are

11

capable of gas phase oxidation of the free analyte atoms, thereby reducing the analyte free atom concentration and thus decreasing the analyte absorbance signal. The existence of the oxidizing species $NO_2$ and $SO_2$ within a graphite furnace atomizer has been confirmed by Yasuda and Kakigama.[5] Their studies were conducted using relatively massive amounts of material and thus may mask the ability of graphite to remove oxidants through the formation of CO or $CO_2$. Since the analyte absorbance signal persists for only a short period of time, gas phase coincidence of the interferent and analyte rather than the percentage decomposition may be the major factor in determining which nitrate or sulfate salt would exhibit the greatest signal depression.

Steady state experiments in which a large amount of the pure metal was placed in one well of the filament atomizer and either $Na_2SO_4$, $K_2SO_4$, $NaNO_3$, or $KNO_3$ was placed in an adjacent well were conducted using the filament type atomizer. The temperature of the atomizer was raised and held at a constant value between 1300 and 1600 K. These experiments demonstrated that gas phase coincidence of the analyte and the interferent oxidant is

possible. It was suggested that the magnitude of the signal reduction was related to the concentration of the interferent in the gas phase, e.g., $NaNO_3$ caused a greater signal depression than $KNO_3$ since its equilibrium constant for decomposition ($1.60 \times 10^{-18}$ at 800 K) is approximately $10^{10}$ larger than is the equilibrium constant for $KNO_3$ ($8.84 \times 10^{-27}$ at 800 K). For the sulfates, $K_2SO_4$ caused a greater signal depression than did $Na_2SO_4$. This again was consistent with the larger decomposition vapor pressures present using $K_2SO_4$.[1]

Transient experiments using the filament atomizer, in which nanogram amounts of sample and interferent were placed on the atomizer and the atomizer rapidly heated to 2000 K, also showed that these salts cause significant signal depressions for Ag, Cu, and Ga.

Other workers have obtained possibly contradictory results using the graphite filament atomizer. West et al have studied the effects of nitrates and sulfates on the absorbance signal of several elements.[6-8] Depending upon the element, the addition of nitric or sulfuric acid to the matrix generally produced depressions, but in some cases enhancements were obtained.

## 2.2 Kinetic Studies

In 1979, Holcombe, Eklund, and Smith[9] presented the thesis that kinetics may play an important role in gas phase interferent reactions above a graphite filament atomizer. Because of the small concentration of sample and interferent in the gas phase, local chemical equilibrium resulting from molecular collisions may not be established. Kinetics can be used to predict the extent of interference reactions.

For the bimolecular reaction:

$$M + AB \rightleftharpoons MA + B$$
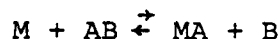
where M is the analyte species and AB is the interferent the rate expression for the disappearance of the analyte with time is given as

$$\frac{-\delta [M]}{\delta t} = k[M][AB]$$

where k is the second order rate constant. Assuming an excess of interferent AB, the rate equation may be reduced to a pseudo-first order kinetic expression

$$\frac{-\delta [M]}{\delta t} = k'[M]$$

where $k' \simeq k[AB]$. Integration of the above rate equation allows the prediction of the rate of disappearance of the analyte with time.

$$\ln \frac{[M]_t}{[M_o]} = -k't$$

where $[M]_t$ is the concentration of the analyte at time t and $[M_o]$ is the concentration of the metal at time t in the absence of interferent AB.

Steady state studies of Fe, Sn, Cu, and Ga, with and without the addition of $O_2$ to the sheath gas, demonstrated that $O_2$ was effective in reducing the analyte absorbance signal. The reactivity of analyte with $O_2$ was experimentally determined to be Sn>Ga>Fe>>Cu while the order of reactivity based on thermodynamic prediction is Sn>Fe>Cu>Ga.[3]

Salmon and Holcombe[10] have expanded on these studies using the transient absorbance signal, both with and without $O_2$, to ascertain a relative rate of reaction for various metals. A more detailed description of this mode of obtaining relative kinetic data can be found in reference 9.

The results of these experiments for the metals investigated in this study are shown in Table I. As can be seen, the relative rates of reactivity for $O_2$ decrease in the order of Sn>>Cr>>Fe>Cu,Ni>Ag.

TABLE I

| Element | Metal Oxide Bond Strength (kcal/mole) | Relative Second Order Rate Constant $x10^{14}$ (ml/molec-sec) |
|---------|---------|---------|
| Sn | 125 | 2300. |
| Cr | 102 | 300. |
| Fe | 99 | .45 |
| Cu | 96 | .33 |
| Ni | 87 | .30 |
| Ag | 33 | .05 |

## 2.3  Thermodynamic Studies

Thermodynamics was originally used to
explain the appearance temperature of certain
elements by Campbell and Ottaway.[11] They postu-
lated that free analyte atoms were produced by
the reduction of the metal oxide by graphite.

$$MO_{(s)} + C_{(s)} \rightarrow CO_{(g)} + M_{(g)}$$
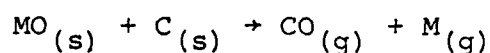
Assuming that this reduction is kinetically fast,
the temperature where $\Delta G^\circ$ of the above reaction
becomes negative was correlated with the appearance
temperature of the analyte in a graphite furnace
atomizer.  Fairly good agreement was obtained for
the majority of the twenty-seven elements studied.

Aggett and Sprott[12] studied the appearance
temperature of several elements using both the
graphite filament atomizer and the Ta ribbon
analyzer.  It was suggested that the appearance
temperature differences between the two atomizers
for the same analyte were indicative of the role
of graphite in the formation of the free metal.
In only four elements (Cu, Fe, Ni, and Sn) out of
fourteen studied was the graphite considered an
effective reducing agent of the MO species.  More
recently, Sturgeon, Chakrabarti, and Langford[13]

studied the mechanism of atom formation in the graphite furnace atomizer. Assuming equilibrium within the furnace, the activation energy of the atomization process was determined for several elements. Based on different activation energies, three mechanisms of atomization were proposed. Atomization can occur either by thermal dissociation of the metal oxide, thermal dissociation of the metal chloride, or reduction of the metal oxide by graphite followed by sublimation of the metal.

Frech and Cedergren investigated high temperature equilibria in graphite furnace atomizers.[14-16] Using a sophisticated computer model, they studied the equilibria in several multicomponent interference systems. For the analysis of Pb in concentrated NaCl solutions, the addition of $HNO_3$ to the matrix resulted in the formation of $NaNO_3$ salts. If these salts were not removed during the ash stage of atomization the partial pressure of the oxygen generated during atomization was calculated to exceed $10^{-5}$ atmospheres. The decrease in sensitivity for Pb at low ash temperatures was attributed to the formation of lead oxide in the gas phase. They

also assumed that, in general, equilibrium within

the graphite furnace atomizer can be rapidly

obtained at temperatures above 1000 K.

References for Chapter II

1.  R.H. Eklund and J.A. Holcombe, Anal. Chim. Acta, 109, 97 (1979).

2.  S. Yasuda and H. Kakiyama, Anal. Chim. Acta, 84, 291 (1976).

3.  K.H. Stern, J. Phys. Chem. Ref. Data, 1, 747 (1972).

4.  K.H. Stern and E.L. Weise, High Temperature Properties and Decomposition of Inorganic Salts, Part 1, Sulfates, National Bureau of Standards Bulletin 7, U.S. Government Printing Office, Washington, D.C., (1966).

5.  S. Yasuda and H. Kakiyama, Bunseki Kagaku, 24, 377 (1975).

6.  D. Clark, R.M. Dagnall, and T.S. West, Anal. Chim. Acta, 63, 11 (1973).

7.  K.W. Jackson and T.S. West, Anal. Chim. Acta, 59, 187 (1972).

8.  K.W. Jackson and T.S. West, Anal. Chim. Acta, 64, 363 (1973).

9.  J.A. Holcombe, R.H. Eklund, and J.E. Smith, Anal. Chem., 51, 1205 (1979).

10. J.A. Holcombe, R.H. Eklund, and S.G. Salmon, Lecture, XXI CSI & ICAS, (1979).

11. W.C. Campbe   and J.M. Ottaway, Talanta, 21,

12. J. Aggett and A.J. Sprott, Anal. Chim. Acta, 72, 49 (1974).

13. R.E. Sturgeon, C.L. Chakrabarti, and C.H. Langford, Anal. Chem., 48, 1792 (1976).

14. W. Frech and A. Cedergren, Anal. Chim. Acta, 82, 83 (1976).

15. W. Frech, Anal. Chim. Acta, 77, 43 (1975).

16. W. Frech and A. Cedergren, Anal. Chim. Acta, 88, 57 (1977).

# CHAPTER III.  EQUIPMENT

## 3.1  Commercial Graphite Furnace Atomizer Apparatus

The Varian Techtron CRA 90 graphite furnace atomizer is composed of two units, the workhead assembly and the atomizer power supply.  The graphite furnace is 9 mm long with an inside diameter of 3 mm and is an adapted Massmann-type atomizer.  The furnace is supported in the workhead assembly by two spring-loaded graphite support electrodes.  These support electrodes are clamped to separate water-cooled metal support blocks on the workhead assembly.  Both the furnace and support electrodes are made from pyrolytically-coated graphite.  A laminar flow sheath gas with a flow rate of approximately 6 liters/minute surrounds the atomizer.  The sheath gas is normally Ar or $N_2$, but it is possible to mix up to approximately 10% $H_2$ with these gases for certain analyses.  The atomizer is resistively heated by the power supply which employs a voltage feedback circuit to attempt reproducible temperature-controlled heating of the atomizer.

The atomizer power supply has both time and temperature settings for the dry, ash, and atomize

22

stages. The dry temperature may range from room temperature to 300°C, while the dry time is variable from five to ninety seconds. During the ash stage temperatures up to 1700°C may be held for zero to sixty seconds. When the atomize cycle begins, the atomizer temperature is ramped at a rate between 25 and 800 degrees per second to any preset final temperature less than 3000°C and held at the final temperature from zero to five seconds. The maximum power fluctuation is claimed at ±4%.[1]

At the start of the atomization cycle the atomizer supplies a trigger input to the spectrophotometer. This circuit, which is activated by the closing of a relay in the power supply, synchronizes the measurement cycle with the atomization of the analyte.

Samples in liquid form are automatically deposited in the graphite furnace atomizer by the ASD 53 automatic sample dispenser. Sample volumes of either 2μl, 5μl, or 10μl are selected by changing a cam within the automatic sampler. Up to nine repetitions of 25 different samples may be selected for analysis.

The AA 375 spectrophotometer is a dual-beam spectrophotometer employing pulsed modulation of the

hollow cathode lamp and lock-in amplifiers to improve the signal-to-noise ratio. This spectrometer is capable of background correction using a deuterium lamp and will measure either the peak height or the peak area of the absorbance signal. A microprocessor automatically converts the transmittance readings, correcting for background absorbance if that option has been selected, into a three-decimal-place digital absorbance measurement which is displayed on the front of the instrument.

The same absorbance signal is fed through a manufacturer-supplied interface to a Hewlett-Packard HP 97 calculator where a permanent record of the absorbance signal is produced. Programs are available on the HP 97 which will correct for any absorbance of the blank, build an analytical working curve from the standards, and calculate the concentration of each unknown sample. For these studies, the instrument was used in the absorbance mode only and the calculator programmed to provide statistical information after a preselected number of repetitive samples were analyzed. The statistical program provides both an average absorbance and the relative standard deviation.

The transient absorbance signals are also supplied to a strip chart recorder as an analog input. For these studies a Linear Instruments Model 285/MM strip chart recorder was used to record the absorbance profile of the analyte.

## 3.2   Graphite Filament Atomizer and Optical System

A block diagram of the apparatus is shown in figure 1.  A hollow cathode lamp (HCL) is used to provide the spectrum of the element under study.  The lens (L) collimates the light from the hollow cathode lamp to provide nearly uniform light intensity in the region being viewed.  The atomizer is a modified West-type filament atomizer that has been partially enclosed to minimize the entrainment of air.  The filament is pyrolitically coated using the method of Szydolski et al.[5]  A laminar flow of Ar, typically at a flow rate of 2.5 liters/minute, further sheaths the filament from the outside environment.  The atomizer power supply is capable of very rapidly raising the temperature of the atomizer at a rate of approximately 5000°/second. The final temperature of the atomizer is controlled by means of a photodiode feedback circuit which allows the atomizer to be reproducibly stepped and held at the selected final temperature.  A trigger circuit provides a trigger pulse input to the Biomation Model 805 Waveform Recorder (Gould, Inc.; Biomation Division) when the atomizer temperature reaches a preselected value.  A more complete description of the atomizer circuit is presented
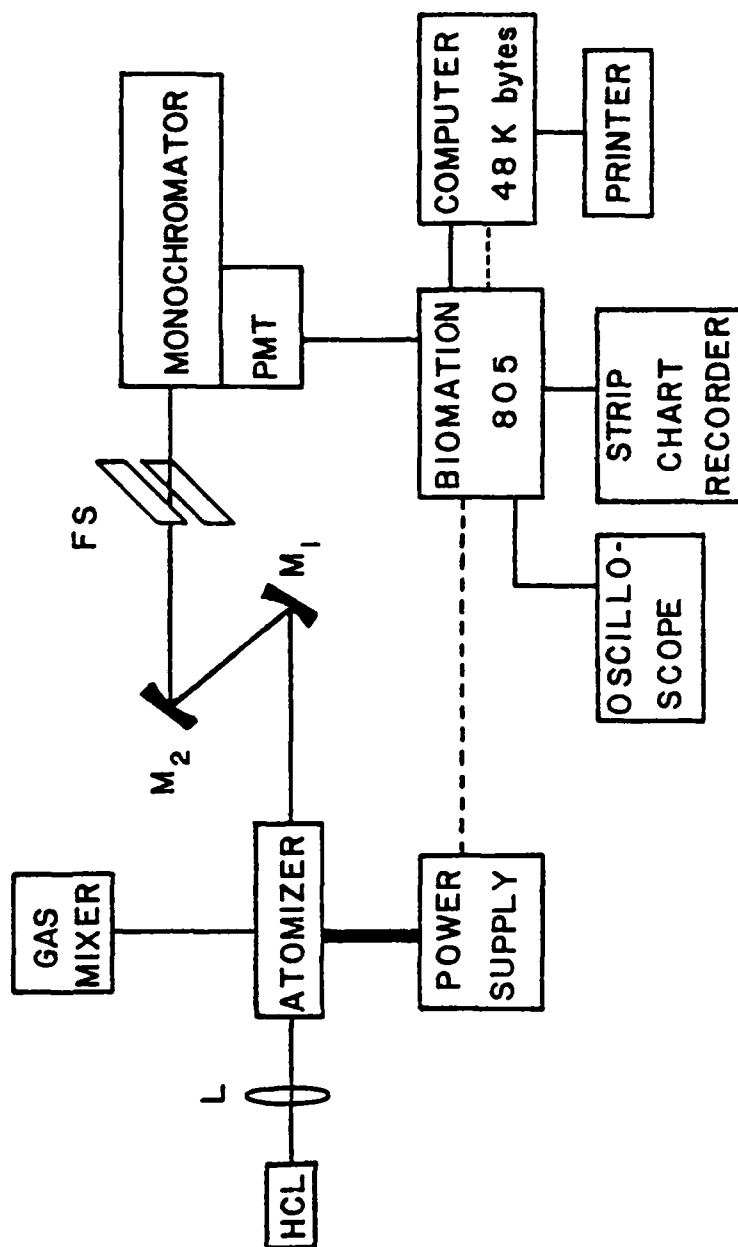
Figure 1. Block Diagram of Filament Atomizer Apparatus

in reference 2. The height of the filament is adjusted to insure that the viewing zone is immediately above the atomizer surface.

The optical system for gathering simultaneous time and spatial absorbance information above a graphite filament atomizer has been described in the literature.[3,4] Basically it employs off-axis imaging to produce the astigmatic tangential and sagittal images. Figure 2 is a representation of the basic optical system. The sagittal image is placed on the entrance slit of the monochromator, thereby allowing increased spectral intensity to reach the photomultiplier tube. The tangential image is repeatedly scanned by means of a precision-made rotating spatial isolation wheel (SIW) which has 60 radial slits (0.4 mm wide, 4.5 cm long) uniformly spaced around the 23 cm diameter wheel. The resolution of this apparatus has been experimentally determined to be limited by the slit width of the SIW, viz., 0.4 mm. It is this repeated scanning of the area above the graphite filament which provides the simultaneous time and spatial absorbance data.

The two $MgF_2$-overcoated front surfaced spherical concave mirrors are arranged in an
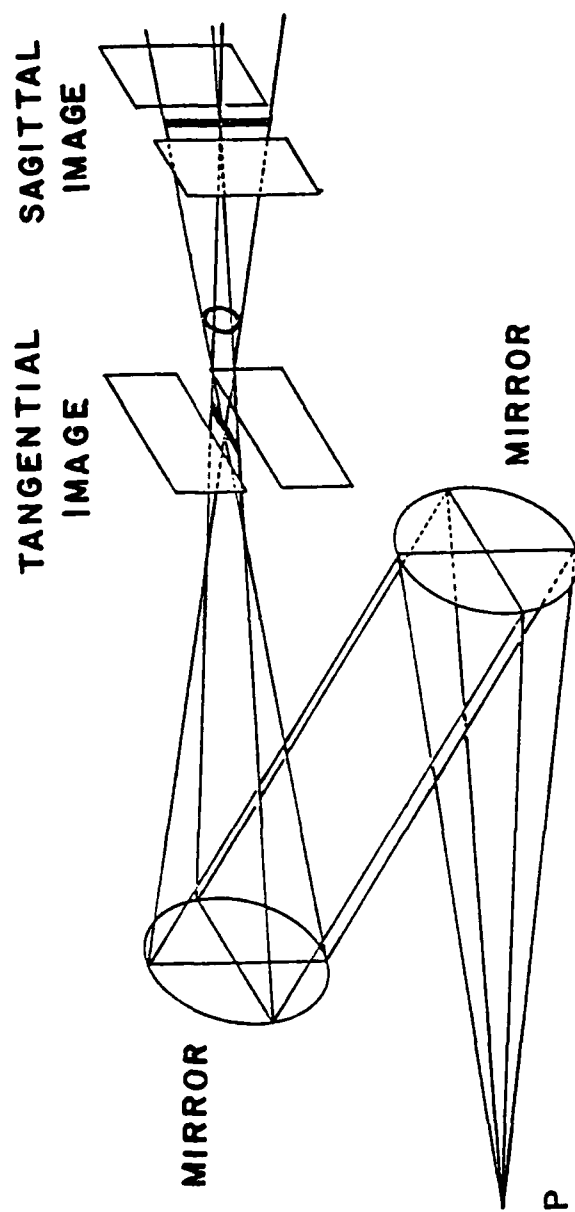
Figure 2. Optical System for Producing Astigmatic Images

over-and-under configuration which provides the
off-axis imaging.  The spatial isolation wheel is
located at the tangential image and is rotated
at either 25, 50, or 100 rpm by means of precision-
geared pulleys (PIC Design Corp.) and a no-slip
positive drivebelt driven by a 100 rpm reluctance
type synchronous motor (Hurst Mfg. Corp.).  The
selection of rotational speeds is dependent on the
length of time the transient analyte signal persists.

The monochromator is a Jarrell Ash 0.5 m
Ebert mount with an 0.5 mm entrance slit and a
0.6 mm exit slit.  The output current of the
1 P28 photomultiplier tube (PMT) is passed through
a parallel combination of a .33M$\Omega$ resistor and
.1$\mu$F capacitor to provide an output voltage with
some high frequency noise rejection.  The voltage
drop across this resistor-capacitor pair is then
fed to the Biomation recorder.  The Biomation
samples the PMT output at a predetermined rate,
digitizes the analog input, and stores the signal in
the 2048 eight-bit memory.  This instrument has the
capability of recording the data before and after
the input trigger, delaying a predetermined amount
of time and then recording, or recording the data
immediately upon receipt of the trigger pulse.  The

Biomation is interfaced to a microcomputer (Vector

Graphics Model Vector 1) equipped with dual floppy

disk drive which accomplishes data reduction,

storage, and averaging.  Generally five repetitions

of each different sample or condition are recorded

and averaged to produce a representative absorbance

profile.

### 3.3 Optical System for Spatial Viewing Within the Graphite Furnace

The optical system used with the graphite filament was modified to allow gathering of simultaneous time and spatial absorbance data within the Varian CRA-90 atomizer (see figures 3 and 4). The filament atomizer assembly was removed from the system and an optical rail was installed upon which was mounted the hollow cathode lamp and its lens $L_1$, the commercial furnace atomizer, and a magnification lens $L_2$. Lens $L_1$ has a focal length of 12.5 cm, while lens $L_2$ is composed of two lens mounted back-to-back resulting in a focal length of 7 cm. Since the inside diameter of the furnace was only 3 mm, while the SIW apparatus and associated computer software was capable of viewing 9 one-mm zones, the furnace was magnified by a factor of three times by lens $L_2$. Due to chromatic aberrations inherent in lenses, the furnace and $L_2$ must be repositioned along the optical rail for each element under study, i.e., for each change in wavelength. Since the basic graphite filament optical system provides unit magnification and optical resolution on the vertical plane above the filament atomizer, the furnace optical system is focused on this plane. The
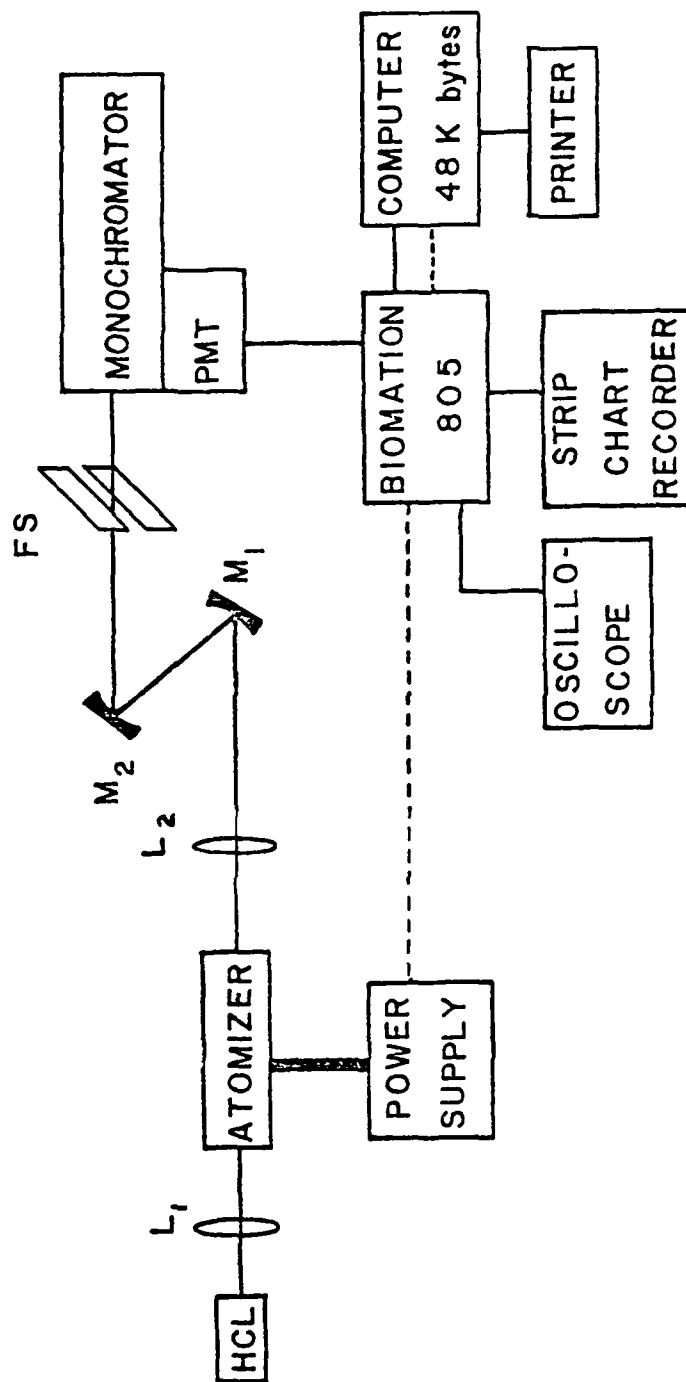
Figure 3.  Block Diagram of Spatially Resolved Furnace Apparatus
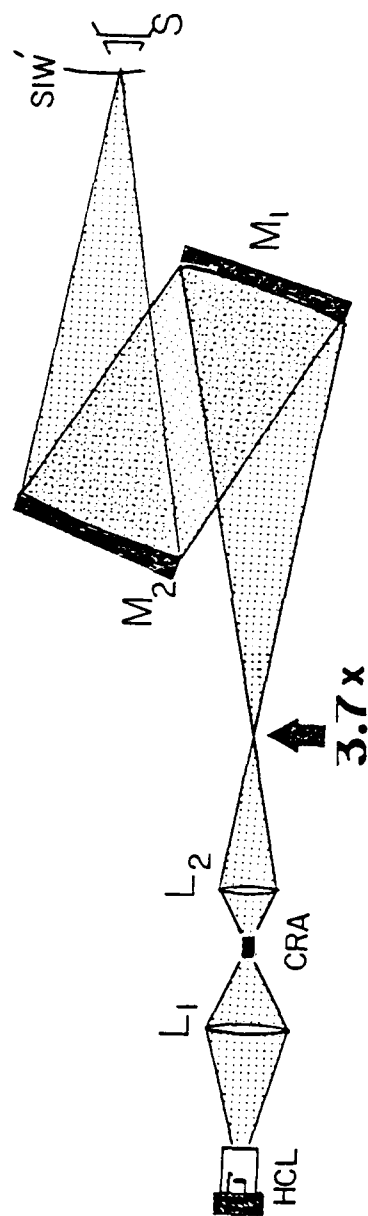
Figure 4. Optical System for Spatial Viewing Within the Furnace Atomizer

spatial resolution has been calculated at less than 220μm (see appendix A).

The furnace is aligned by rotating the SIW and viewing the PMT output on an oscilloscope. An approximate magnification was obtained from the visual image of the furnace on the SIW with the image of the furnace centered on the SIW field stops. The atomizer was brought into sharp focus by means of a horizontal grid which was clamped into the workhead assembly in place of the furnace. The furnace was then reinserted into the workhead assembly and the image centered on the monochromater entrance slit. If the magnification is correct, all nine zones of the SIW trace on the oscilloscope are illuminated. Overmagnification can be detected by moving the atomizer assembly horizontally a short distance. Since the optical system is now viewing a vertical chord of the furnace which is smaller than the furnace diameter, the display on the oscilloscope should indicate that not all nine zones of the SIW output are illuminated. If the alignment is incorrect, the furnace and/or the magnification lens is repositioned and the alignment procedure repeated.

At temperatures above 2100°C flare from the

magnification lens became a problem, especially for
those elements whose resonance line was closer to
the visible spectrum.  The flare was minimized by
placing an adjustable iris diaphram between the
lens and the first mirror.  The aperture was reduced
until it interfered with the magnitude of the PMT
output.  For all wavelengths used in this study,
this was sufficient to reduce the magnitude of rod
emission below detectability.

Because the optical system was extended
by approximately one meter and the image magnified
approximately three times, the hollow cathode lamp
light intensity striking the photomultiplier tube
was reduced.  To restore the signal to an acceptable
level required increasing the photomultiplier tube
voltage and/or focusing the hollow cathode lamp
output down into the furnace.  Both these procedures
introduced noise into the system.

A Hamilton $10\mu l$ syringe was used to place a
$2\mu l$ aliquot of the test solution into the furnace
through the sample introduction port in the
atomizer.  The furnace was heated by the commercial
power supply to dry, ash, and atomize the sample.
The trigger circuit in the atomizer power supply
was modified to provide a positive trigger pulse to

the Biomation at the start of the atomization cycle.
A battery was used to charge a capacitor to 1.5
volts.  At the start of the atomization cycle, a
relay in the commercial power supply closes allowing
the capacitor to discharge through a resistor,
thereby providing the trigger pulse to the Biomation.

The digital data from the Biomation is fed
to the microcomputer (Vector Graphics Model Vector
1) where the different spatial zones are identi-
fied and the absorbance values calculated from the
transmittance data.  Another data reduction program
averages together all the repetitions of each
sample or condition to produce a representative
profile.  This program obtains the best alignment
of the absorbance profiles for the first three
spatial zones by shifting the data in time rather
than just averaging together all the time-resolved
absorbance data.  This program calculates the
percent deviation of each data set from the averaged
profile and has the ability to eliminate one "bad"
data set (>45% deviation in the first three zones)
which exceeds the deviation criteria and calculates
such fundamental parameters as appearance time,
$T_1$, $T_2$, peak location, peak half width, in addition

to peak height and peak area.

## References for Chapter III

1.  B.R. Culuer and D.E. Shrader, Amer. Lab.,
    8, 59 (1976).

2.  R.H. Eklund, Electrothermal Atomization in
    Atomic Absorption Spectrometry: Fundamental
    Causes of Interference Effects and a Study of
    an Exploding Thin Film Atomizer, Dissertation,
    The University of Texas at Austin, Austin,
    Texas  (1979).

3.  S.G. Salmon and J.A. Holcombe, Anal. Chem.,
    51, 648 (1979).

4.  S.G. Salmon and J.A. Holcombe, Anal. Chem.,
    50, 1714 (1978).

5.  F.J. Szydolski, E. Peck, and B. Bax, Appl.
    Spectrosc., 32, 402 (1978).

# CHAPTER IV:   RESULTS AND DISCUSSION

## 4.1   Thermodynamics

Gas phase interferent reactions in flameless atomic absorption spectroscopy require that an interferent spcies must exist or be produced, that the interferent and analyte be temporally coincident, that thermodynamics favor the formation of the molecular species involving the analyte, and that the kinetics of the analyte-interferent reaction be sufficiently fast to deplete the gas phase analyte concentration.

Yasuda and Kakigama[1] have confirmed the existence of oxidizing species produced by the decomposition of nitrate and sulfate salts within the furnace atomizer.  Eklund and Holcombe,[2] in transient studies with the filament atomizer, have demonstrated that temporal coincidence of analyte and interferent is possible for selected elements.  The kinetic data of Holcome, Eklund, and Smith[3] for the analyte oxygen reaction above a graphite filament atomizer suggest that Sn and Cr are kinetically fast and that a sufficient time may exist for equilibrium to be established.  As shown in Table I, the other elements in this study

(Cu, Fe, Ni, Ag) are three to four orders of magnitude slower in their reaction with oxygen, and thus equilibrium may or may not be obtained.

To examine the role of thermodynamics in predicting or explaining the extent of interferent reactions, the following equilibrium expressions were considered:

$$2O_{(g)} + C_{(s)} \rightleftarrows CO_{2(g)} \qquad K_1 = \frac{P_{CO_2}}{(P_O)^2}$$

$$O_{(g)} + C_{(s)} \rightleftarrows CO_{(g)} \qquad K_2 = \frac{P_{CO}}{P_O}$$

$$\tfrac{1}{2}O_{2(g)} \rightleftarrows O_{(g)} \qquad K_3 = \frac{P_O}{(P_{O_2})^{\frac{1}{2}}}$$

$$M_{(s)} \rightleftarrows M_{(g)} \qquad K_4 = P_M$$

$$M_{(g)} + O_{(g)} \rightleftarrows MO_{(g)} \qquad K_5 = \frac{P_{MO}}{(P_M)(P_O)}$$

$$M_{(g)} + 2O_{(g)} \rightleftarrows MO_{2(g)} \qquad K_6 = \frac{P_{MO_2}}{(P_M)(P_O)^2}$$
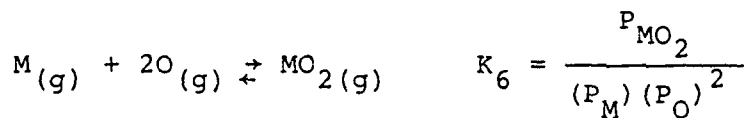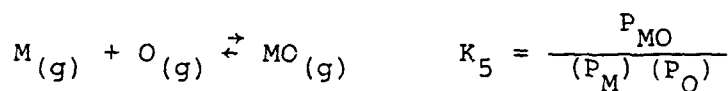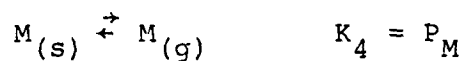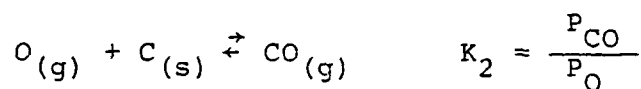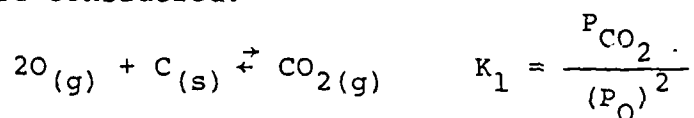
The total partial pressure of the metal ($P_m^O$) is the sum of the partial pressures:

$$P_M^O = P_M + P_{MO} + P_{MO_2}$$

The total partial pressure of oxygen ($P_O^O$) is

also the sum of the component partial pressures:

$$P_O^O = P_O + 2P_{O_2} + P_{CO} + 2P_{CO_2} + P_{MO} + 2P_{MO_2}$$

From these equations an expression in terms of the partial pressure of oxygen $(P_O^O)$, the partial pressure of the metal $(P_M^O)$, and the equilibrium constants may be derived.

$$P_O^4(2K_3^2K_6 + 2K_1K_6) + P_O^3(K_6 + K_2K_6 + 2K_3^2K_5 +$$
$$2K_1K_5) + P_O^2(-P_O^O K_6 + K_5 + K_2K_5 + 2K_3^2 + 2K_1 +$$
$$2P_M^O K_6) + P_O(-P_O^O K_5 + 1 + K_2 + P_M^O K_5) - P_O^O = 0 \quad (1)$$

The equilibrium constants at different temperatures were obtained from high temperature thermodynamic data[4] and the relationship:

$$K_{eq} = e^{-\Delta G/RT} \quad (2)$$

If no thermodynamic data were available, the equilibrium constants were calculated from bond strengths and entropies of translation and rotation at various temperatures. The equation for entropy of translation[5] is:

$$S_{TRANS} = R[\frac{5}{2} + \ln\frac{(2\pi mkT)^{3/2}}{h^3} v]$$

where:

R = ideal gas constant, 1.987 cal/mole -K

m = atomic mass in kg

$k$ = Boltzman constant, $1.38 \times 10^{-23}$ J/K

$T$ = temperature, Kelvin

$h$ = Planck's constant, $6.62 \times 10^{-34}$ J sec

$v$ = molar volume at temperature T, $m^3$

For a diatomic molecule the entropy of rotation is:[6]

$$S_{ROT} = R(1 + \ln \frac{8\pi IkT}{h^2})$$

where I is the moment of inertia as calculated by:[7]

$$I = \frac{m_1 m_2}{m_1 + m_2} r^2$$

The internuclear distance is $r$, and $m_1$ and $m_2$ are the respective masses of the atoms. The entropy of vibration is small and was neglected for these studies.

The total change in entropy ($\Delta S$) of the metal oxide MO, free metal M, oxygen O system is:

$$\Delta S = S_{MO} - (S_M + S_O)$$

where S represents the summation of the translational and rotational entropies of the respective species. Due to the lack of heat capacity data, the change in enthalpy of the metal oxide bond with temperature was assumed small.

From these data, the free energy of reaction, $\Delta G$, for the reaction $M_{(g)} + O_{(g)} \rightarrow MO_{(g)}$ was calculated using the relationship:

$$\Delta G = \Delta H - T\Delta S$$

Equation 2 was then used to extract the equilibrium values. The results of these calculations were compared with published thermodynamic data at elevated temperatures for several metals and agreement to within 10% was found.

A computer program was developed to calculate the equilibrium distribution of the various species using equation 1. Without considering the role of graphite, i.e. omitting the first two equilibrium expressions, figures 5 and 6 illustrate the effects of an initial concentration of $10^{-3}$ atm of $O_2$ on the various elements. This oxygen concentration is comparable to the oxygen generated from the dissociation of 2 $\mu$l of 100 ppm $KNO_3$ solution. In general these calculations would predict significant signal depressions from the metal-oxygen reactions below 2500 K. However, these calculations presume coincidence of interferent and analyte, do not consider the reaction kinetics leading to the formation of the metal oxide, and neglect the chemical role of graphite. When graphite is included in these calculations and its activity is assumed equal to one, greater than 95% of the metal is present as the free metal at

temperatures above the appearance temperatures of
these metals. Thus in comparison to the filament
atomizer where the analyte atoms are vaporized
into free space, the furnace atomizer, which
contains the analyte atoms within the high temper-
ature graphite walls for a relatively longer
period of time, should be more effective in
minimizing interference due to metal oxygen reactions.

Due to the lack of a recording optical
pyrometer with which to calibrate the filament
and furnace atomizers, literature values of
appearance temperatures of the elements were used
throughout this study. L'vov[8] has compiled various
literature values of the appearance temperature
and averaged them together to obtain a representative
value. The arrows on figures 5 and 6 indicate the
appearance temperatures of Cr (1740K), Ni (1675K),
Fe (1580K), Cu (1460K), Sn (1620K), and Ag (1120K).
These graphs may now be used to predict the
relative effect of oxygen on the various metals
in the study. Thus the depressive effect of oxygen
on the analyte absorbance signal is greatest for
Sn, followed in order by Fe, Cu, Cr, Ni, and Ag.
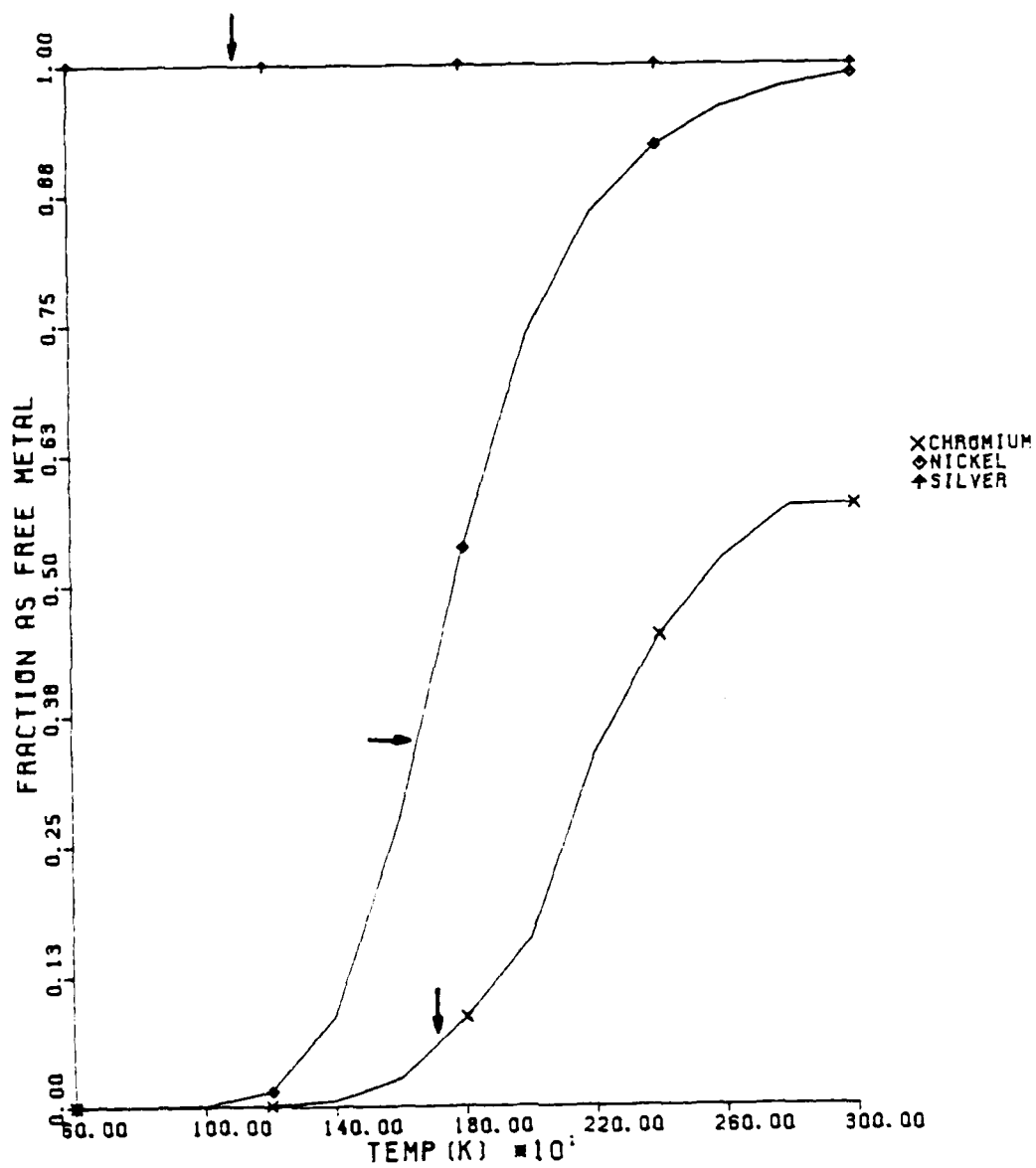
Figure 5.   Results of Thermodynamic

Calculations for Cr, Ni, Ag
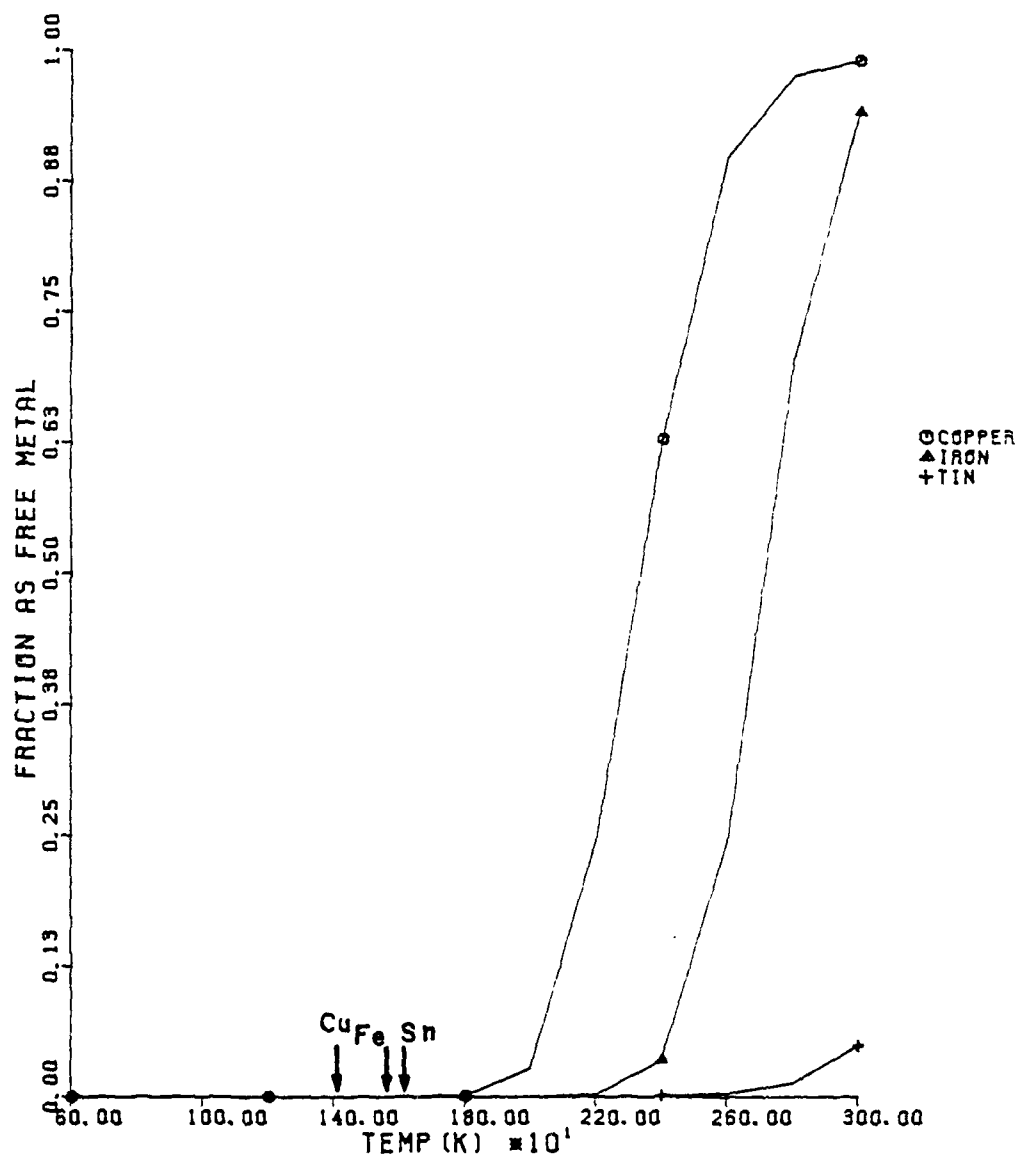
Figure 6.   Results of Thermodynamic

Calculations for Cu, Fe, Sn

## 4.2 Experimental Procedure

The experimental parameters of the elements studied are given in Table II. Test solutions were prepared each day by dilution from concentrated stock solutions. Deionized, doubly-distilled water was employed for all dilutions. All glassware was cleaned with and stored in dilute $HNO_3$. Prior to use, the glassware was thoroughly rinsed with the deionized, distilled water.

The wavelengths chosen for analysis were the most sensitive wavelengths recommended[9] with certain exceptions. The intensity of the hollow cathode lamp at the most sensitive tin line, 234.8 nm, was so low that the 286.3 nm line was used. Photomultiplier tube noise was a major factor in the choice of wavelengths for the spatially resolved furnace studies. Thus the choice of the second most sensitive wavelenths for Ag, Ni, and Fe, as shown in Table II, permitted a lower baseline noise level.

In general, five repetitions of each sample or condition were conducted and the data averaged to produce a representative absorbance profile. The analyte solution without added interferent was normally analyzed both before and after the solutions containing interferent to verify that the atomizer

TABLE II

**FILAMENT**

| | Cr | Ni | Cu | Fe | Ag | Sn |
|---|---|---|---|---|---|---|
| $\lambda$ (nm) | 357.9 | 232.0 | 324.8 | 248.3 | 328.1 | 286.3 |
| analyte mass (g) | $5\times10^{-10}$ | $2\times10^{-9}$ | $5\times10^{-10}$ | $2\times10^{-9}$ | $2\times10^{-10}$ | $6.25\times10^{-9}$ |
| final atomization temperature (°C) | 2300 | 2300 | 1800 | 1800 | 1800 | 1800 |

**FURNACE**

| | Cr | Ni | Cu | Fe | Ag | Sn |
|---|---|---|---|---|---|---|
| $\lambda$ (nm) | 357.9 | 232.0 | 324.8 | 248.3 | 328.1 | 286.3 |
| analyte mass (g) | $5\times10^{-10}$ | $2\times10^{-9}$ | $5\times10^{-10}$ | $1.25\times10^{-9}$ | $2\times10^{-10}$ | $6.25\times10^{-9}$ |
| | | | $2.5\times10^{-10}$ | $2\times10^{-9}$ | | $2.5\times10^{-9}$ |
| final atomization temperature (°C) | 2400 | 2200 | 2000 | 2200 | 1800 | 2300 |
| ramp rate (°C/sec) | 700 | 700 | 700 | 700 | 700 | 600 |

**SPATIALLY RESOLVED FURNACE**

| | Cr | Ni | Cu | Fe | Ag | Sn |
|---|---|---|---|---|---|---|
| $\lambda$ (nm) | 357.9 | 352.5 | 324.8 | 372.0 | 338.3 | 286.3 |
| analyte mass (g) | $1.5\times10^{-10}$ | $2\times10^{-9}$ | $3.5\times10^{-10}$ | $1\times10^{-9}$ | $1\times10^{-9}$ | $2.5\times10^{-9}$ |
| final atomization temperature (°C) | 2500 | 2300 | 2000 | 2200 | 1800 | 2100 |
| ramp rate (°C/sec) | 700 | 700 | 700 | 700 | 700 | 700 |

surface and other experimental variables had not changed. The interferent solutions consisted of the analyte to which was added either a ten-fold or a hundred-fold excess (weight-to-weight) of interfering anion to analyte. The interferent was either $Na_2SO_4$, $K_2SO_4$, $NaNO_3$, or $KNO_3$. Ashing temperatures were minimized in the furnace atomizer and the ash stage bypassed in the filament atomizer to insure the presence of interferent at the start of the atomization cycle.

The elements were selected for analysis based on their relative reaction rates with oxygen, the strength of the metal oxide bond, and their atomization temperatures. As shown in Table I, tin and chromium are both kinetically fast reactors with oxygen, yet the Sn absorbance signal appears some 120°C lower than Cr. Copper, iron, and nickel react moderately fast with oxygen. Nickel's appearance temperature is about that of Cr, while the appearance temperatures for Fe and Sn are approximately the same. Silver has the lowest appearance temperature of the elements studied and is also kinetically the slowest for the metal-oxygen reaction.

The experimental results for each element

are comprised of the peak absorbance measurements
from the commercial apparatus, the time and spa-
tially resolved studies above the graphite filament
atomizer, and the time and spatially resolved
studies within the furnace atomizer.  These
results are presented by element in the order of
decreasing appearance temperature.

## 4.3  Chromium

As shown in Table I, chromium exhibited
the second fastest reaction rate for the metal
oxygen reaction.  Its metal oxide bond strength
of 102 kcal/mole is indicative of the thermodynamic
driving force for this reaction.  When the analyte
absorbance signal is superimposed on the thermo-
dynamic calculations (figure 7) it can be seen that
different partial pressures of oxygen greatly affect
the free Cr atom concentration.  Utilizing figure 7,
a partial pressure of oxygen greater than $10^{-4}$ atm.
should produce significant signal depressions.
These calculations presume coincidence of analyte
and interferent oxygen, assume that kinetics are
sufficiently fast to produce equilibrium, and
discount the role of graphite in the equilibrium
calculations.

FILAMENT ATOMIZER:  Figures 8 through 11
display the results of the filament studies as a
graph of the Cr peak absorbance signal vs the nine
one mm viewing zones above the graphite filament
atomizer.  For a signal depression to be considered
significant, the criteria was established that the
analyte absorbance signal must decrease by more
than one standard deviation from the absorbance
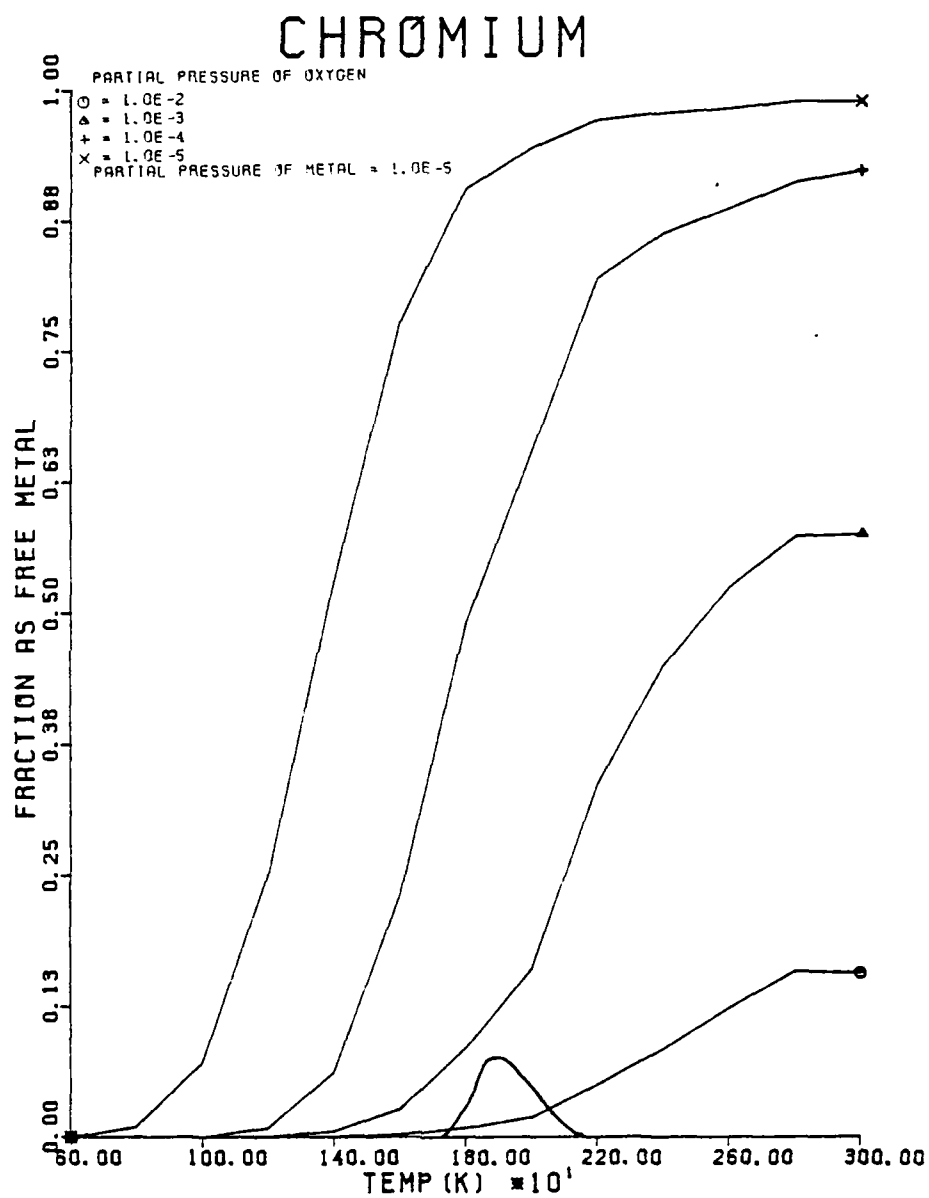
Figure 7.   Results of Thermodynamic
Calculations for Cr

# CHRØMIUM

## PEAK HEIGHT

✱ = ANALYTE +/- ØNE STD. DEV.
⊡ = 10X SØDIUM NITRATE
✕ = 100X SØDIUM NITRATE
✩ = 10X POTASSIUM NITRATE
◇ = 100X POTASSIUM NITRATE
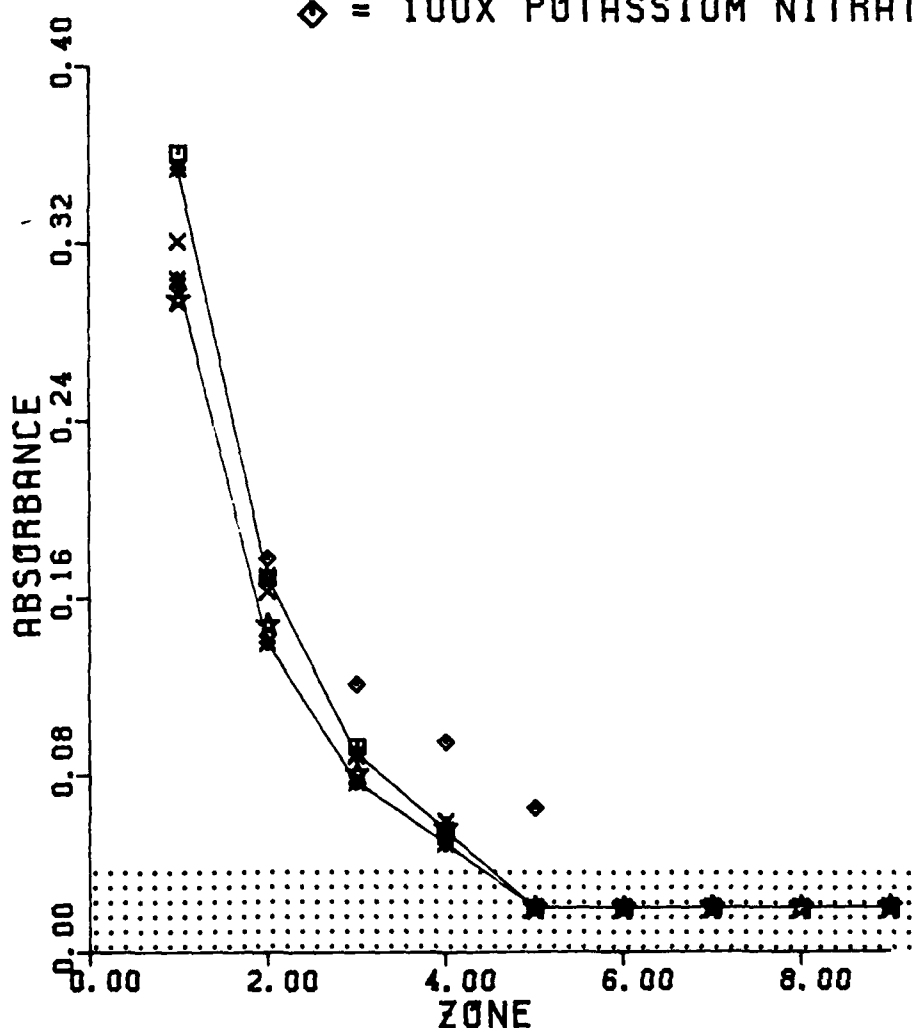


Figure 8.  Filament Atomizer Results

# CHROMIUM

## PEAK HEIGHT

✳ = ANALYTE +/- ONE STD. DEV.
⊡ = 10X SODIUM SULFATE
✕ = 100X SODIUM SULFATE
☆ = 10X POTASSIUM SULFATE
◇ = 100X POTASSIUM SULFATE
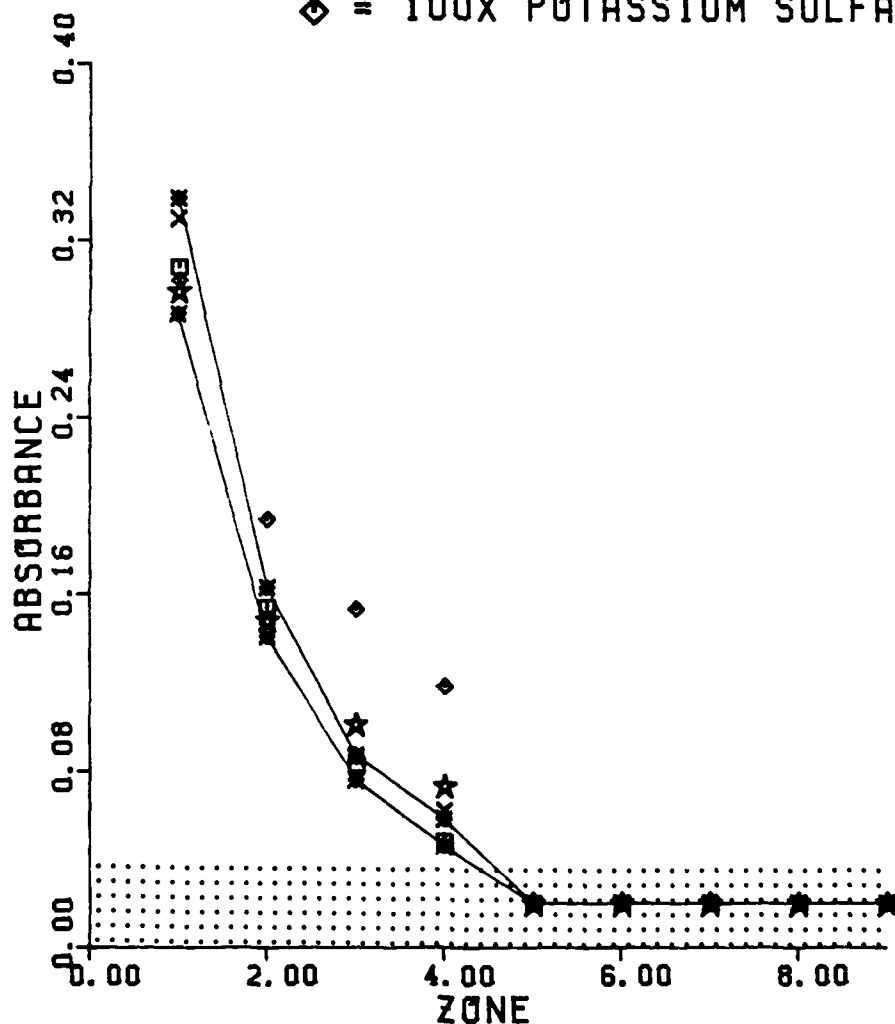


Figure 9.  Filament Atomizer Results

# CHROMIUM

## PEAK HEIGHT

✳ = ANALYTE +/- ONE STD. DEV.
◻ = 10X SODIUM NITRATE
✕ = 100X SODIUM NITRATE
☆ = 10X POTASSIUM NITRATE
◇ = 100X POTASSIUM NITRATE
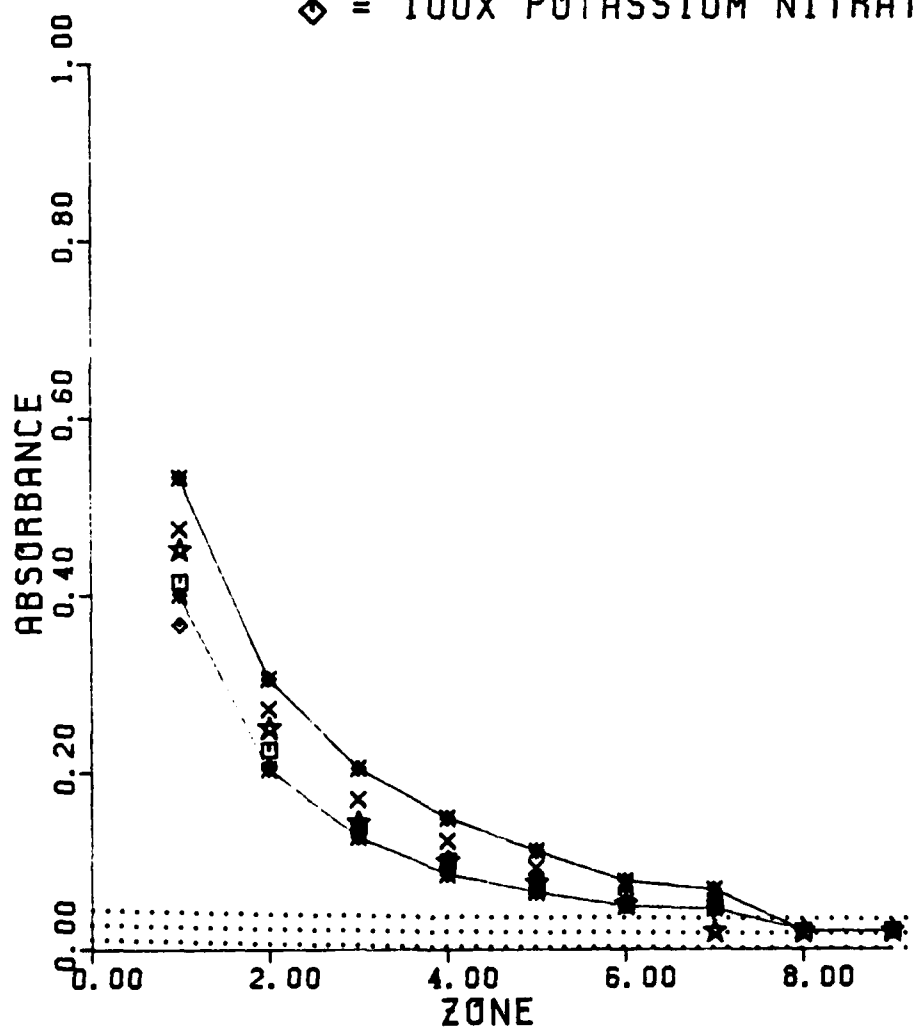
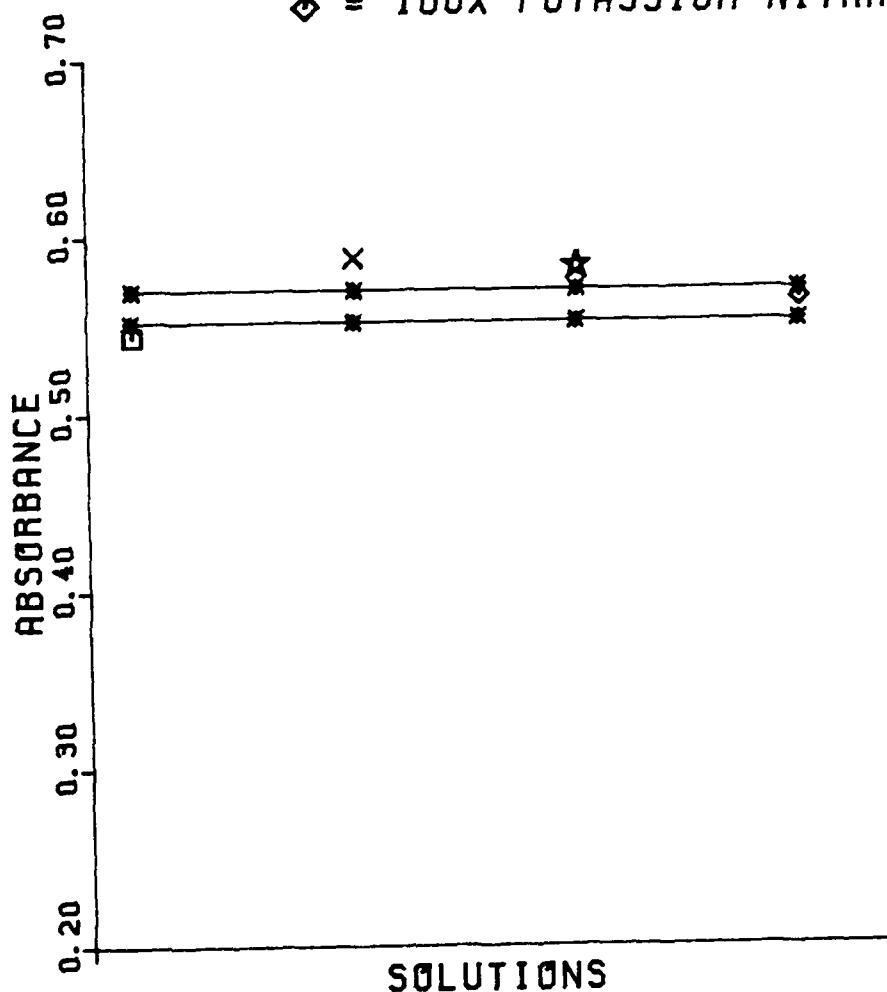Figure 10.  Filament Atomizer Results

# CHROMIUM

## PEAK HEIGHT

* = ANALYTE +/- ONE STD. DEV.
☐ = 10X SODIUM SULFATE
✕ = 100X SODIUM SULFATE
☆ = 10X POTASSIUM SULFATE
◇ = 100X POTASSIUM SULFATE
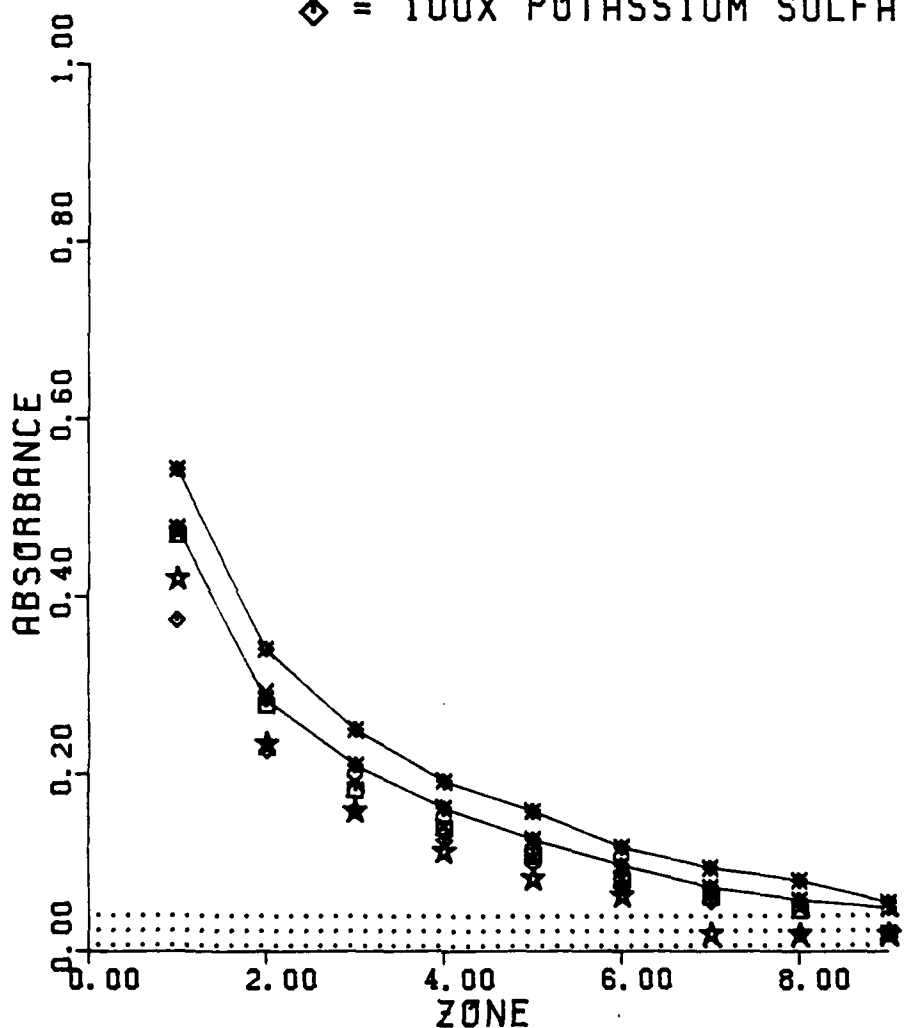


Figure 11.  Filament Atomizer Results

signal of the interferent-free solution. Thus
the solid lines on the graphs represent the ± one
standard deviation absorbance signal for the inter-
ferent-free analyte solutions. In figures 8 and 9,
the chromium absorbance signal decreases very
rapidly from its maximum value closest to the
filament (zone 1) until it disappears into the
baseline noise level at the fifth zone. No
depressions were observed when either the sulfate
or nitrate interferents were added to the analyte.
The solutions containing Cr plus a hundred-fold
excess of $KNO_3$ and the $K_2SO_4$ solutions exhibited
slight enhancements in these viewing zones. The
filament is completely enclosed by copper electrodes
and quartz viewing windows to a height of approxi-
mately 2.5 cm above the filament. This enclosure
is constantly flushed by the argon sheath gas. To
minimize the entrainment of air from the top of the
atomizer, the enclosure height can be increased a
further 7.5 cm by placing a four-sided glass
chimney on top of the atomizer. Figures 10 and 11
suggest that this chimney is effective in minimizing
the entrainment of air into the atomizer. The Cr
absorbance signal persists to at least the
seventh viewing zone above the filament. Slight

depressions were observed for the interferent sulfate solutions.

FURNACE ATOMIZER: As shown in Table II, chromium required the highest final atomization temperature of the elements studied. As shown in figures 12 and 13, no signal depressions were observed for the added nitrates and sulfates. However, the presence of 1% of $O_2$ in the Ar sheath gas reduced the Cr absorbance signal magnitude by about 75%. This suggests that the absence of signal depressions results from the lack of gas phase temporal overlap between analyte and interferent.

SPATIALLY RESOLVED FURNACE ATOMIZER: Figures 14 and 15 illustrate that the Cr atoms are not uniformly distributed across the vertical diameter of the furnace. As discussed in the previous chapter, the optical system for the spatially resolved furnace studies gave a spatial resolution of approximately 0.3 mm in place of about 1 mm viewed in the filament atomizer. Even this magnified view, coupled with the increased residency time of the Cr atoms within the furnace and the potential effectiveness of metal oxide collisions with the hot graphite furnace walls are

# CHROMIUM
## PEAK HEIGHT

✱ = ANALYTE +/- ONE STD. DEV.
⊡ = 10X SODIUM NITRATE
✕ = 100X SODIUM NITRATE
☆ = 10X POTASSIUM NITRATE
◇ = 100X POTASSIUM NITRATE



Figure 12.   Furnace Atomizer Results

# CHRØMIUM

## PEAK HEIGHT

＊ = ANALYTE +/- ONE STD. DEV.
▣ = 10X SØDIUM SULFATE
✕ = 100X SØDIUM SULFATE
✰ = 10X POTASSIUM SULFATE
◇ = 100X POTASSIUM SULFATE
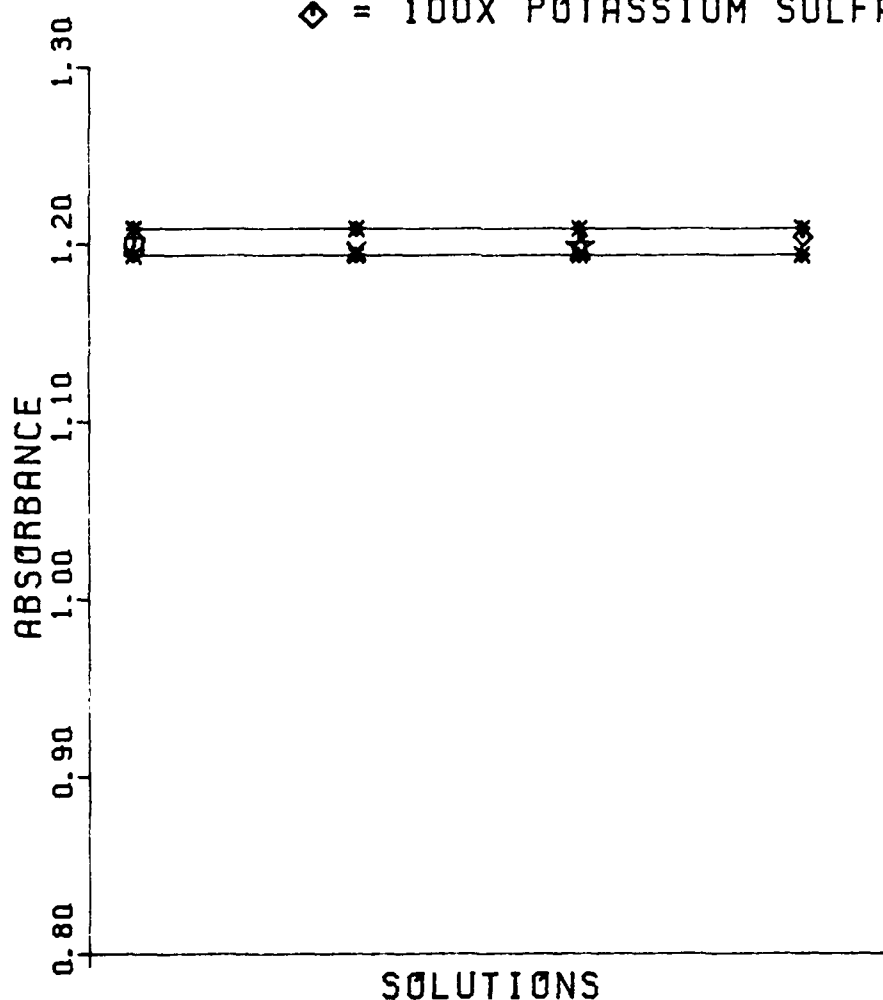


Figure 13.   Furnace Atomizer Results

# CHROMIUM

## PEAK HEIGHT

✳ = ANALYTE +/- ONE STD. DEV.
⊡ = 10X SODIUM NITRATE
✕ = 100X SODIUM NITRATE
✪ = 10X POTASSIUM NITRATE
◇ = 100X POTASSIUM NITRATE
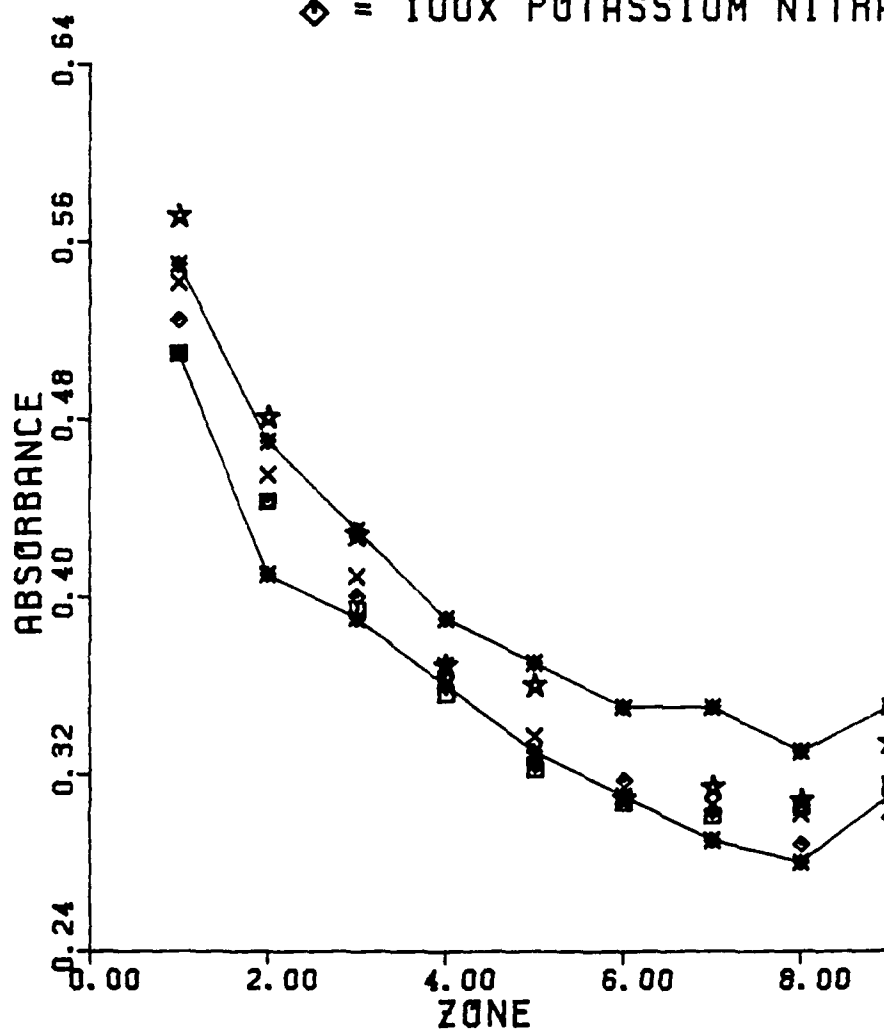


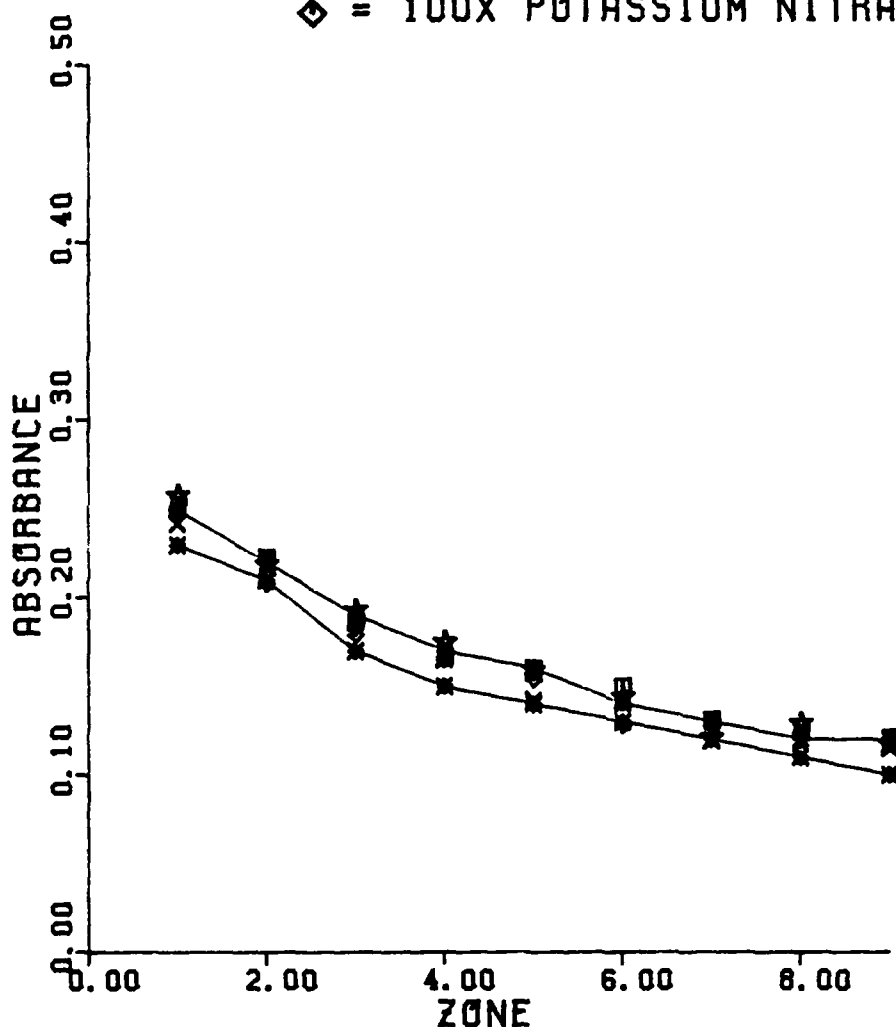Figure 14.  Spatially Resolved Furnace Results

# CHROMIUM

## PEAK HEIGHT

✳ = ANALYTE +/- ONE STD. DEV.
⊞ = 10X SODIUM SULFATE
✕ = 100X SODIUM SULFATE
✰ = 10X POTASSIUM SULFATE
◇ = 100X POTASSIUM SULFATE
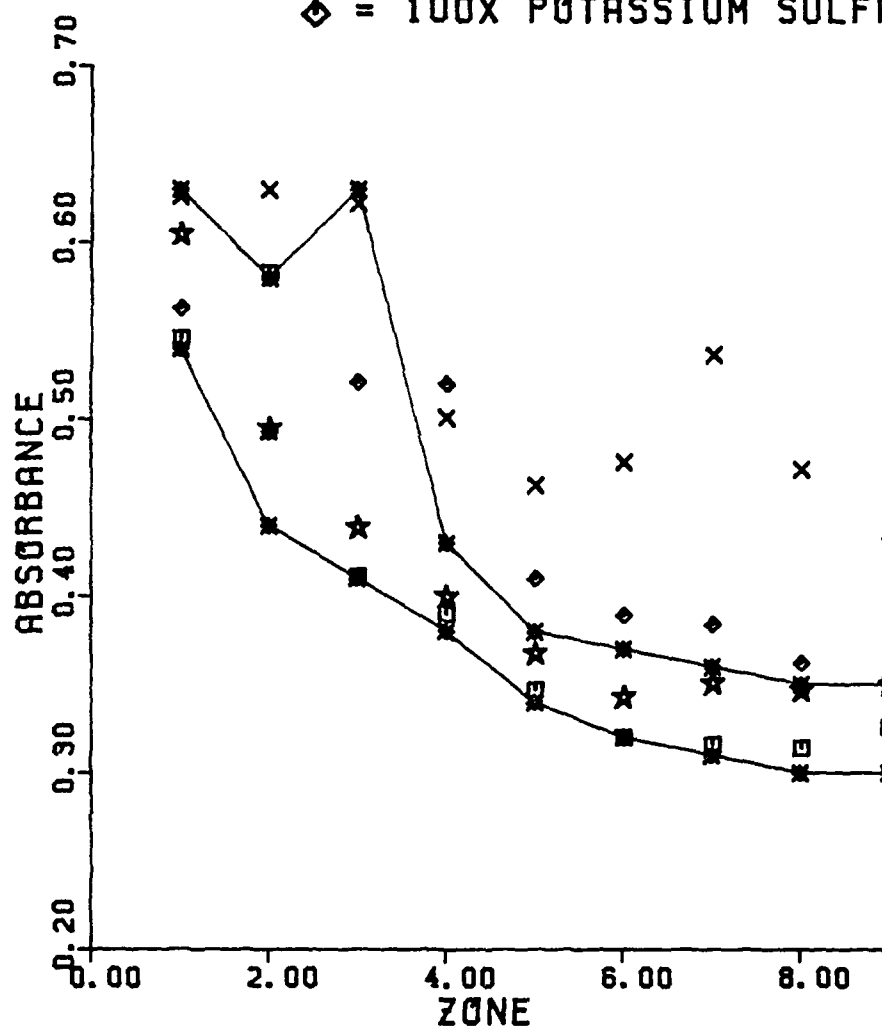


Figure 15. Spatially Resolved Furnace Results

insufficient to achieve uniform distribution of
chromium atoms in the furnace atomizer. The three
dimensional absorbance-zone-time graphs provide
a picture of the entire absorbance profile. As
shown in figure 16, the absorbance signal persists
for about 800 msec. The absorbance is much higher
in zone one, closest to the base of the furnace
than in zone nine which is closest to the top of
the furnace. The exact cause of the reduced free
atom density near the center of the furnace is not
known at this time. Similarly, the failure of the
absorbance signal in zone 9 to reach the magnitude
shown in zone 1 is inconsistent with a system at
equilibrium if one assumes rapid diffusive mixing
and a thermal gradient which is radially symmetrical.
The signal enhancements due to the addition of a
hundred-hold excess of $Na_2SO_4$ to the Cr solution
were not observed on subsequent repetitions of
this experiement on different days.
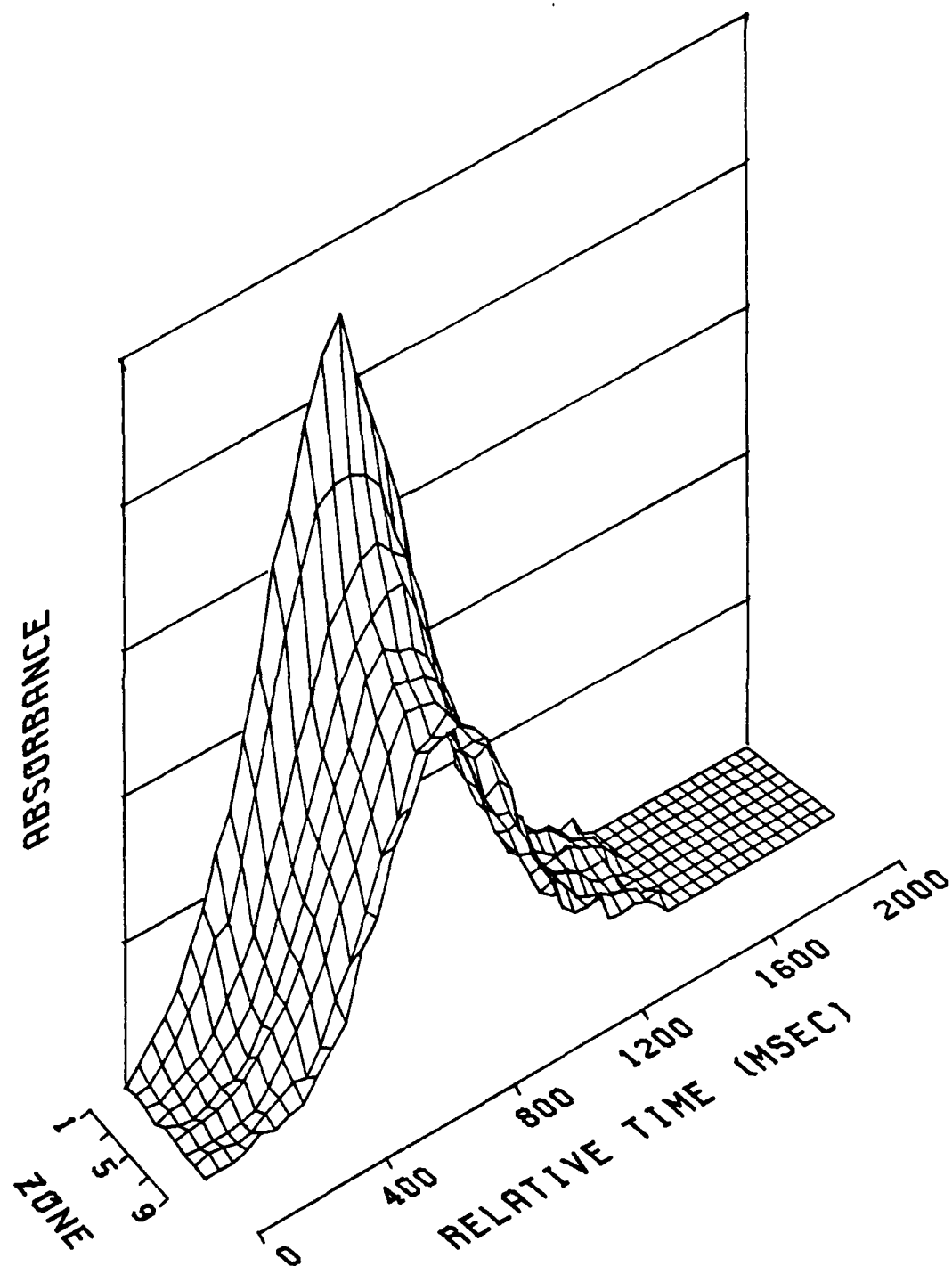
Figure 16. Absorbance Profile for Cr

## 4.4  Nickel

Nickel is comparable to Cr in its appearance and final atomization temperatures, yet the metal oxygen reaction for Ni is approximately $10^3$ times slower for Ni than for Cr.  As shown in Table I, the nickel-oxygen bond strength of 87 kcal/mole is about 20% lower than that of Cr.  When the appearance temperature of Ni is superimposed on the results of the thermodynamic studies, as indicated by the arrow in figure 17, a partial pressure of oxygen in excess of $10^{-3}$ atm is required to significantly reduce the Ni free metal concentration.  However, if graphite were considered in the equilibrium calculations, almost all the Ni would appear as the free metal even at an oxygen partial pressure as high as $10^{-2}$ atm.

FILAMENT ATOMIZER:  Figure 18 demonstrates that the nitrate interferents produced no significant signal depressions using the graphite filament atomizer.  Figure 19 shows similar results for added sulfates with the exception of a hundred-fold excess of $K_2SO_4$.  The three dimensional profile for the filament atomizer shown in figure 20 illustrates that in contrast to Cr, the analyte absorbance signal decayed less rapidly and
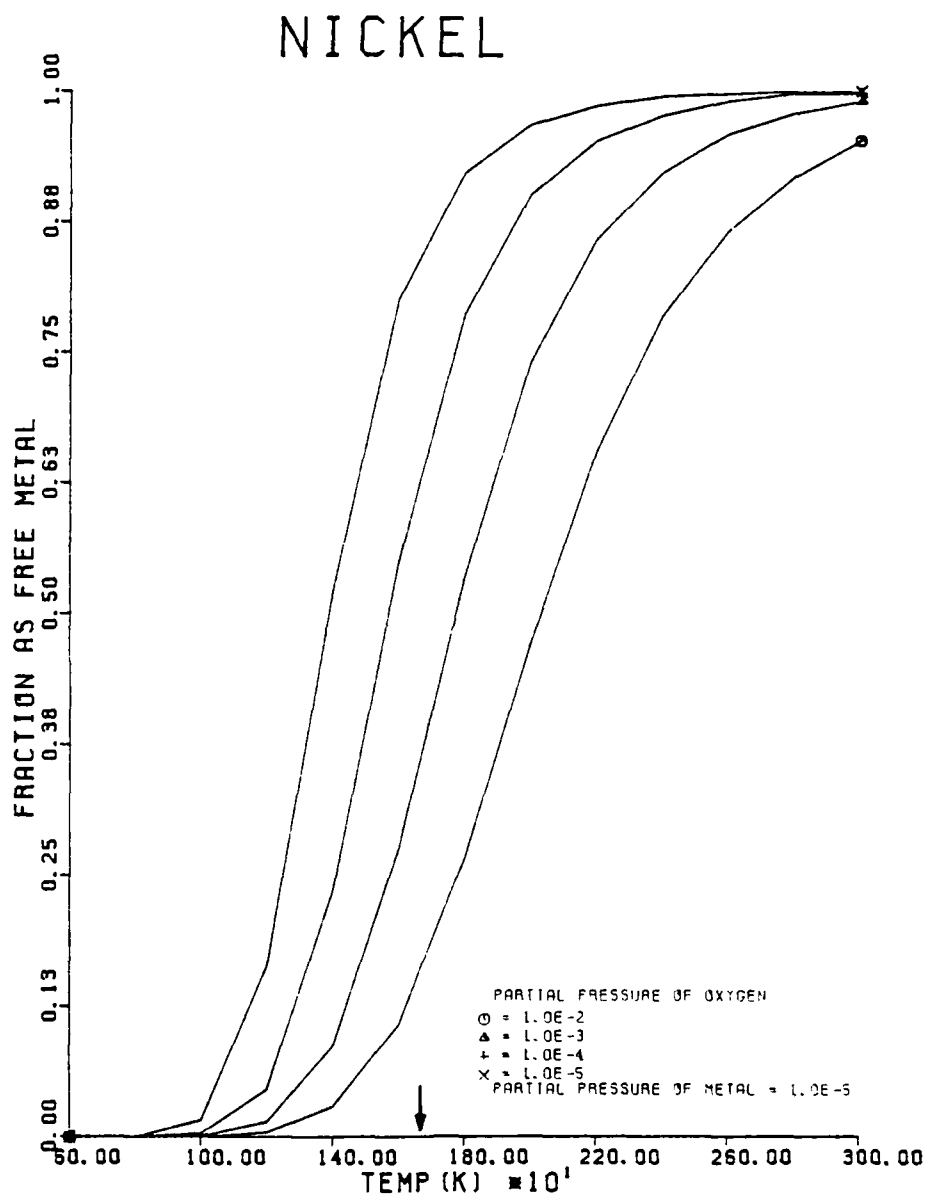
# NICKEL



Figure 17.   Results of Thermodynamic

Calculations for Ni

# NICKEL
## PEAK HEIGHT

✳ = ANALYTE +/- ONE STD. DEV.
⊡ = 10X SODIUM NITRATE
✕ = 100X SODIUM NITRATE
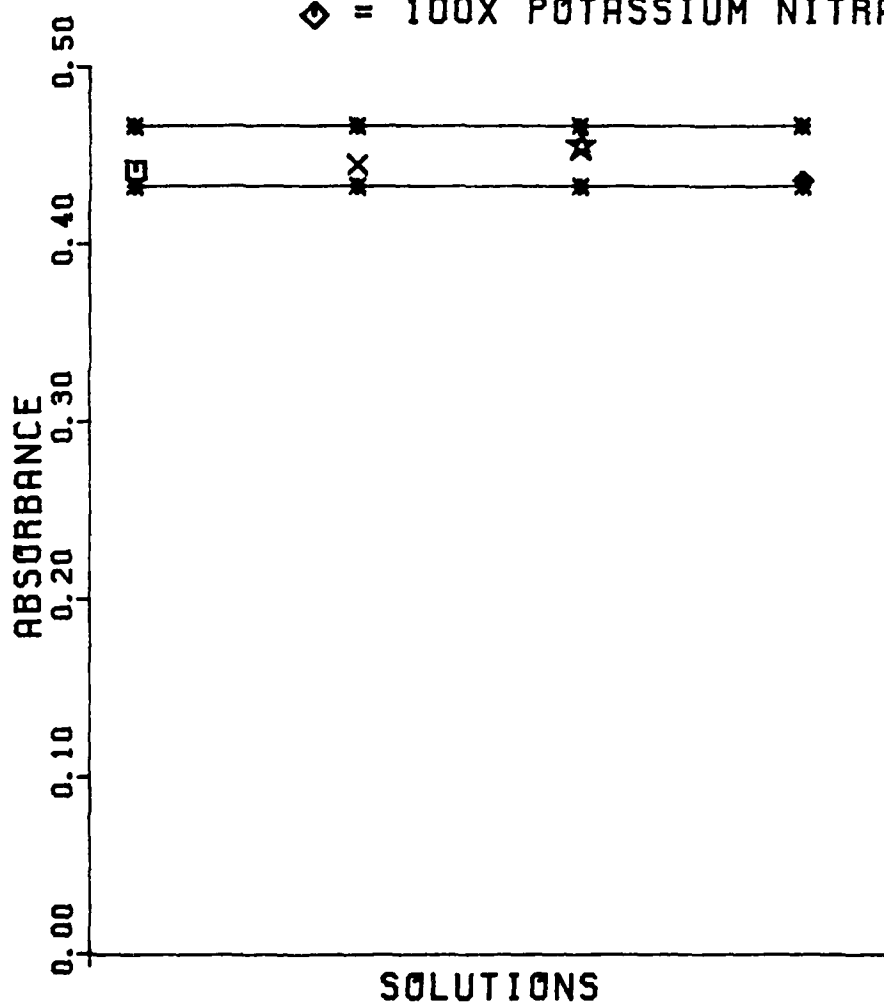✩ = 10X POTASSIUM NITRATE
◇ = 100X POTASSIUM NITRATE



Figure 18.  Filament Atomizer Results

# NICKEL

## PEAK HEIGHT

✳ = ANALYTE +/- ONE STD. DEV.
▣ = 10X SODIUM SULFATE
✕ = 100X SODIUM SULFATE
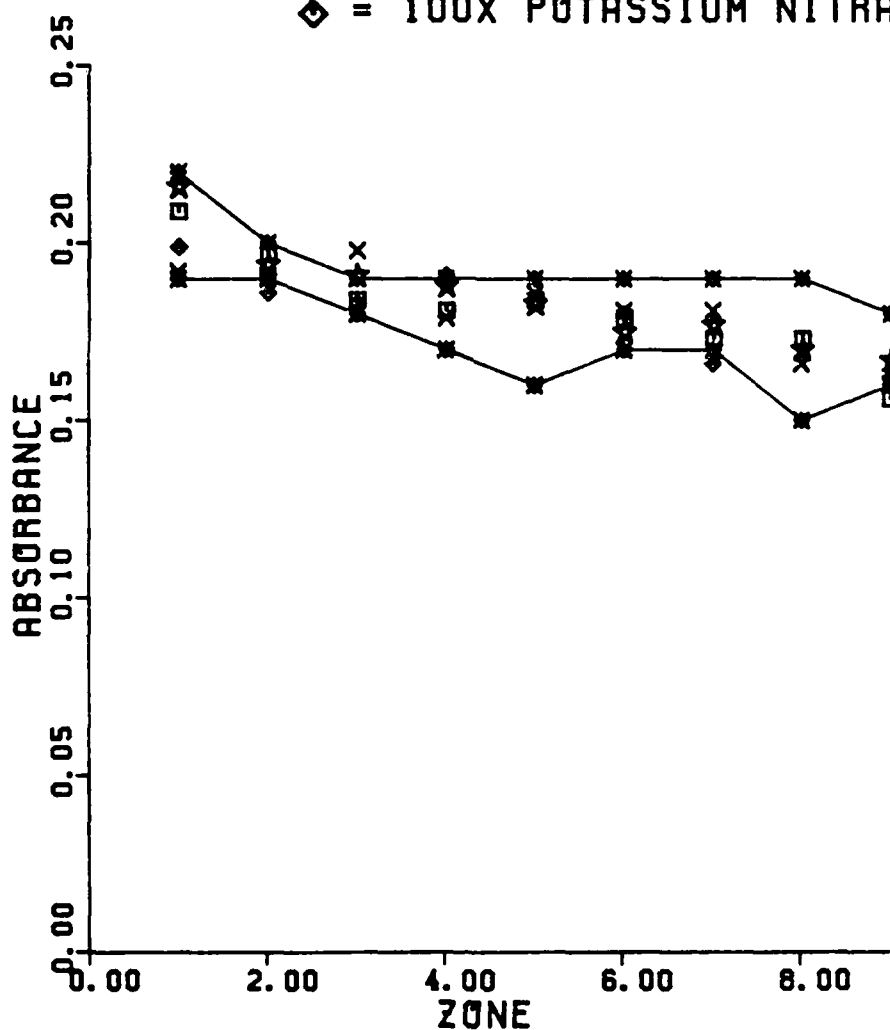☆ = 10X POTASSIUM SULFATE
◇ = 100X POTASSIUM SULFATE
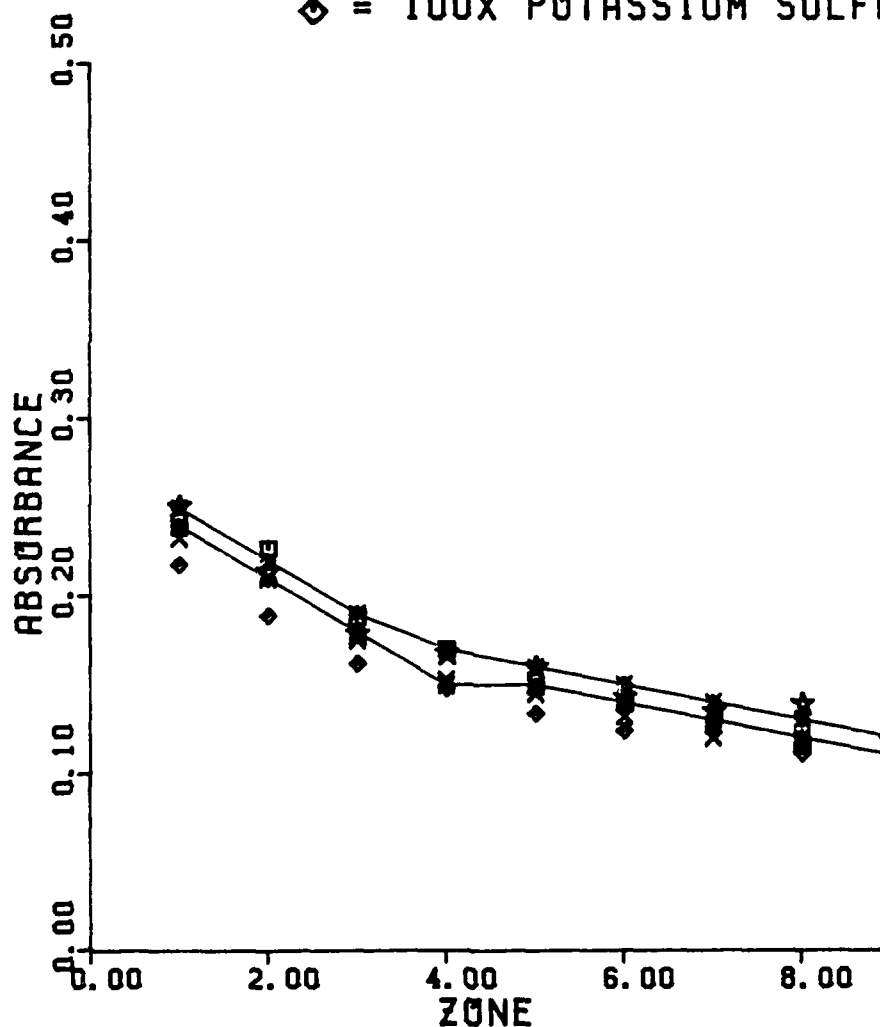


Figure 19.   Filament Atomizer Results
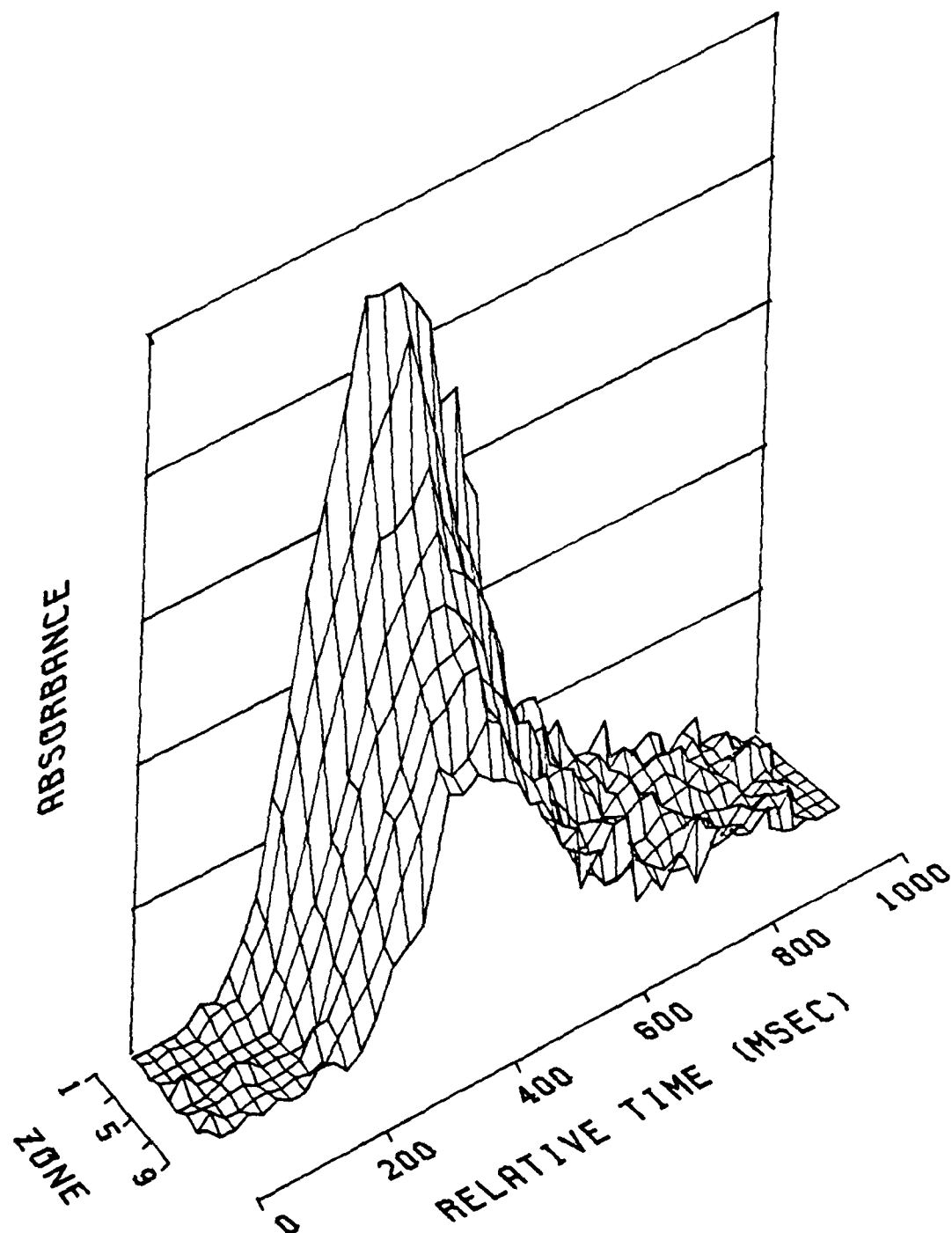
Figure 20.  Absorbance Profile for Ni + 10xNa$_2$SO$_4$

persisted for all nine viewing zones. This is consistent with the weaker Ni-O bond and the reduced reaction kinetics.

FURNACE ATOMIZER: As shown in figures 21 and 22, there were no absorbance signal depressions observed with the commercial apparatus. As with Cr, the absence of depressions may be attributed to the lack of gas phase coincidence of analyte and interferent. Additionally, as mentioned above, both kinetics and equilibrium considerations more strongly favor the existence of the free atomic species.

SPATIALLY RESOLVED FURNACE ATOMIZER: As illustrated in figures 23, 24, and 25, the free nickel atoms are fairly uniformly distributed throughout the vertical diameter of the furnace atomizer. That the maximum absorbance signal for each of the nine viewing zones occurs at approximately the same time indicates that diffusion from the bottom to the top of the atomizer is fairly rapid.

# NICKEL

## PEAK HEIGHT

✳ = ANALYTE +/- ONE STD. DEV.
⊡ = 10X SODIUM NITRATE
✕ = 100X SODIUM NITRATE
✩ = 10X POTASSIUM NITRATE
◇ = 100X POTASSIUM NITRATE

Figure 21. Furnace Atomizer Results

# NICKEL

## PEAK HEIGHT

✳ = ANALYTE +/- ONE STD. DEV.
⊞ = 10X SODIUM SULFATE
✕ = 100X SODIUM SULFATE
✰ = 10X POTASSIUM SULFATE
◇ = 100X POTASSIUM SULFATE
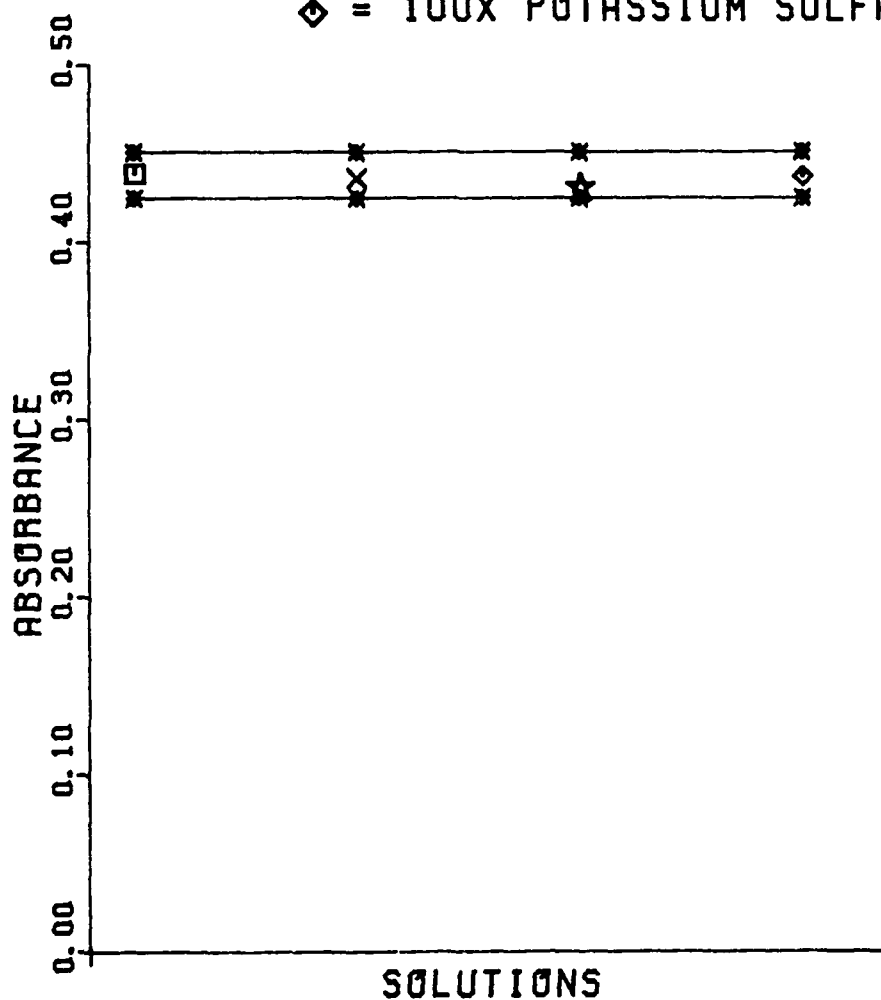


Figure 22.   Furnace Atomizer Results

# NICKEL

## PEAK HEIGHT

✳ = ANALYTE +/- ONE STD. DEV.
⊡ = 10X SODIUM NITRATE
✕ = 100X SODIUM NITRATE
✩ = 10X POTASSIUM NITRATE
◈ = 100X POTASSIUM NITRATE



Figure 23. Spatially Resolved Furnace Results

# NICKEL

## PEAK HEIGHT

✳ = ANALYTE +/- ONE STD. DEV.
🄴 = 10X SODIUM SULFATE
✕ = 100X SODIUM SULFATE
☆ = 10X POTASSIUM SULFATE
◇ = 100X POTASSIUM SULFATE
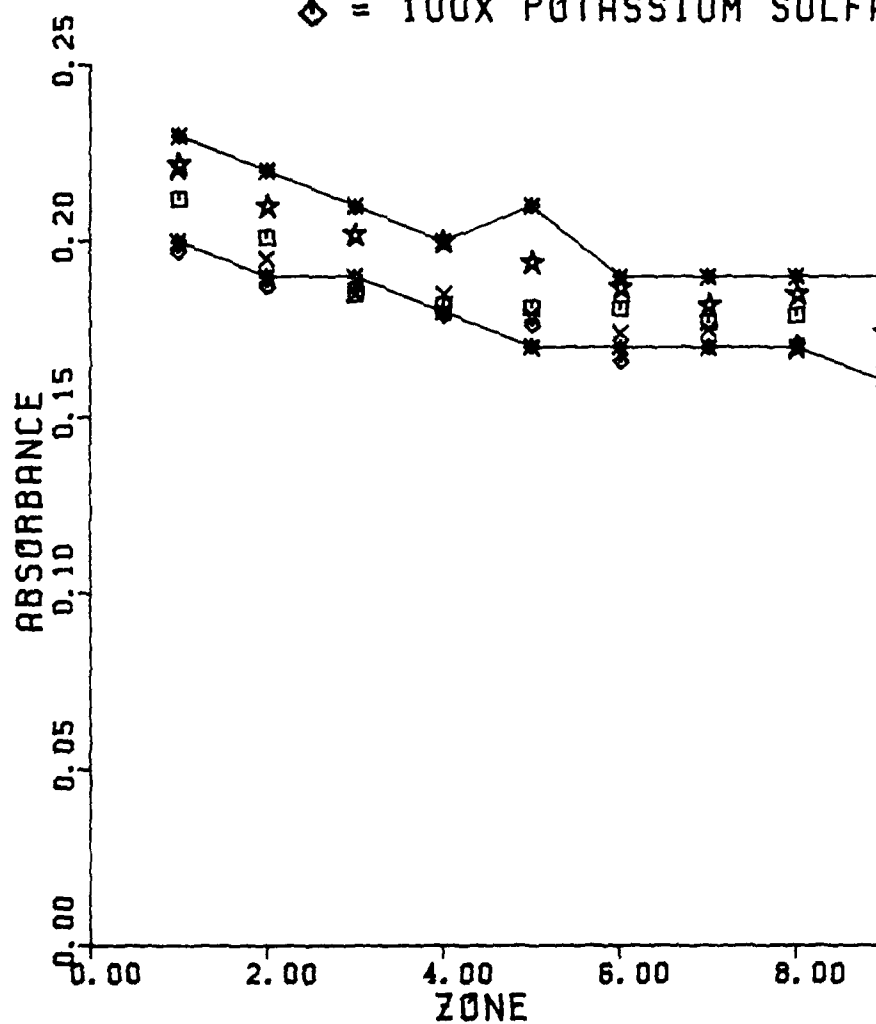


Figure 24.   Spatially Resolved Furnace Results
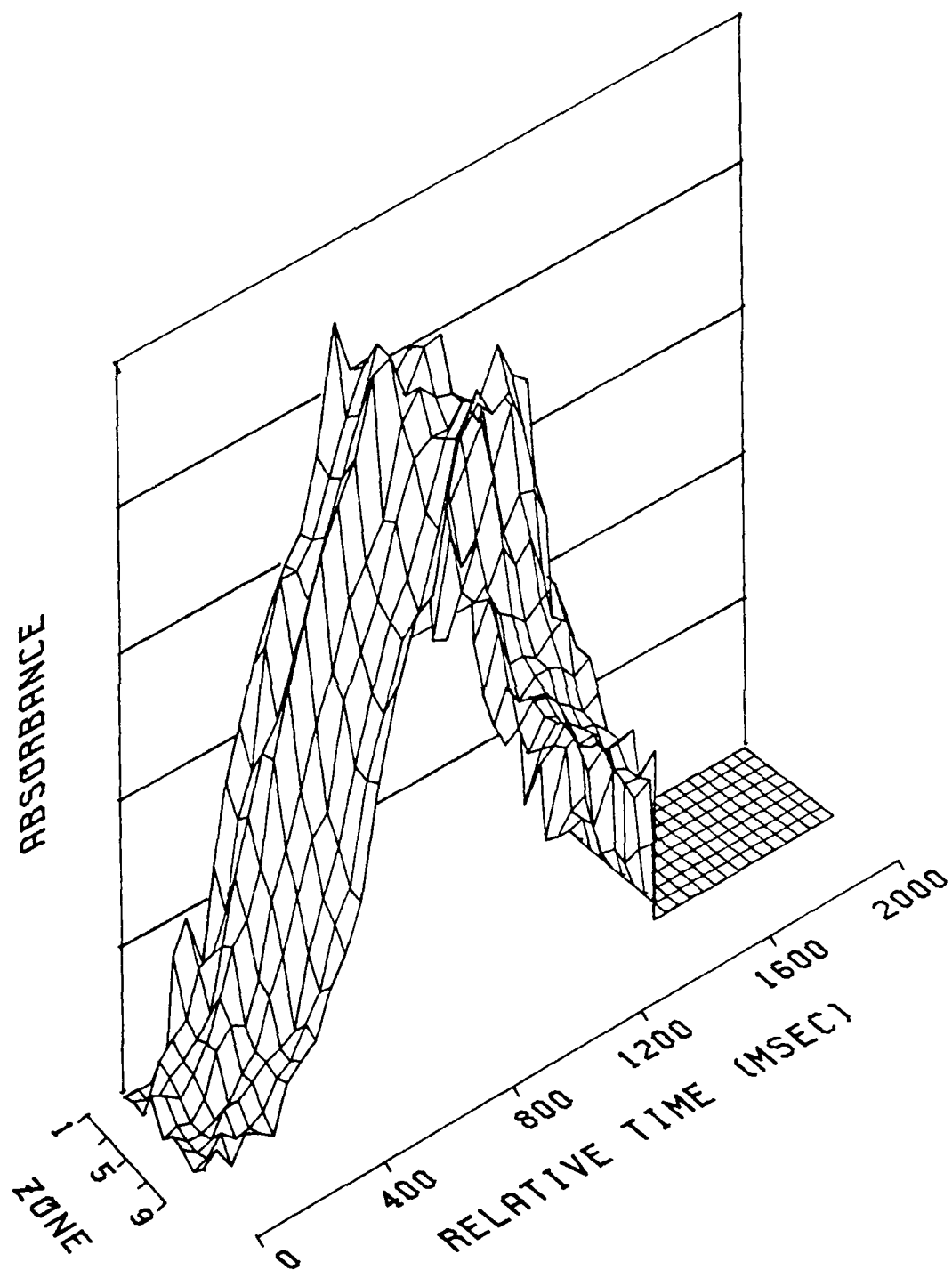
Figure 25. Absorbance Profile for "i

## 4.5 Iron

Many of the properties of iron are very
similar to copper, e.g., its metal oxide bond
strength (99 kcal/mole vs. 96 kcal/mole for
$Cu$[10]), and the kinetic rates for the formation
of the metal oxide (.45 x $10^{-14}$ ml/molecule-sec
vs. .33 x $10^{-14}$ ml/molecule-sec for Cu). Similarly,
the equilibrium distribution diagrams for the two
metals, ignoring the presence of graphite, as shown
in figure 26 for Fe and figure 27 for Cu are very
much alike. The tabulated average appearance
temperature compiled by L'vov[8] contain some
temperatures which are inconsistent with the
other values for the same element. The appearance
temperature for Cu of 1730K, as observed by
Campbell and Ottaway, is at least 300 degrees
higher than the other Cu appearance temperatures.
By removing this value, the recalculated Cu
appearance temperature becomes 1367K. If the
two graphs are shifted to superimpose the two
appearance temperatures, which are indicated by
arrows on the graphs, the thermodynamic profiles
become almost identical. Thus, the similar
response of the two metals to the added inter-
ferents may be explained by the thermodynamic

# IRØN



PARTIAL PRESSURE OF OXYGEN
⊙ = 1.0E-2
△ = 1.0E-3
+ = 1.0E-4
X = 1.0E-5
PARTIAL PRESSURE OF METAL = 1.0E-5
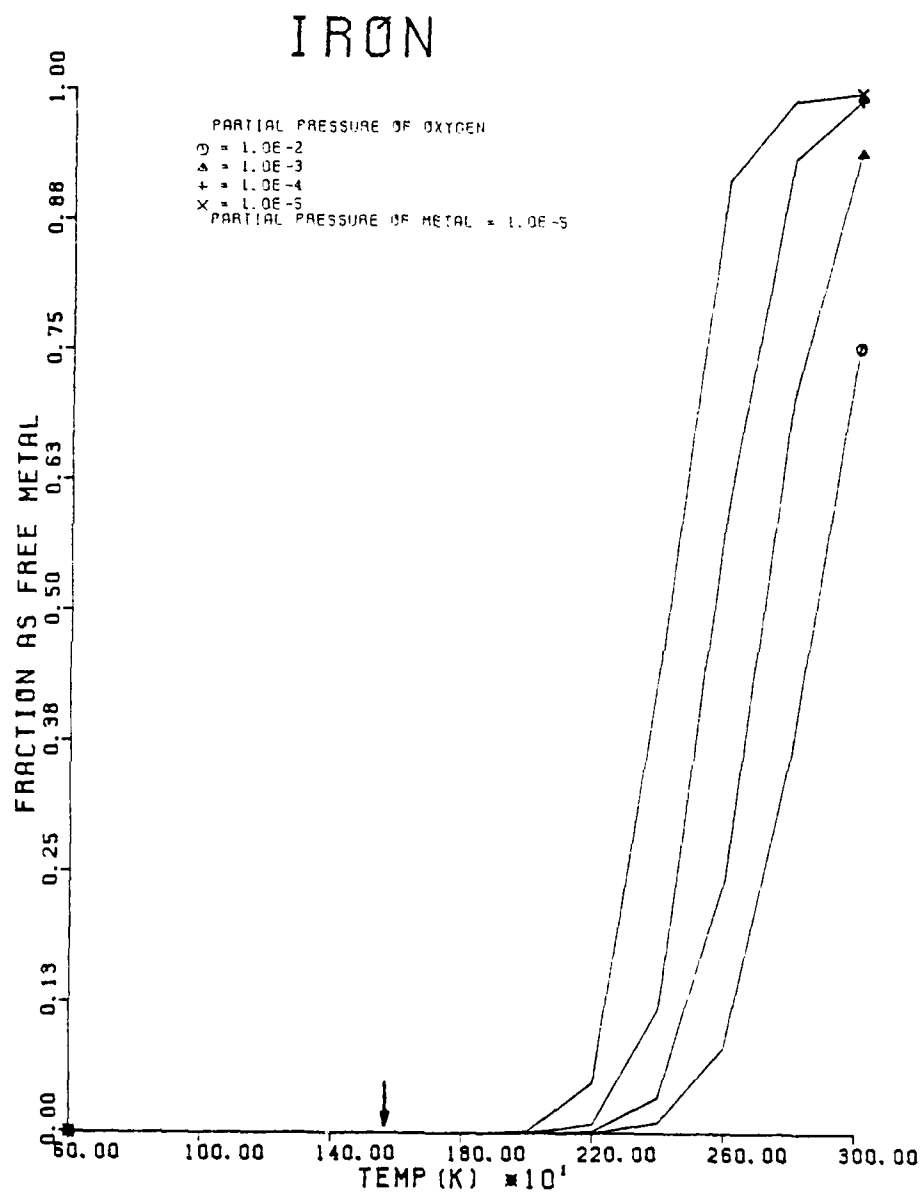
Figure 26.   Results of Thermodynamic

Calculations for Fe

# COPPER



PARTIAL PRESSURE OF OXYGEN
O ≈ 1.0E-2
△ ≈ 1.0E-3
+ ≈ 1.0E-4
× ≈ 1.0E-5
PARTIAL PRESSURE OF METAL ≈ 1.0E-5

FRACTION AS FREE METAL

TEMP (K)  *10$^1$
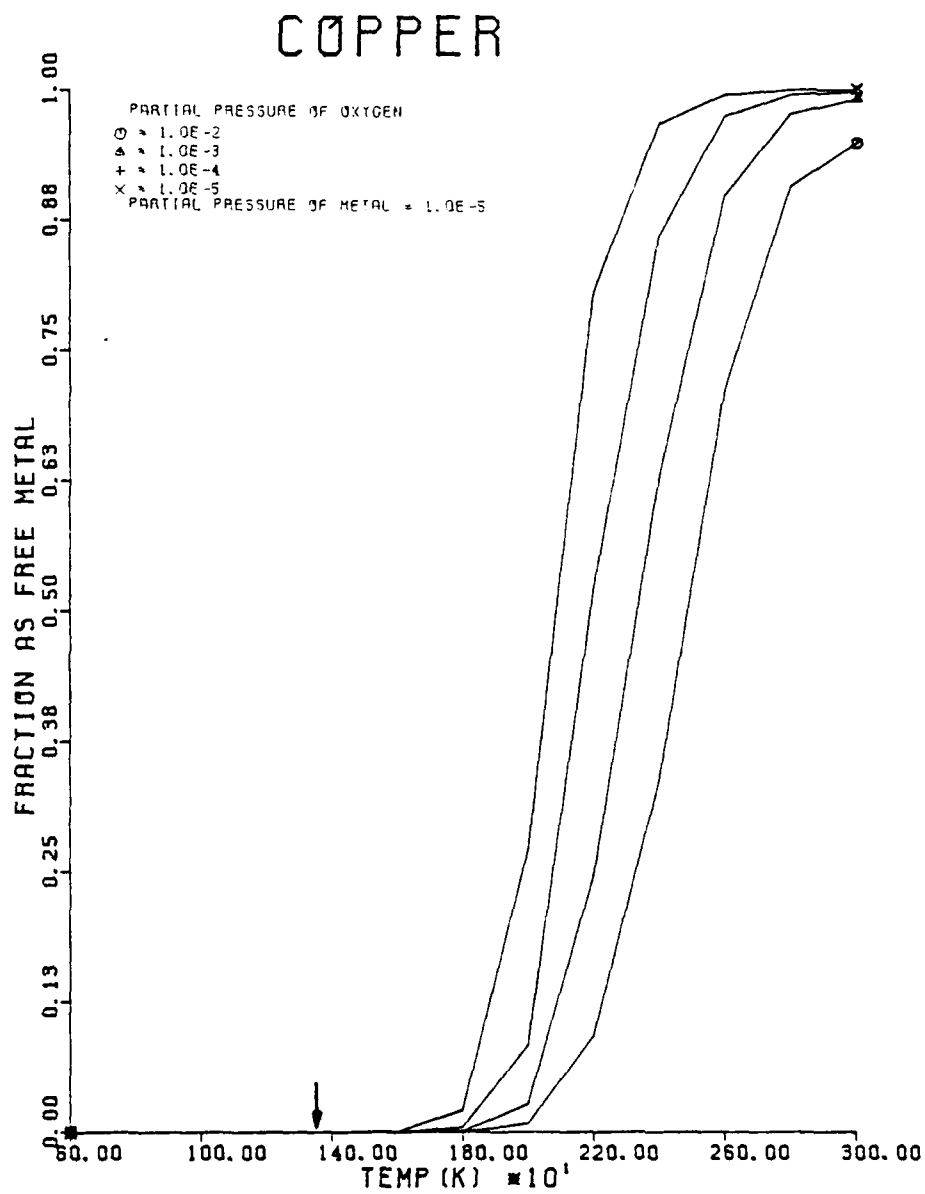
Figure 27.   Results of Thermodynamic

Calculations for Cu

studies.

FILAMENT ATOMIZER:  The peak absorbance
signal vs. height above the filament atomizer
are shown in figures 28 and 29.  Slight depressions
at elevated zones were observed for $KNO_3$ solutions.
All the sulfate salts, with the exception of a
ten-fold excess of $Na_2SO_4$ produced depressions.  The
depressions produced by the potassium sulfates
were greater than those produced by the sodium
sulfates.  Figures 30 and 31 illustrate the
absorbance-height-time profiles for the pure metal
and Fe plus a hundred-fold excess of $K_2SO_4$.

FURNACE ATOMIZER:  As shown in figures 32
and 33, the interferents produced depressions in
the furnace atomizer.  The depressions appear to
be fairly independent of interferent concentration
and the type of interferent.  This random ordering
of depressions may be due to changes in the activity
of the graphite.  As noted earlier, if graphite
was considered to have unit activity almost all
the analyte (greater than 95%) would exist as the
free metal at temperatures greater than the
appearance temperature.  Thus, small changes in
the activity of graphite would account for the
day-to-day variation in the magnitude and order

# IRØN

## PEAK HEIGHT

✳ = ANALYTE +/- ONE STD. DEV.
☐ = 10X SØDIUM NITRATE
✕ = 100X SØDIUM NITRATE
☆ = 10X POTASSIUM NITRATE
◇ = 100X POTASSIUM NITRATE
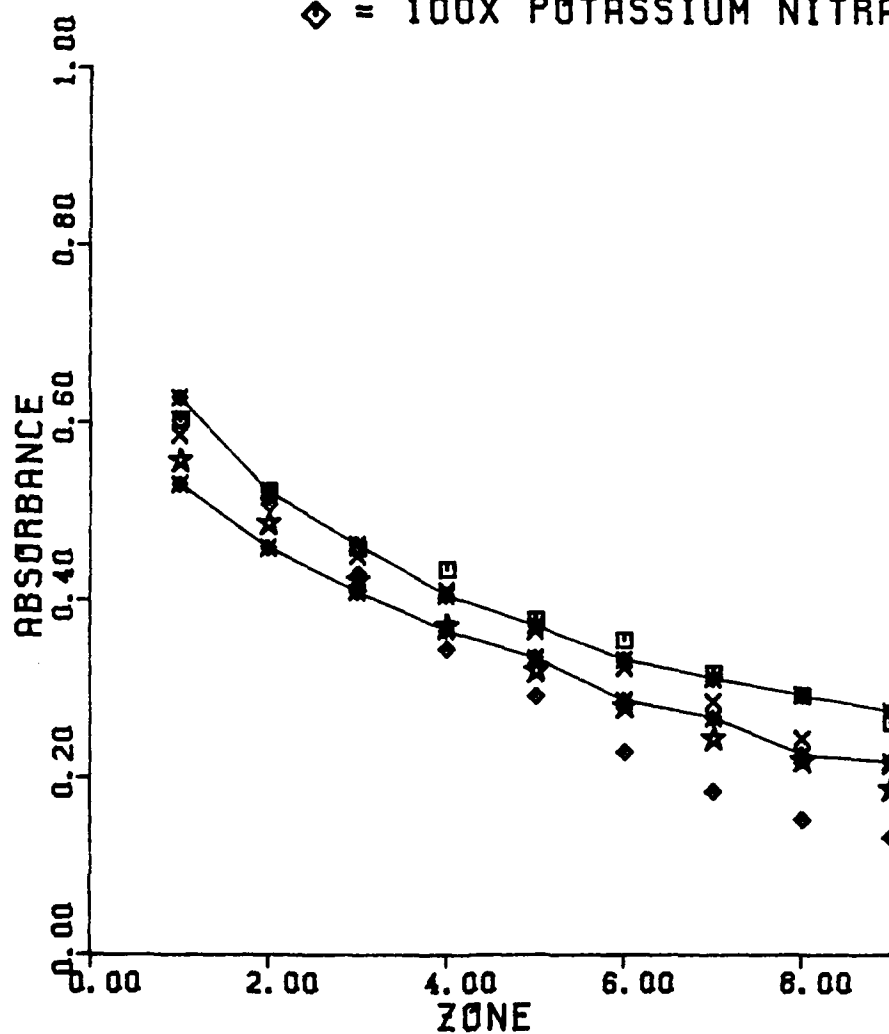


Figure 28.   Filament Atomizer Results

# IRON

## PEAK HEIGHT

✳ = ANALYTE +/- ONE STD. DEV.
⊡ = 10X SODIUM SULFATE
✕ = 100X SODIUM SULFATE
✩ = 10X POTASSIUM SULFATE
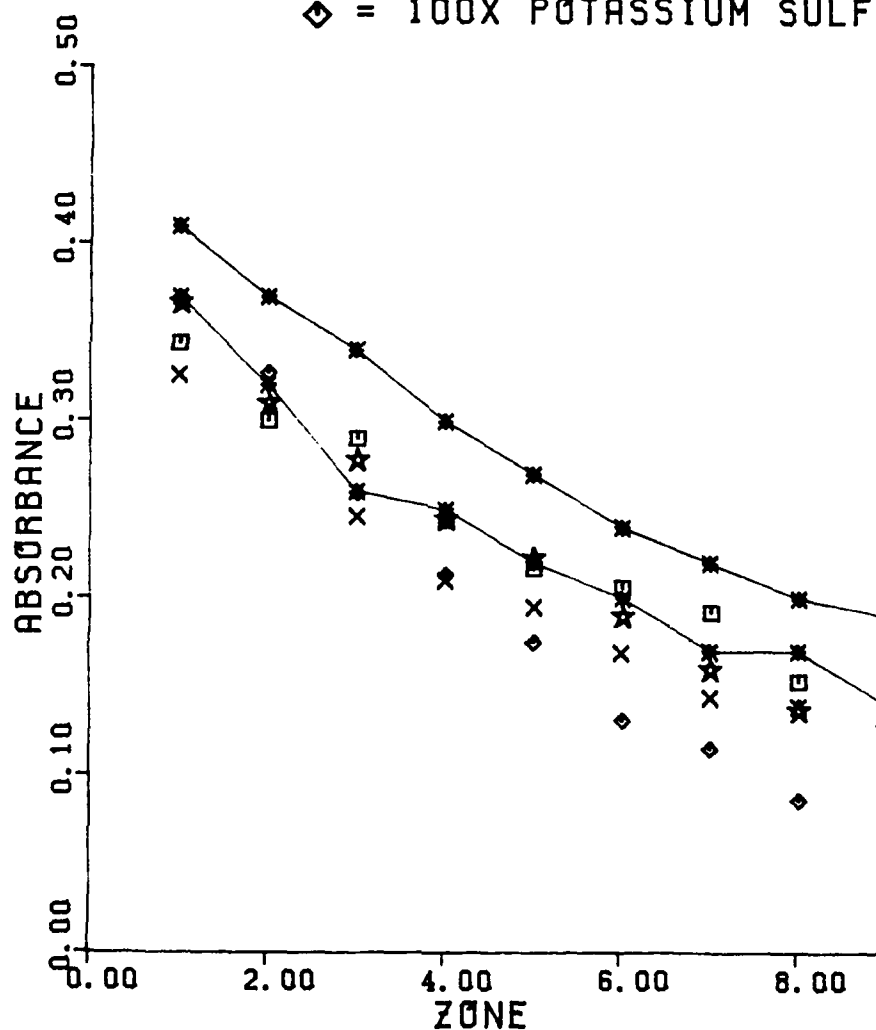◇ = 100X POTASSIUM SULFATE
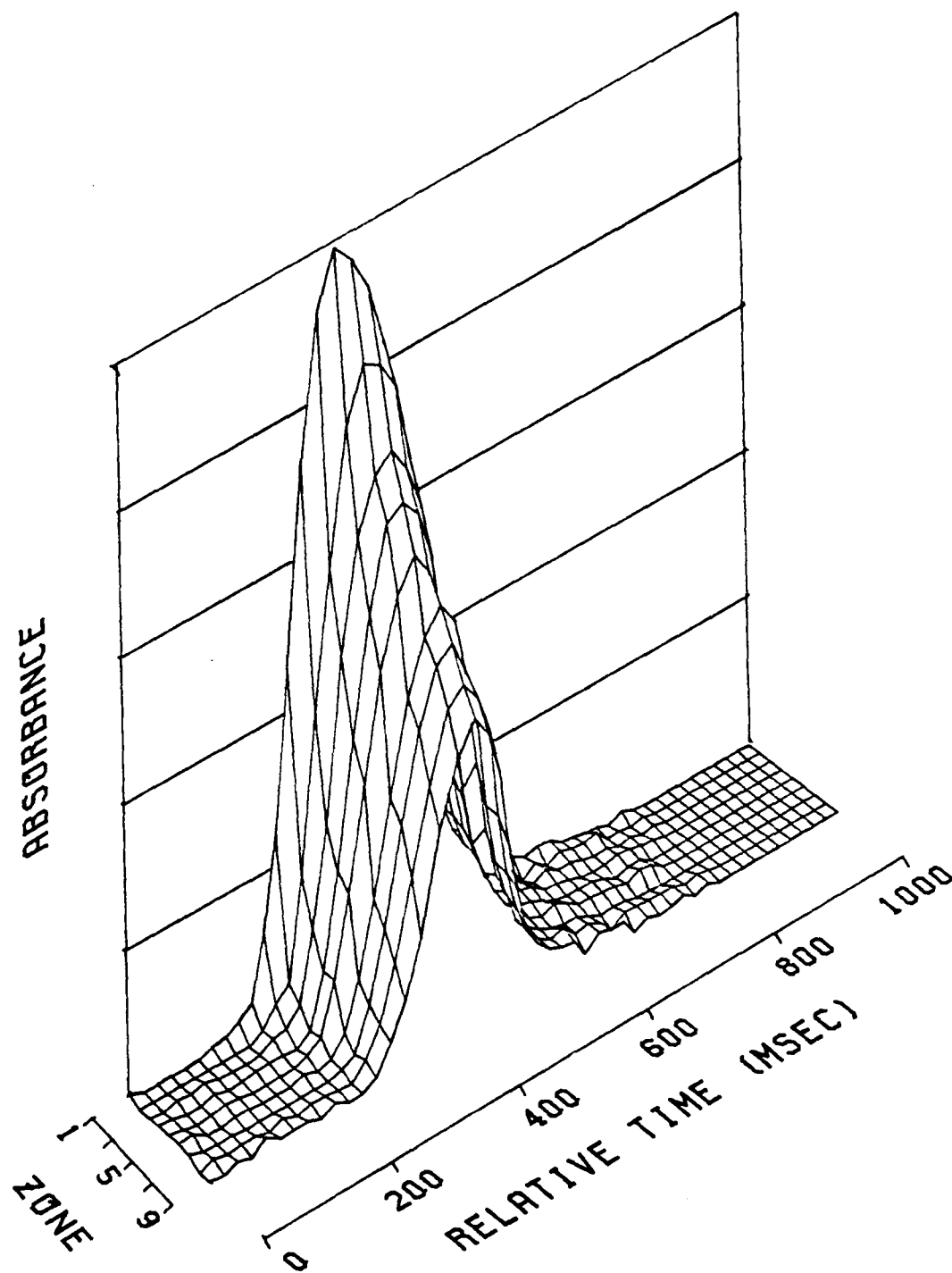


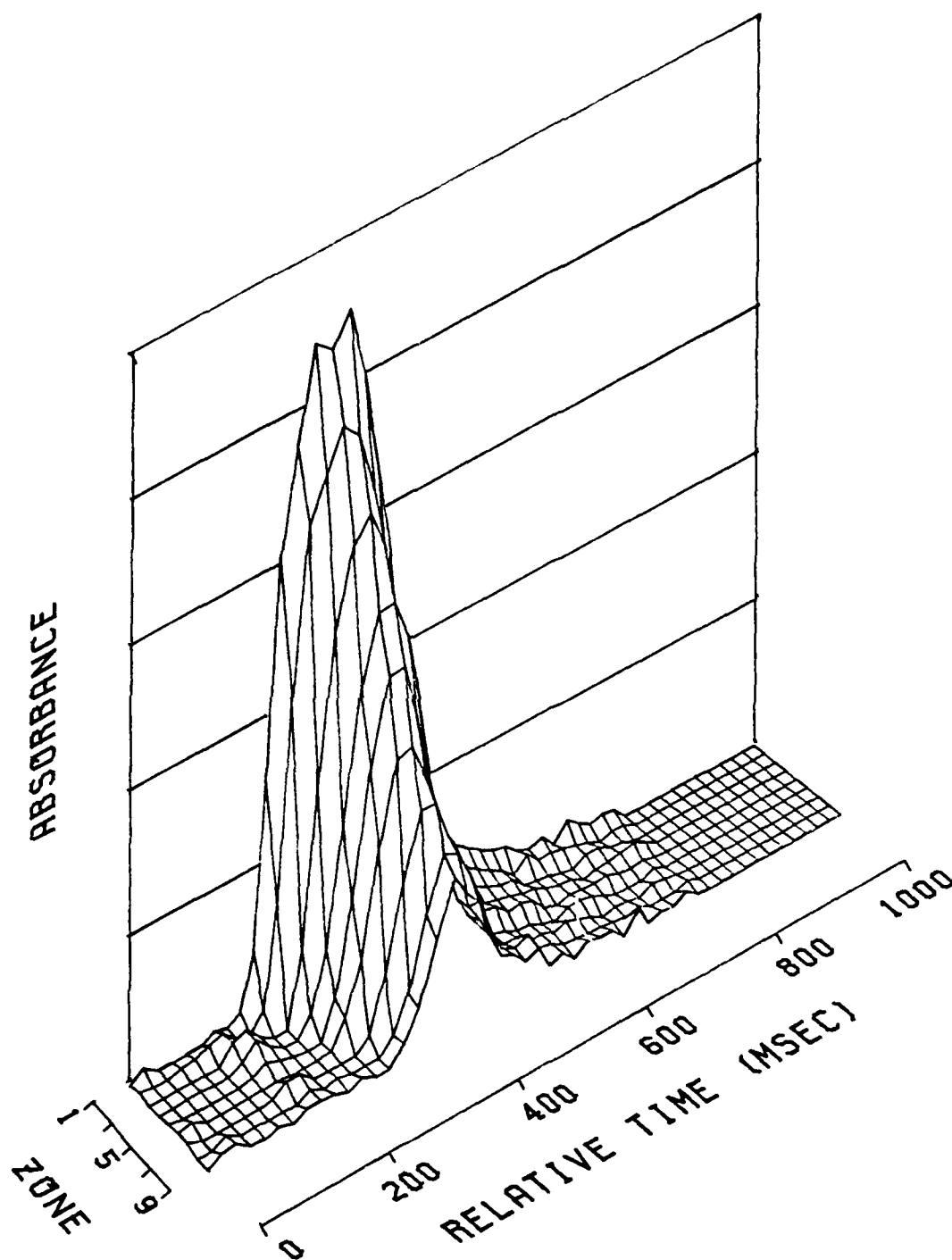Figure 29.   Filament Atomizer Results

Figure 30. Absorbance Profile for Fe

Figure 31. Absorbance Profile for Fe + 100xK$_2$SO$_4$

# IRØN

## PEAK HEIGHT

✳ = ANALYTE +/- ONE STD. DEV.
⊡ = 10X SØDIUM NITRATE
✕ = 100X SØDIUM NITRATE
☆ = 10X POTASSIUM NITRATE
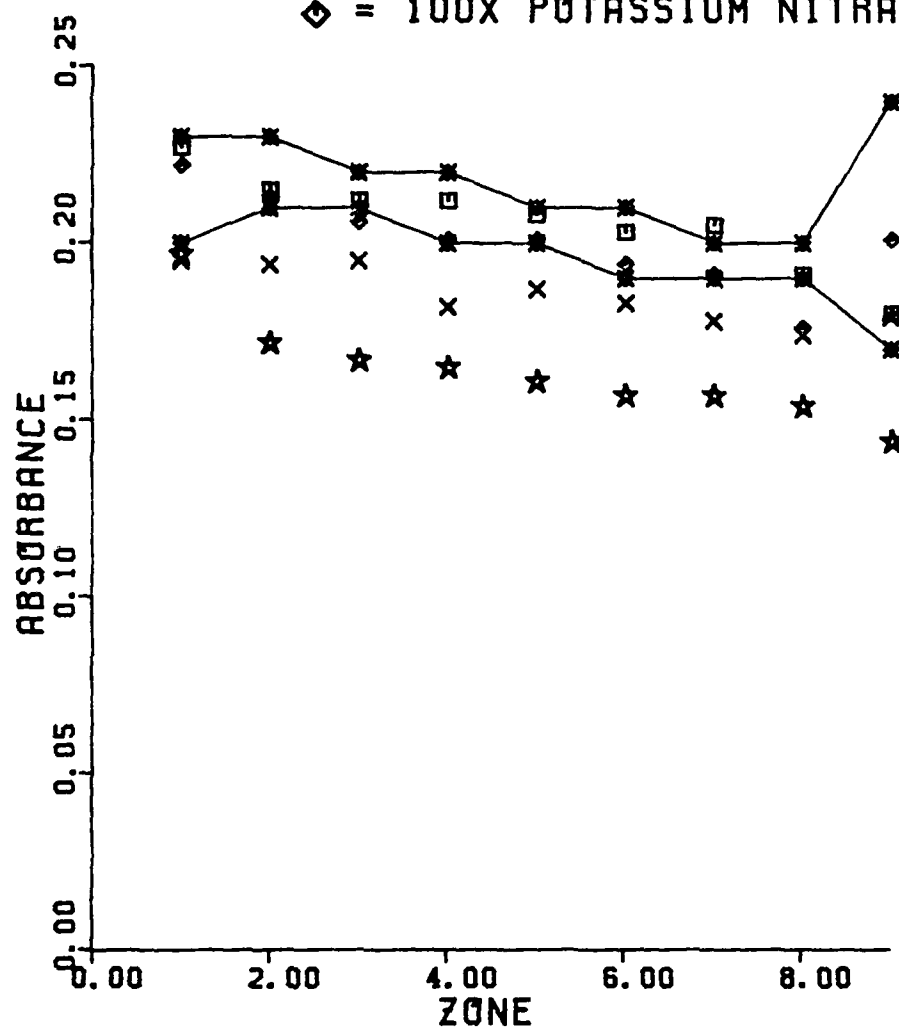◇ = 100X POTASSIUM NITRATE
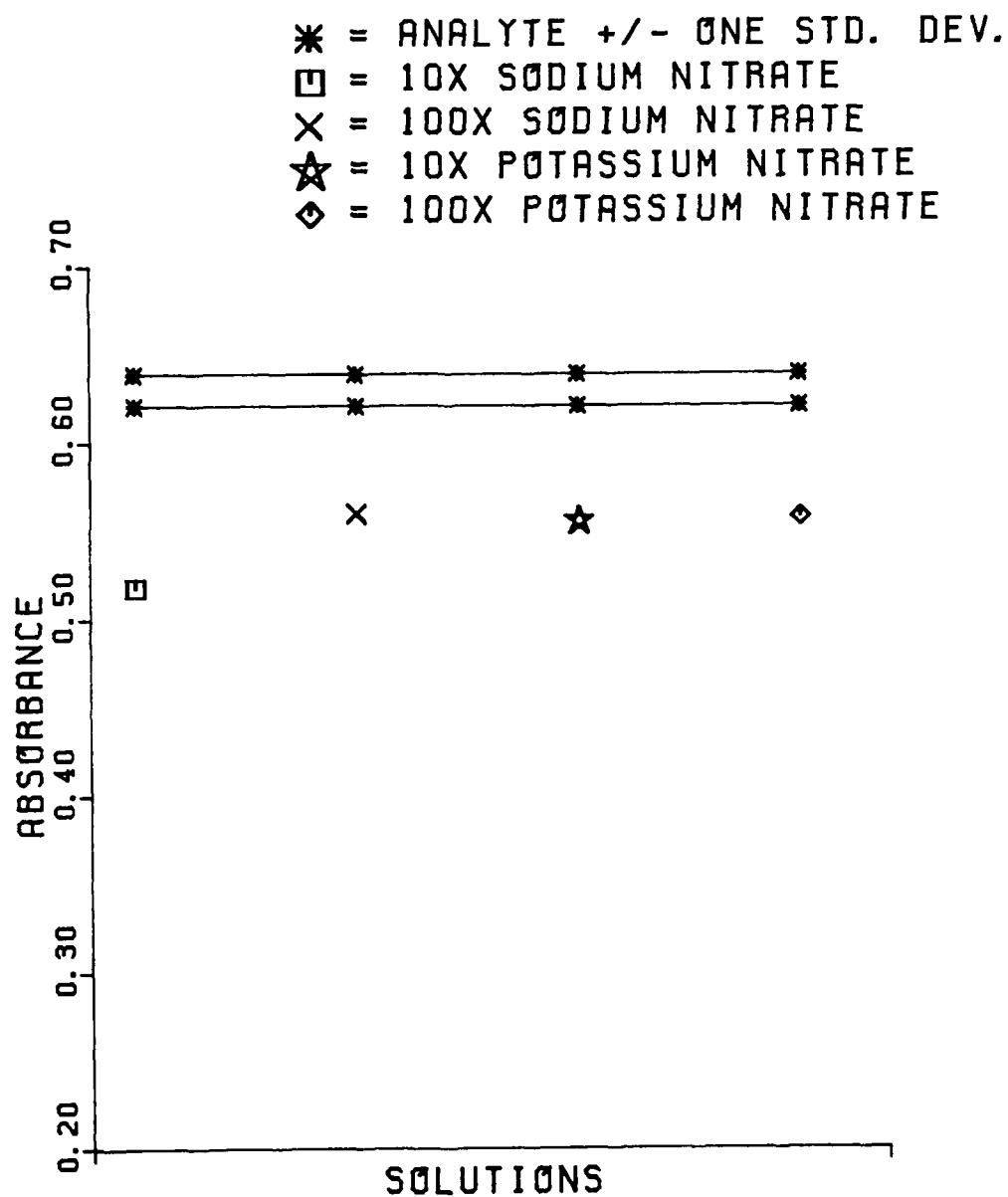


Figure 32.  Furnace Atomizer Results

# IRØN

## PEAK HEIGHT

✳ = ANALYTE +/- ONE STD. DEV.
⊡ = 10X SØDIUM SULFATE
✕ = 100X SØDIUM SULFATE
☆ = 10X POTASSIUM SULFATE
◇ = 100X POTASSIUM SULFATE

Figure 33.   Furnace Atomizer Results

of the depressive effects of the interferent salts.

## SPATIALLY RESOLVED FURNACE ATOMIZER:

Depressions were again apparent in the spatially resolved furnace studies. As is shown in figures 34 and 35, these depressions were again in somewhat of a random order. The three-dimensional absorbance-zone-time graphs (figure 36) illustrate that the Fe atoms, like Ni, are fairly uniformly distributed across the vertical diameter of the furnace.

# IRØN

## PEAK HEIGHT

✳ = ANALYTE +/- ONE STD. DEV.
▣ = 10X SØDIUM NITRATE
✕ = 100X SØDIUM NITRATE
✰ = 10X PØTASSIUM NITRATE
◈ = 100X PØTASSIUM NITRATE



Figure 34.  Spatially Resolved Furnace Results

# IRON

## PEAK HEIGHT

✳ = ANALYTE +/- ONE STD. DEV.
⊞ = 10X SODIUM SULFATE
✕ = 100X SODIUM SULFATE
✩ = 10X POTASSIUM SULFATE
◇ = 100X POTASSIUM SULFATE
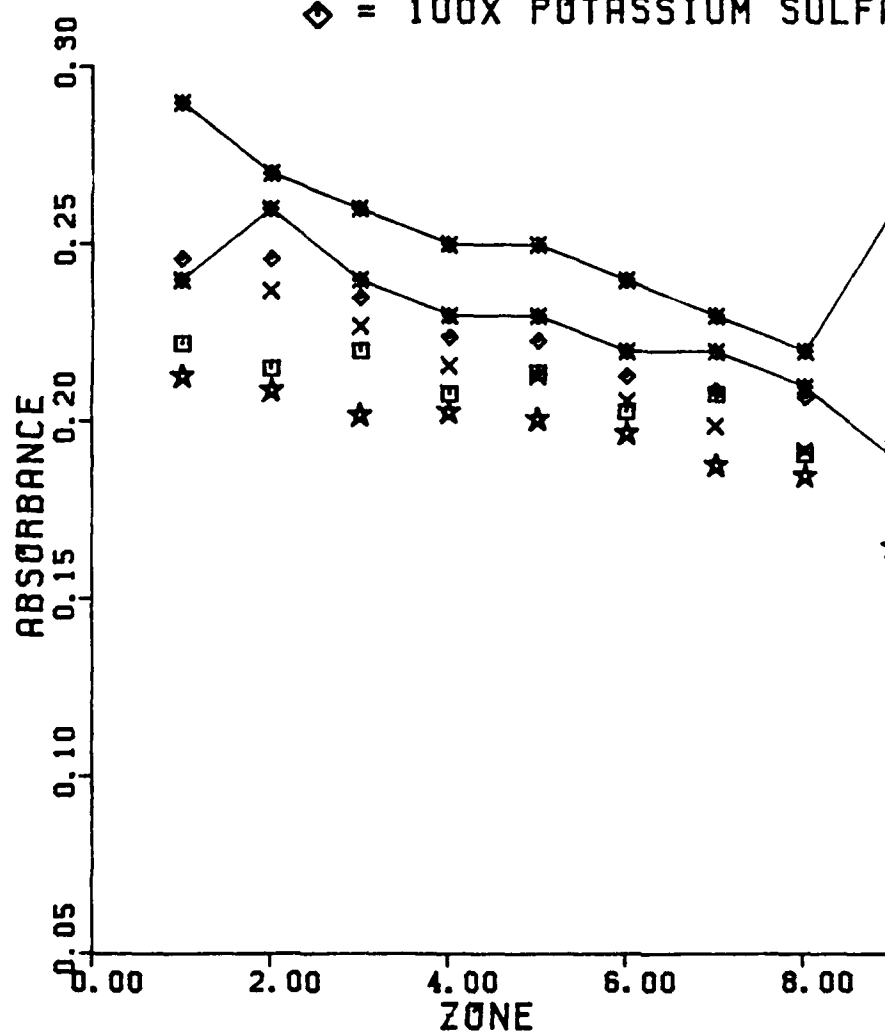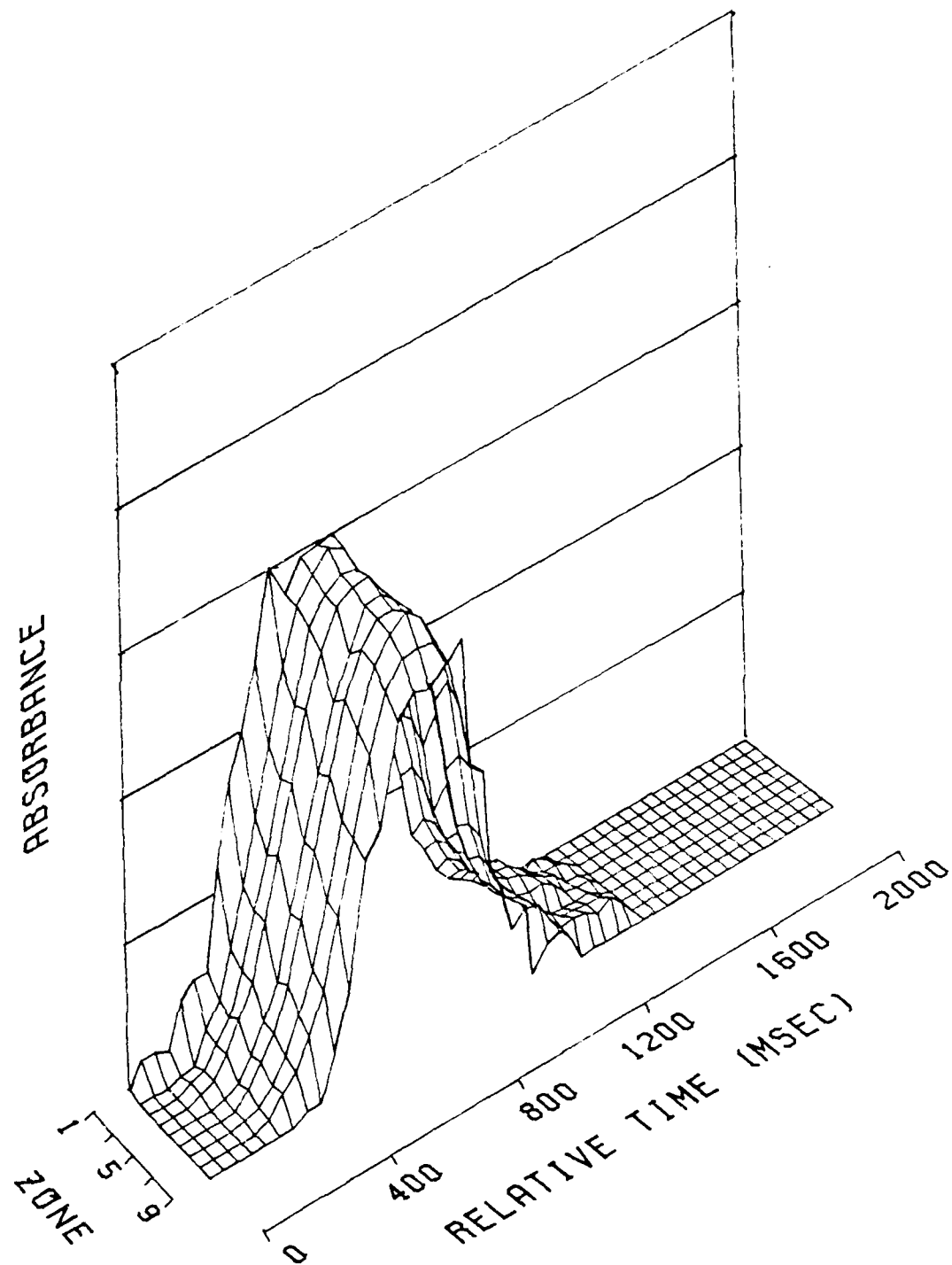


Figure 35. Spatially Resolved Furnace Results

Figure 36. Absorbance Profile for Fe + ......

END
DATE
FILMED
81-2
DTIC

## 4.6  Copper

As noted previously, copper and iron are very similar in their kinetic and thermodynamic properties for the formation of the metal oxide.

FILAMENT ATOMIZER:  Figures 37 and 38 show that the addition of nitrate and sulfate salts to the Cu solution cause significant analyte signal depressions.  As predicted from the relative magnitude of their decomposition constants, $K_2SO_4$ depressed the analyte signal to a greater extent than did $Na_2SO_4$.  For the nitrates, $KNO_3$ showed a greater interferent effect than $NaNO_3$.  The absorbance-height-time profiles for the filament atomizer illustrate that the depressive effects of the concomitant salts are greatest at the elevated zones (figures 39 and 40).  This suggests that reaction.kinetics have yet to produce equilibrium.

FURNACE ATOMIZER:  In the furnace atomizer studies, figures 41 and 42, depressions were again observed, although the day-to-day reproducability was poor.  As with iron, the depressions appear to be independent of the type of salt or concentration.

# COPPER

## PEAK HEIGHT

✳ = ANALYTE +/- ONE STD. DEV.
⊡ = 10X SODIUM NITRATE
✕ = 100X SODIUM NITRATE
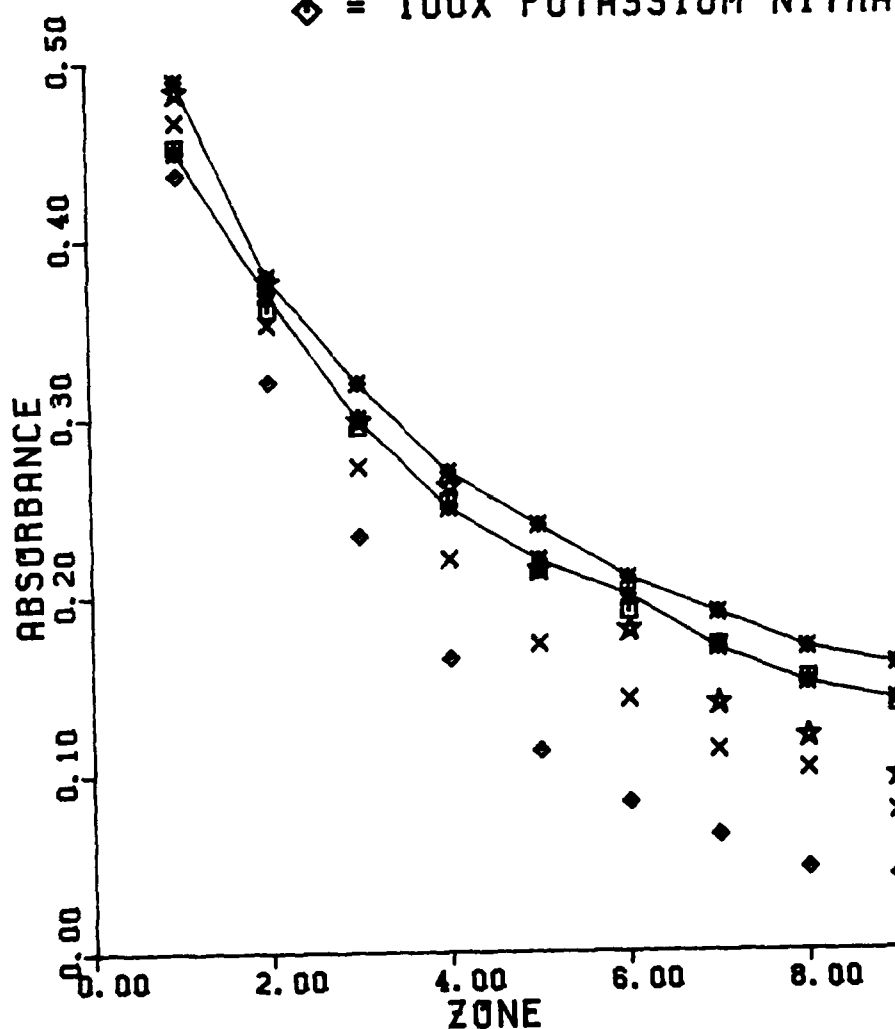✰ = 10X POTASSIUM NITRATE
◈ = 100X POTASSIUM NITRATE



Figure 37.  Filament Atomizer Results

# COPPER

## PEAK HEIGHT

✳ = ANALYTE +/- ONE STD. DEV.
▣ = 10X SODIUM SULFATE
✕ = 100X SODIUM SULFATE
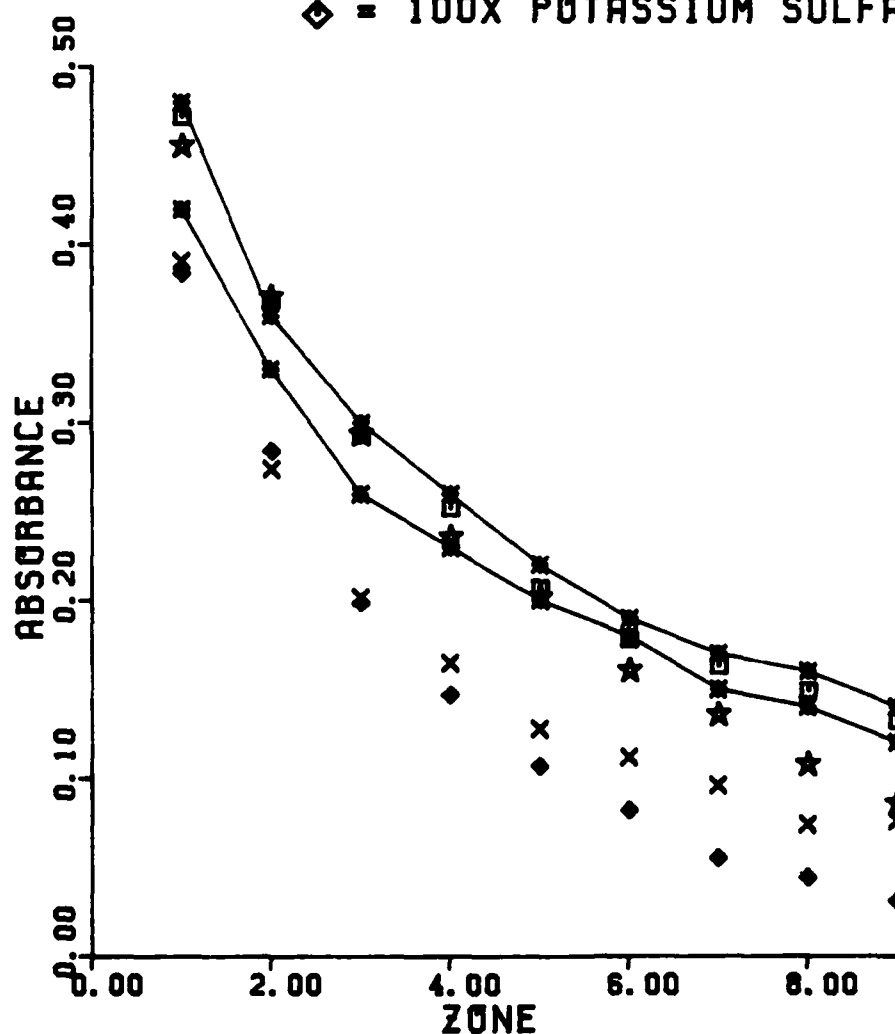★ = 10X POTASSIUM SULFATE
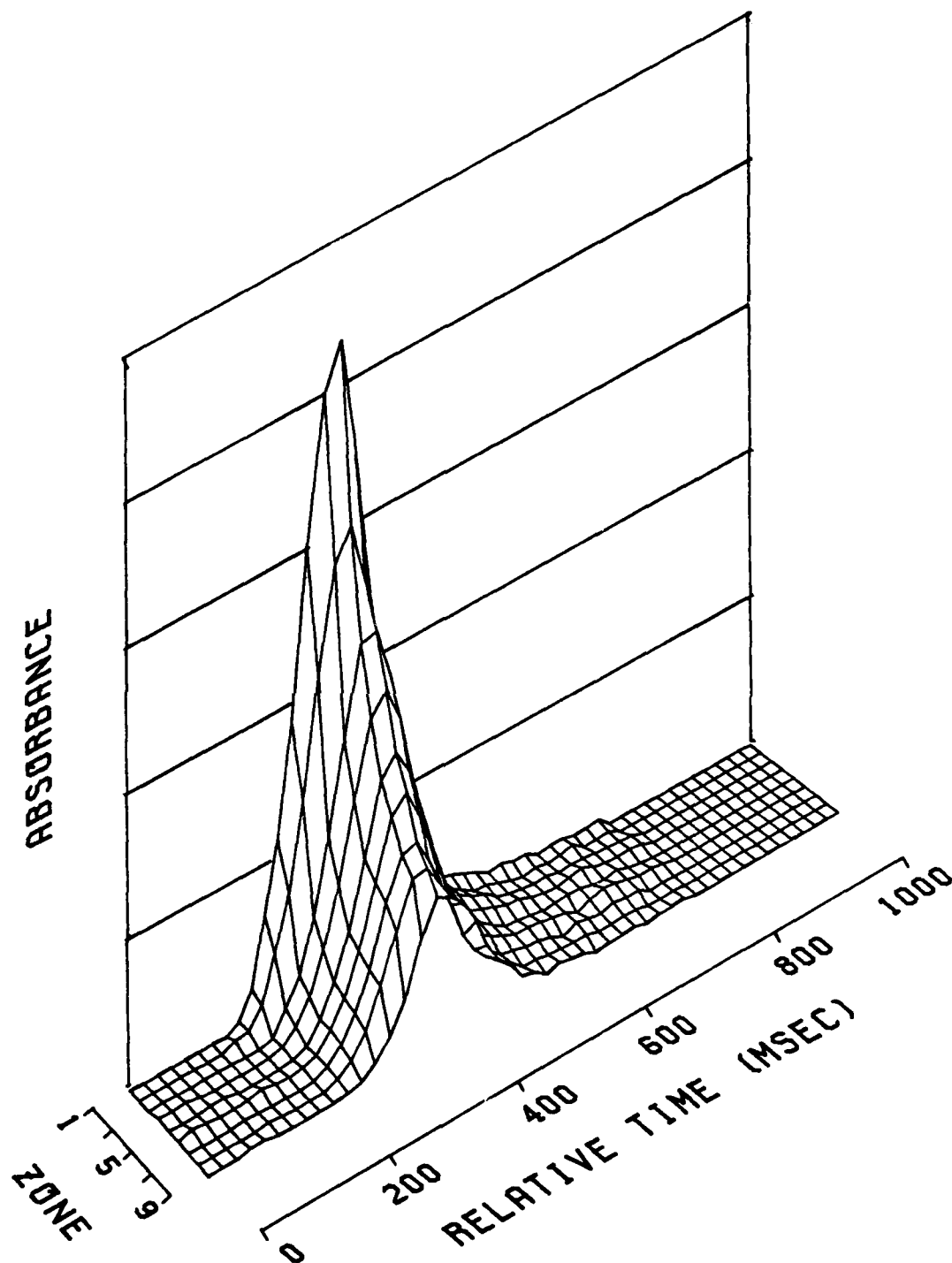◈ = 100X POTASSIUM SULFATE



Figure 38.   Filament Atomizer Results

Figure 39. Absorbance Profile for Cu
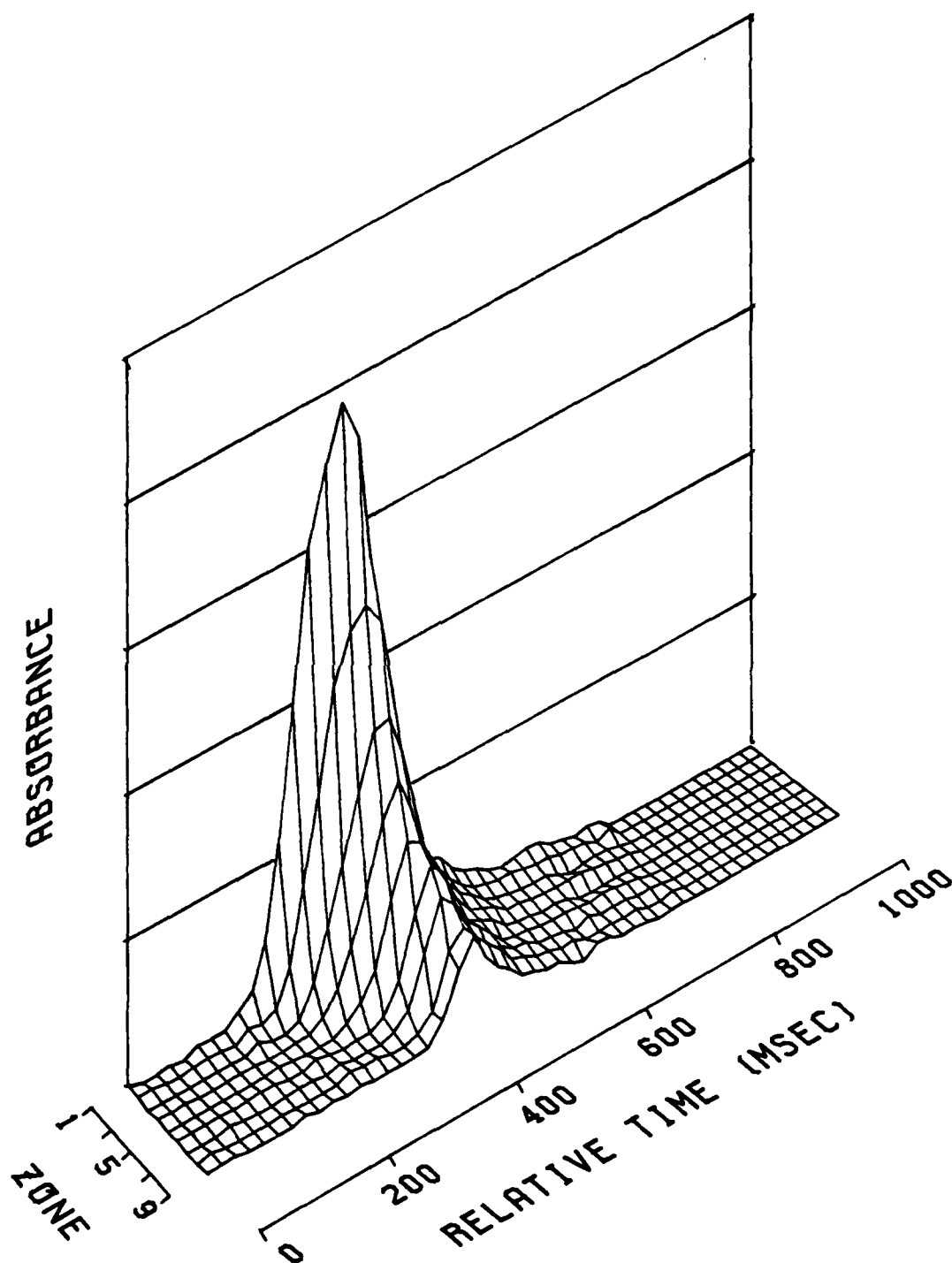
Figure 40.   Absorbance Profile For Cu + 100xNa$_2$SO$_4$

# COPPER

## PEAK HEIGHT

✳ = ANALYTE +/- ONE STD. DEV.
☐ = 10X SODIUM NITRATE
✕ = 100X SODIUM NITRATE
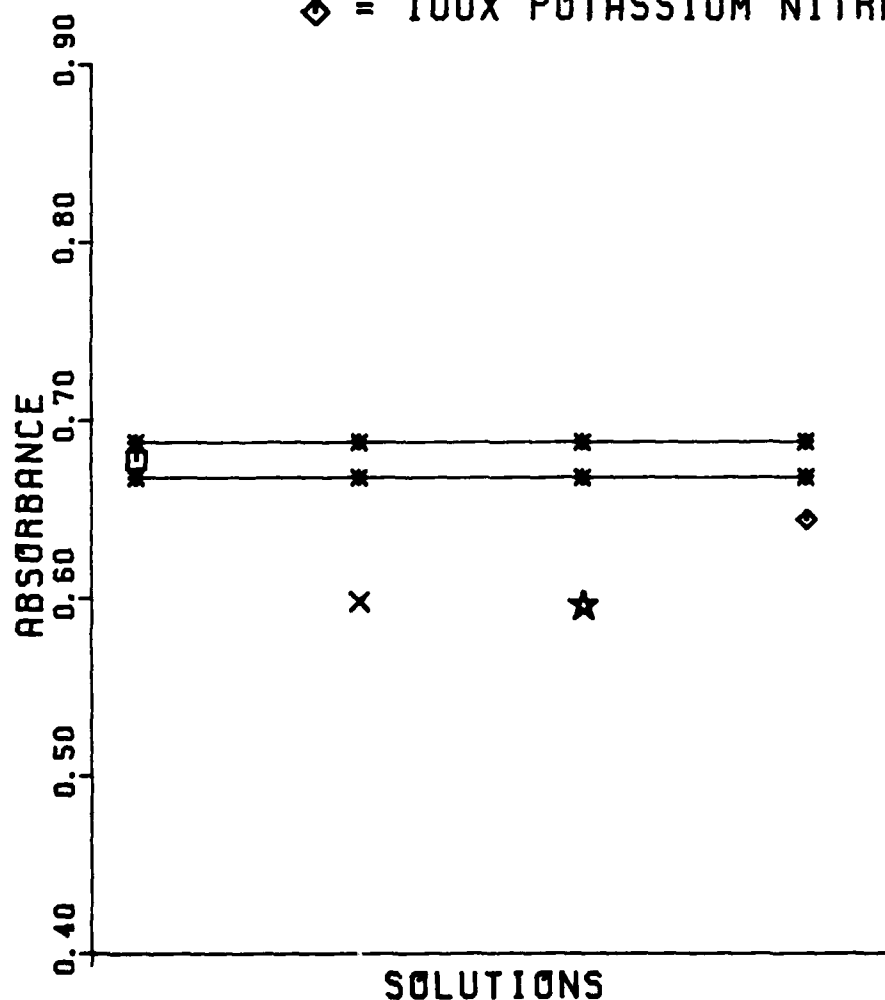★ = 10X POTASSIUM NITRATE
◇ = 100X POTASSIUM NITRATE



Figure 41.   Furnace Atomizer Results

# COPPER

## PEAK HEIGHT

✳ = ANALYTE +/- ONE STD. DEV.
⊡ = 10X SODIUM SULFATE
✕ = 100X SODIUM SULFATE
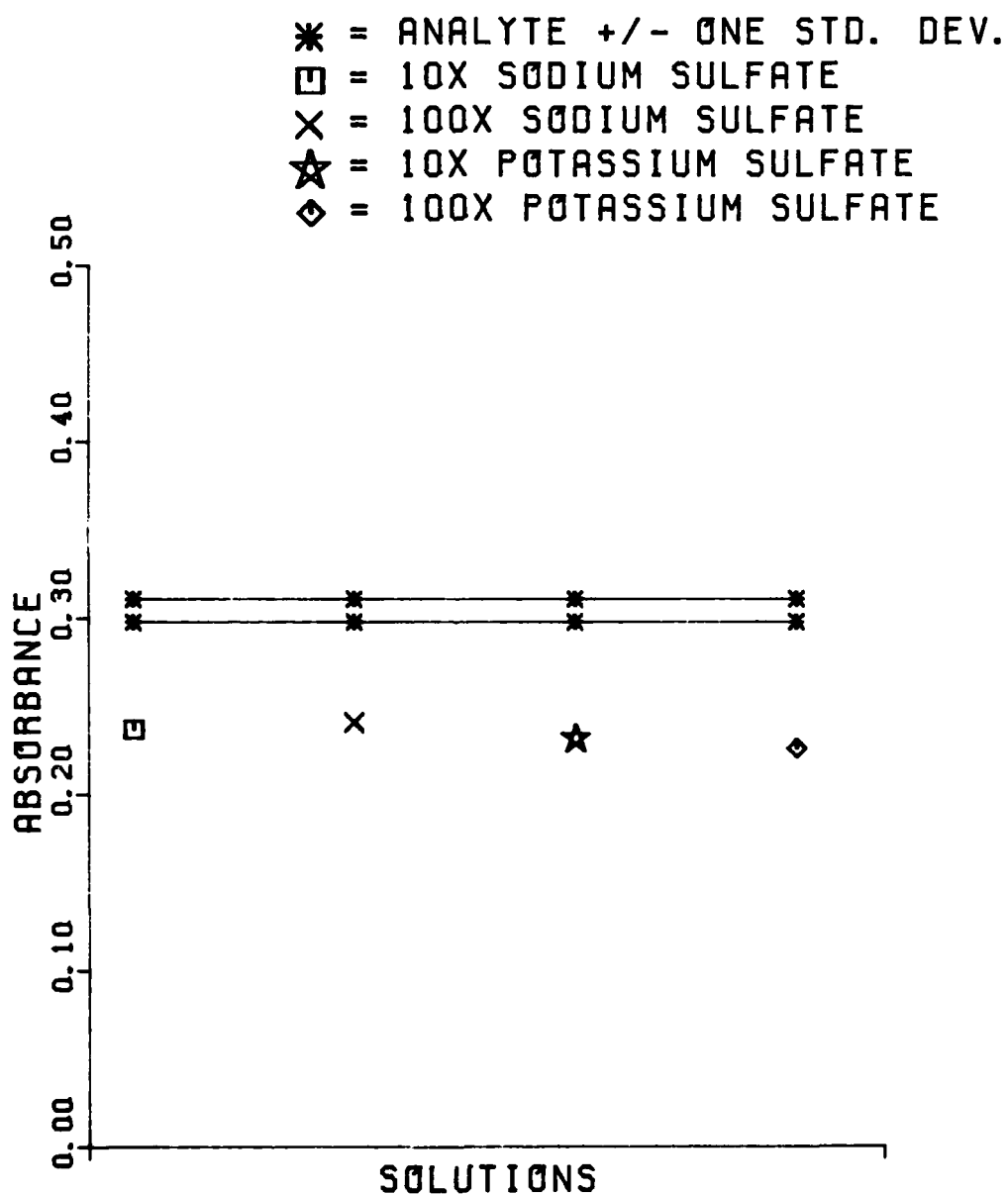✩ = 10X POTASSIUM SULFATE
◇ = 100X POTASSIUM SULFATE



Figure 42.   Furnace Atomizer Results

SPATIALLY RESOLVED FURNACE ATOMIZER:

Depressions were also noted in the spatially
resolved furnace data.  Figures 43 and 44 indicate
that the free copper atoms, while slightly higher
near the furnace base, are fairly evenly distributed
throughout the furnace volume.  The three-dimensional
graphs, figures 45 and 46, illustrate the depressive
effects of the interferent.

# COPPER

## PEAK HEIGHT

✳ = ANALYTE +/- ONE STD. DEV.
⊡ = 10X SODIUM NITRATE
✕ = 100X SODIUM NITRATE
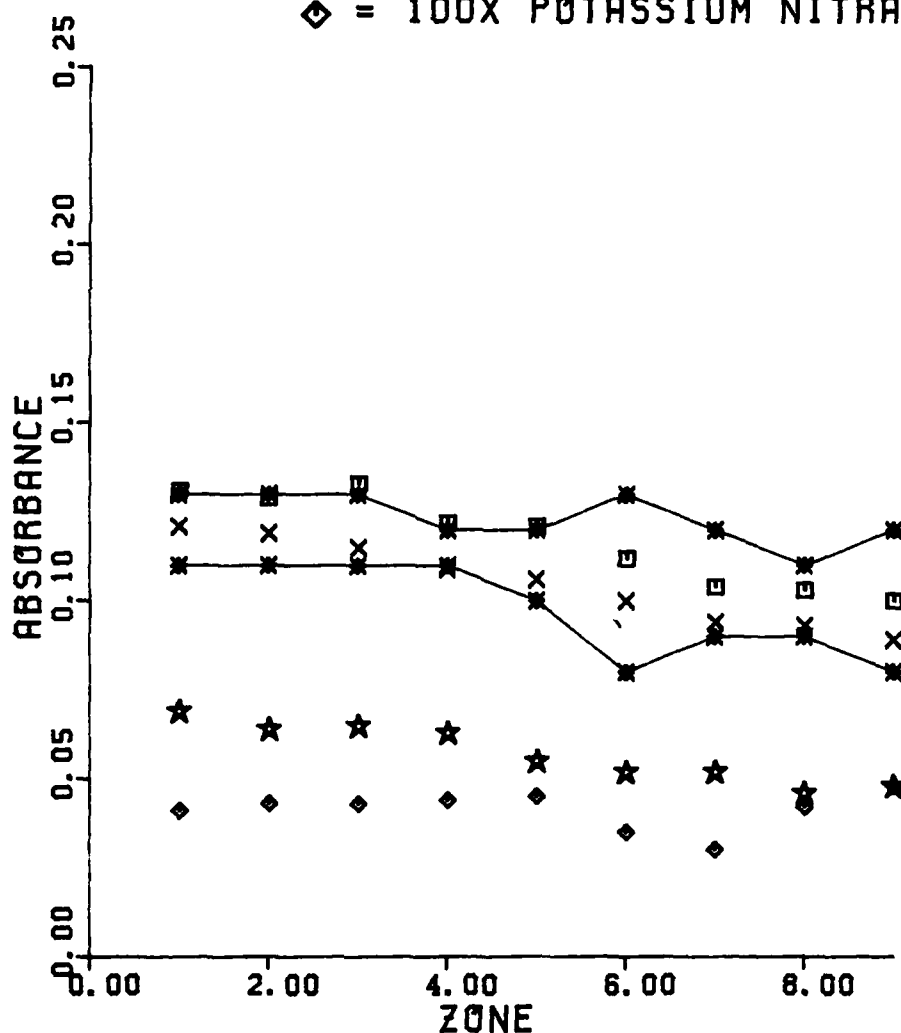☆ = 10X POTASSIUM NITRATE
◇ = 100X POTASSIUM NITRATE



Figure 43.  Spatially Resolved Furnace Results

# COPPER

## PEAK HEIGHT

✳ = ANALYTE +/- ONE STD. DEV.
🔲 = 10X SODIUM SULFATE
✖ = 100X SODIUM SULFATE
✯ = 10X POTASSIUM SULFATE
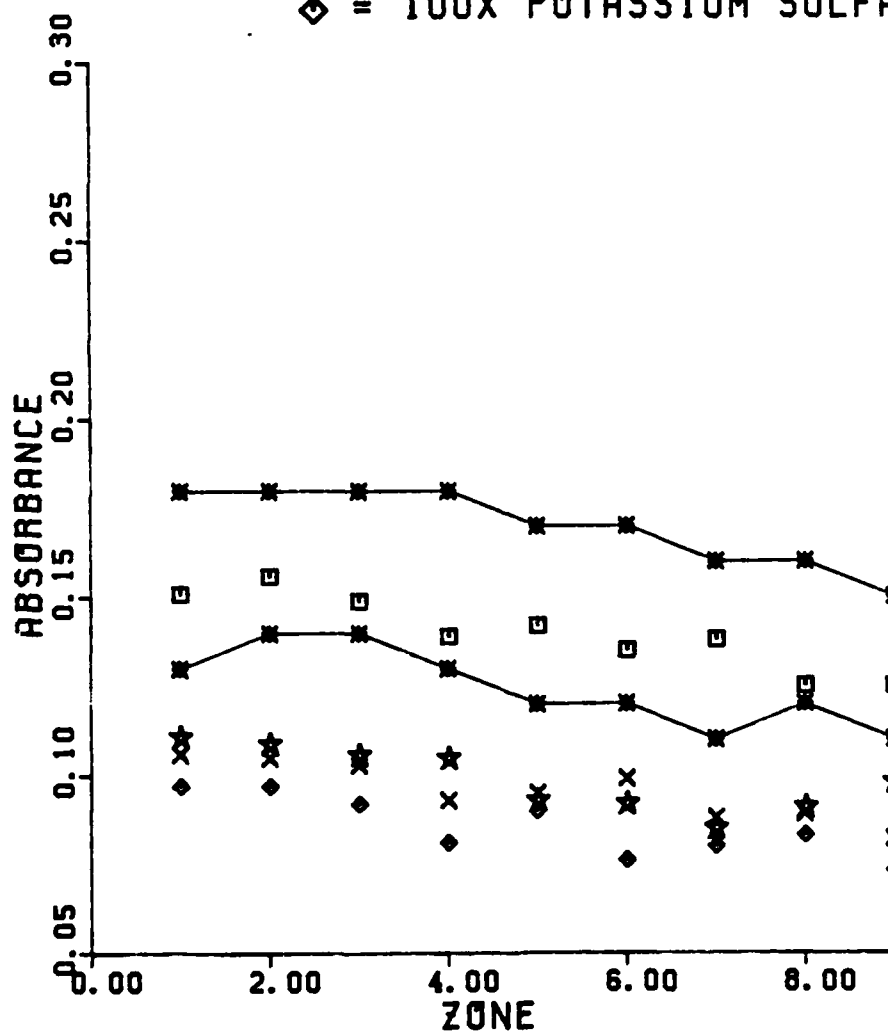◇ = 100X POTASSIUM SULFATE



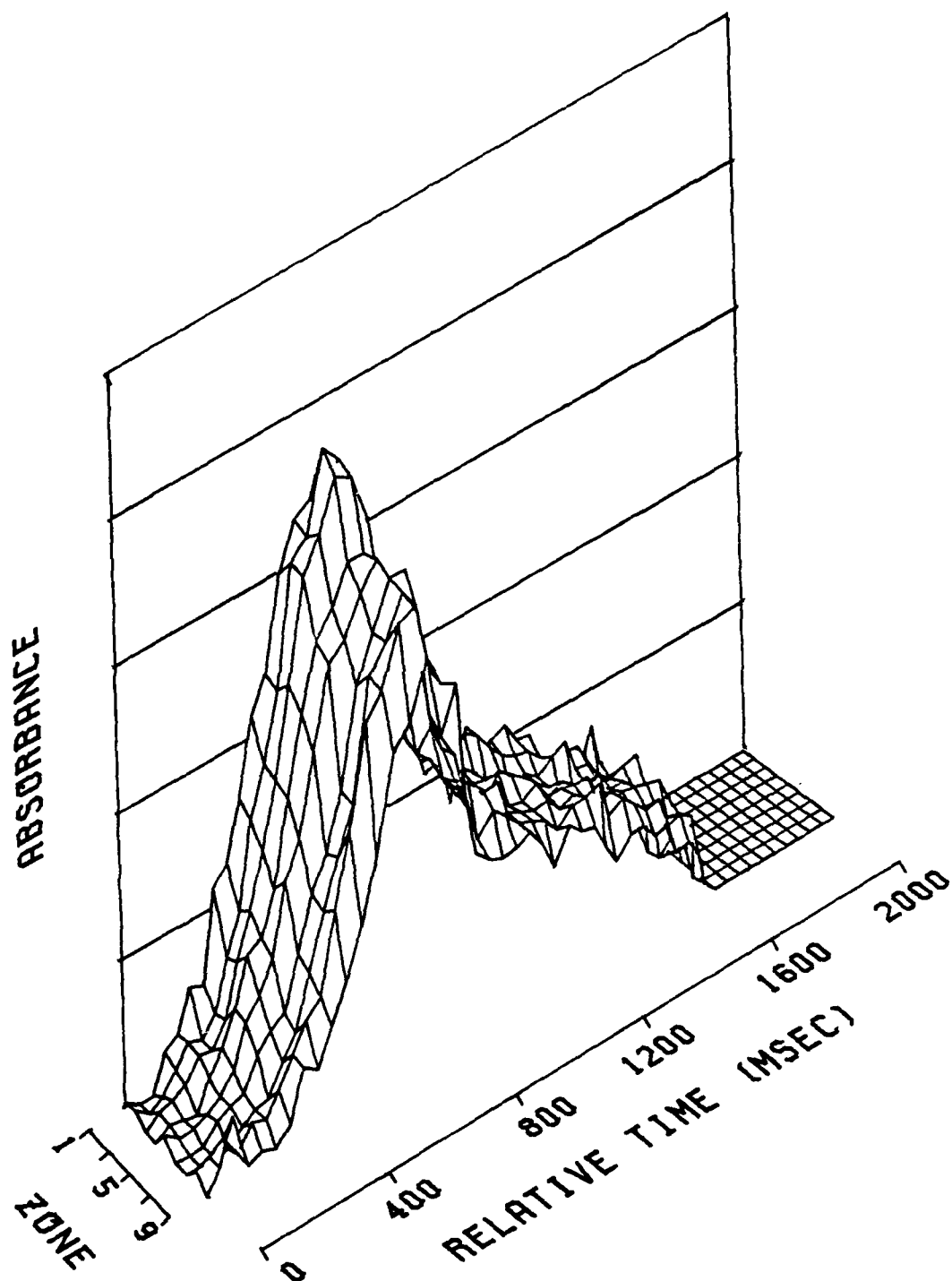Figure 44. Spatially Resolved Furnace Results
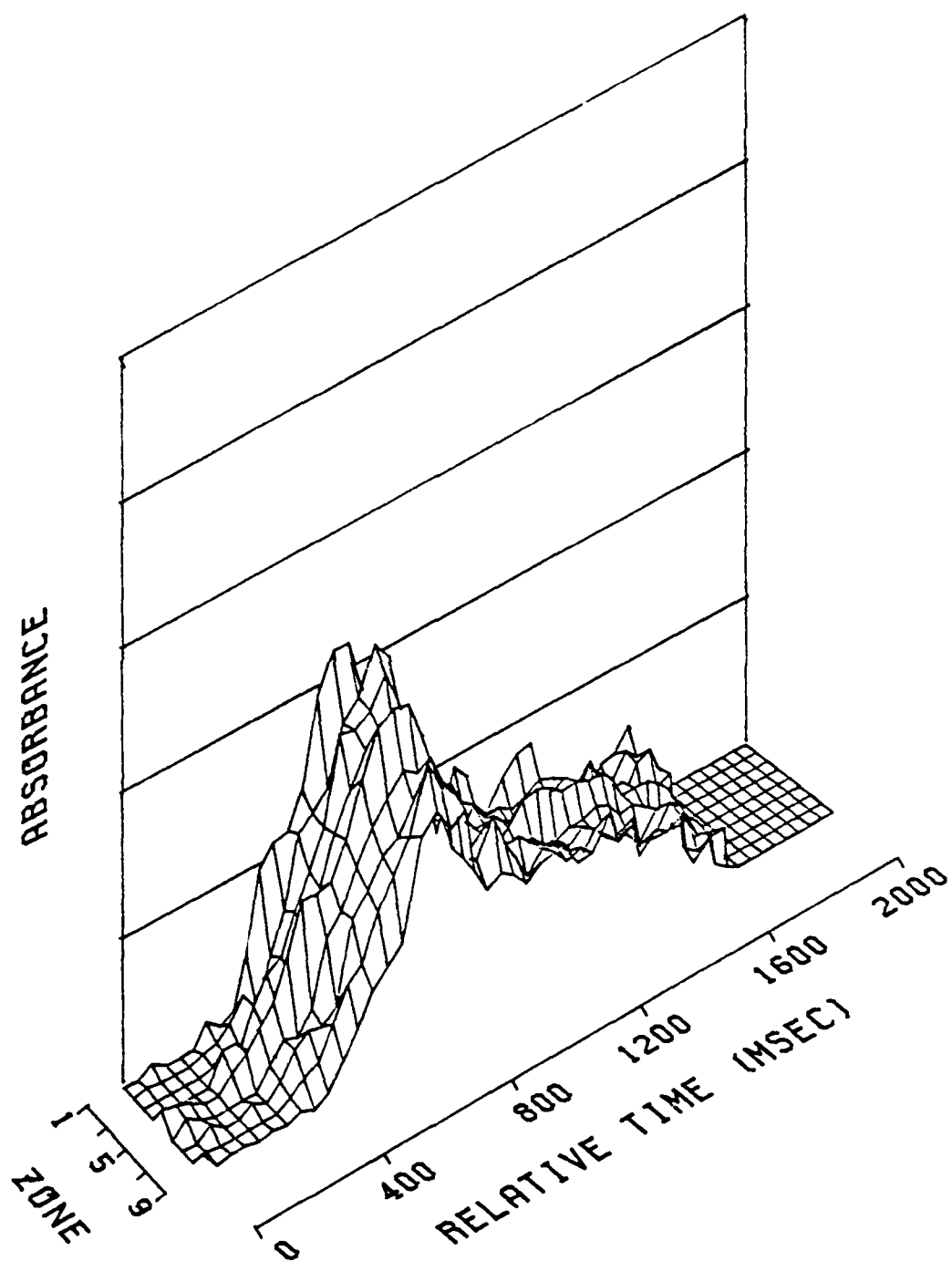
Figure 45.  Absorbance Profile for Cu

Figure 46.   Absorbance Profile for Cu + 100xH$_2$SO$_4$

## 4.7 <u>Tin</u>

Tin was the most interesting element examined. The equilibrium distributions shown in figure 47 indicate that if the role of graphite is ignored, the Sn appearance temperature of 1620K[8] is such that almost all the free metal is removed by the presence of even a small amount of oxygen. However, the inclusion of graphite in the thermodynamic calculations again results in nearly all of the metal being present as the free metal. As shown in Table I, tin has the highest kinetic rate constant for the metal oxygen reaction of the elements studied. Fontijn <u>et al</u>,[13] in studies at room temperature, suggest that the metal oxygen reaction approaches a collision rate limited condition. Its metal oxide bond strength of 125[10] kcal/mole is at least 20% higher than the other elements in this study.

<u>FILAMENT ATOMIZER</u>: The graphite filament atomizer could not be employed for the analysis of Sn. With the present system configuration, the Sn absorbance signal was very erratic in the spatial zone closest to the filament surface and did not persist past the second viewing zone.

# TIN



PARTIAL PRESSURE OF OXYGEN
⊙ = 1.0E -2
△ = 1.0E -3
+ = 1.0E -4
✕ = 1.0E -5
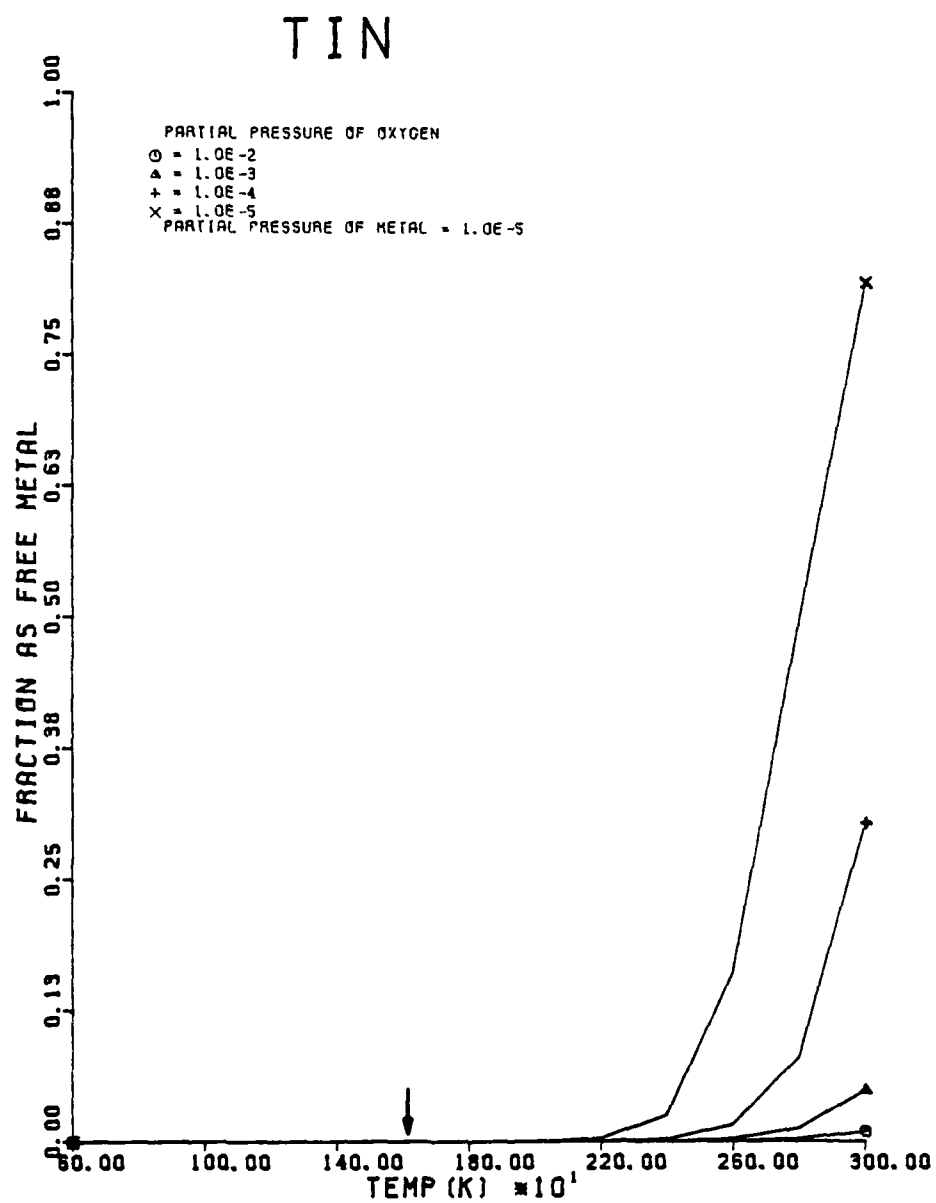PARTIAL PRESSURE OF METAL = 1.0E -5

Figure 47.   Results of Thermodynamic

Calculations for Sn

Perhaps with better exclusion of oxygen, the
filament atomizer could be used for the analysis
of Sn.

FURNACE ATOMIZER:   The entrained oxygen,
which was believed responsible for the failure of
the filament atomizer to generate a reproducible
absorbance signal, was minimized by one of two
methods.  Approximately 10% $H_2$ (flow rate of
.6 1/min) was introduced into the Ar sheath gas
during the ash and atomization cycles.  The
hydrogen provides a strongly reducing environment
for the analyte as well as removing oxygen.
Indeed, a hydrogen-diffused flame is observed
during the atomization cycle.  The commercial
instrument was modified by enclosing the entire
atomizer assembly and the automatic sample
dispenser carrousel in an air-tight box which was
continuously flooded with Ar (figure 48) introduced
through  the gas box of the atomizer.  As the
box filled with the more dense Ar, the entrained
air was purged from the atomizer.  The pressure
within the enclosure box was maintained at slightly
greater than one atmosphere by allowing Ar to
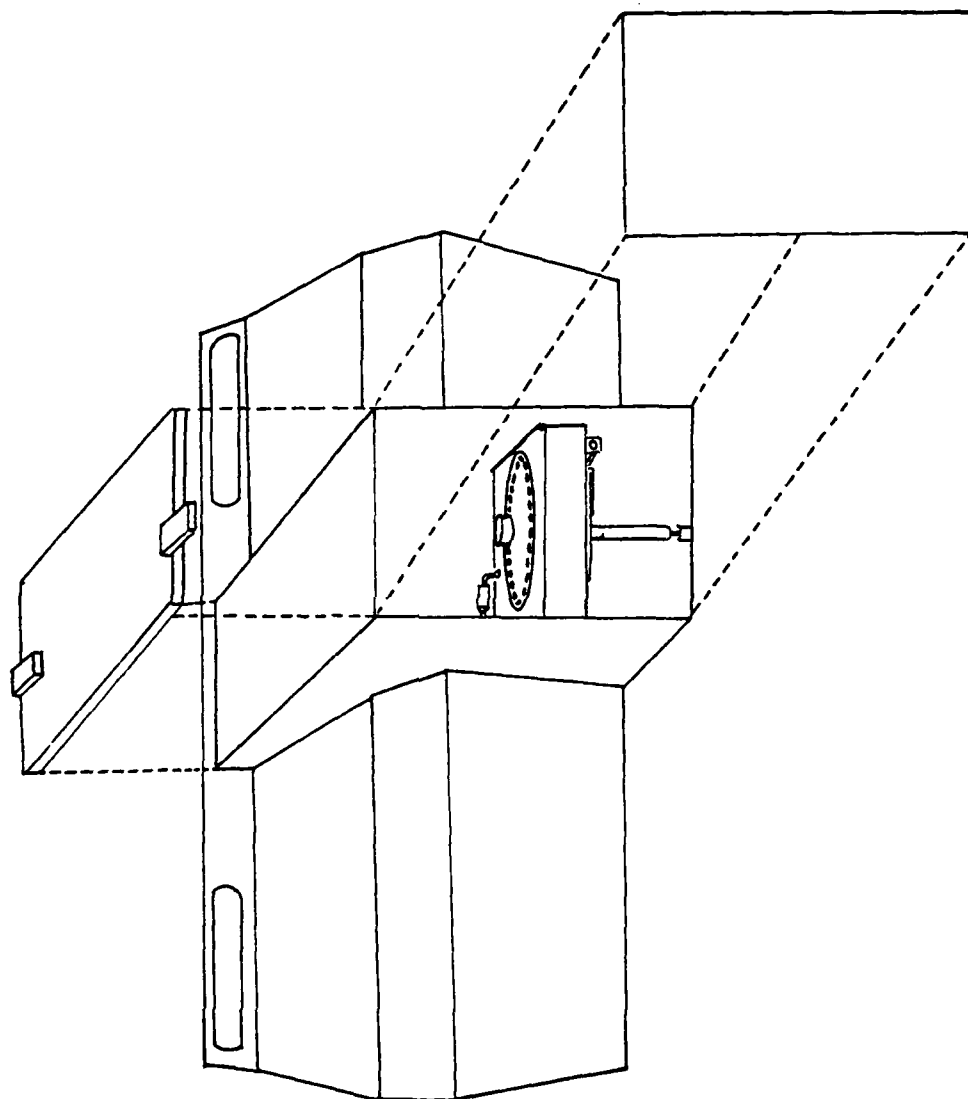escape from the box.

Both the systems proved effective in

Figure 48. Furnace Atomizer Enclosure Box

stabilizing and enhancing the tin absorbance
signal. As is shown in figure 49, a significant
shift in the analyte absorbance appearance time,
which can be related to an atomizer temperature
change of approximately 380°C, was noted for
both the $H_2$ rich environment and the atomizer
enclosure box in comparison to just using Ar
sheath gas in the unmodified atomizer enclosure.
This change in the appearance time suggests a
change in the release mechanism of Sn from the
atomizer surface due to the presence or absence
of oxygen. The exact nature of this change is
not presently known. These results confirm the
importance in minimizing the entrainment of
air as first suggested by Guiochon et al[11] and
Eklund and Holcombe.[12]

Dramatic signal depressions were observed
for the tin and hundred-fold excess of sulfates
while using $H_2$ added to the sheath gas. As can
be seen in figure 50, the tin absorbance signal
is reduced to a value comparable to the background
noise level. The effects of the addition of
equal amounts of sodium or potassium sulfate to
the tin solution are shown in figure 51. While
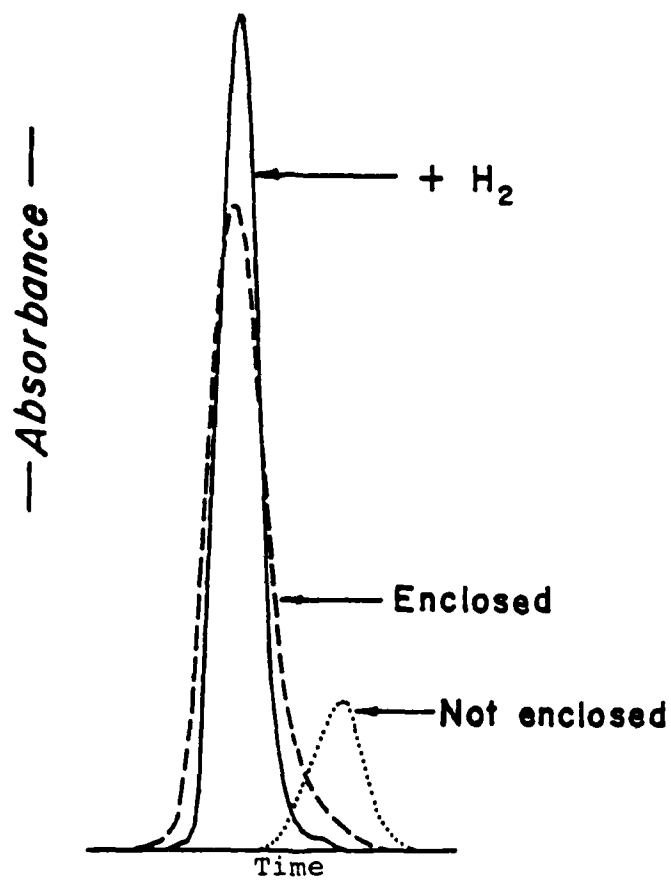a measurable signal was still detected, it was

Figure 49.   Effects of $H_2$ and Atomizer
Enclosure Box on Sn Absorbance Signal

# TIN

## PEAK HEIGHT

✳ = ANALYTE +/- ONE STD. DEV.
☐ = 10X SODIUM SULFATE
✗ = 100X SODIUM SULFATE
☆ = 10X POTASSIUM SULFATE
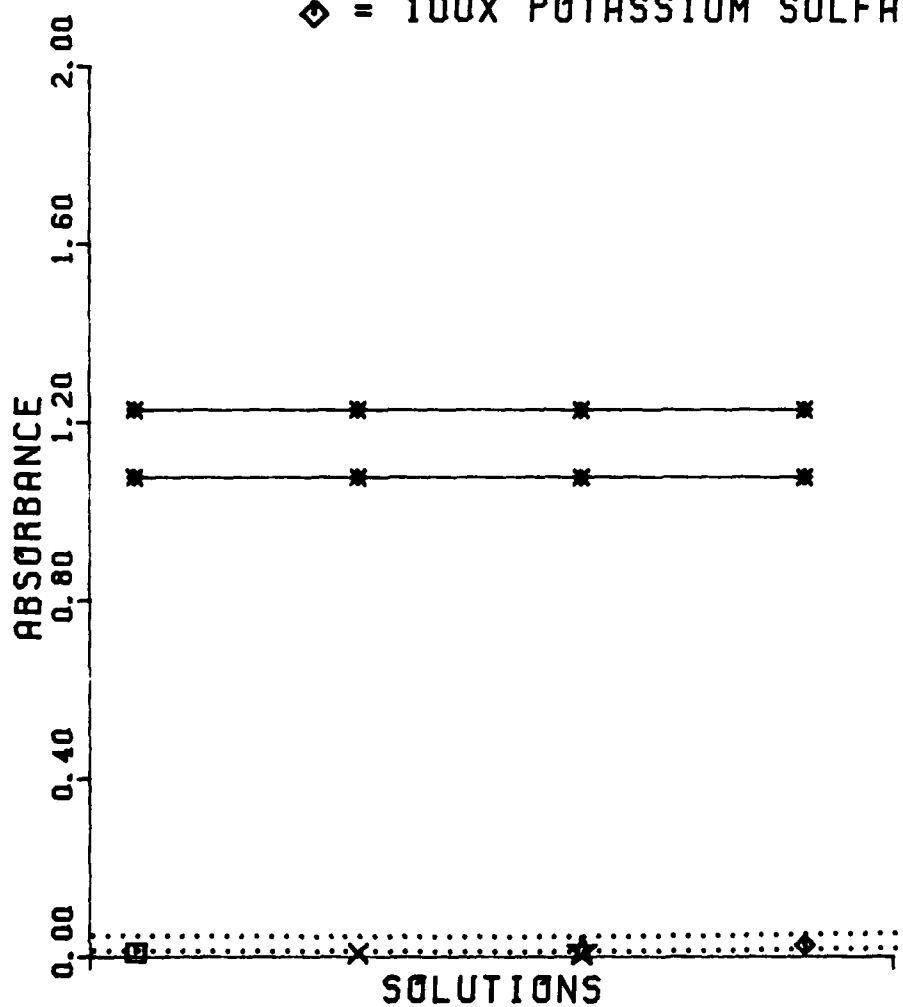◈ = 100X POTASSIUM SULFATE



Figure 50.   Furnace Atomizer Results
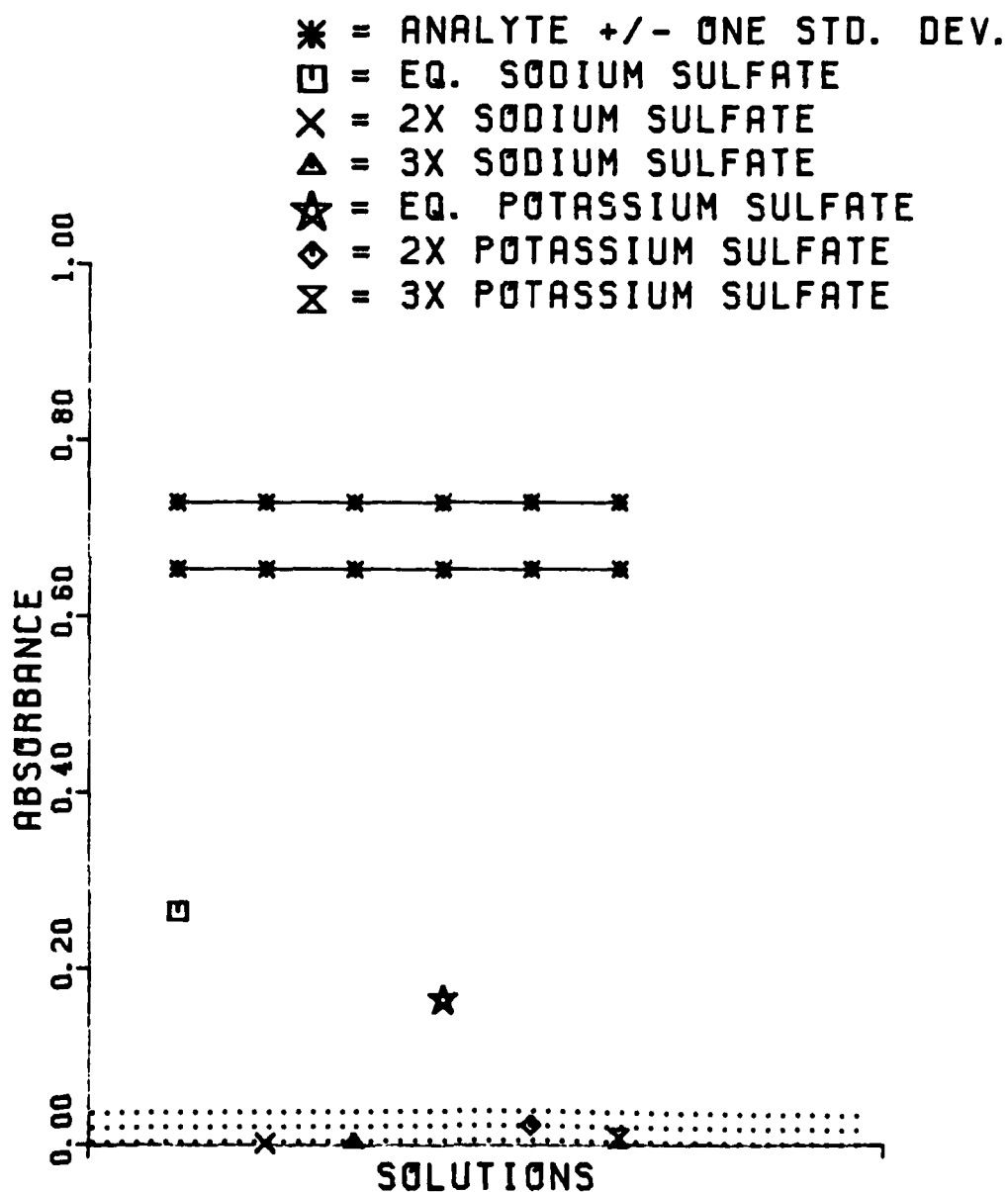
# TIN

## PEAK HEIGHT



Figure 51. Furnace Atomizer Results

significantly depressed. Two- and three-fold excesses of these salts once again completely suppressed the analyte absorbance signal as can be seen in figure 51. Ashing the samples up to 750°C for 20 sec was not sufficient to eliminate the signal depressions. This suggests that the interferent was not decomposed and volatilized during the ashing stage. Ashing at temperatures above 750°C resulted in loss of the analyte. The addition of 1% oxygen to the argon sheath gas while using the atomizer enclosure box also reduced the tin absorbance signal below the level of detectability.

### SPATIALLY RESOLVED FURNACE ATOMIZER:

Spatial studies within the graphite furnace atomizer employing $H_2$ added to the sheath gas also showed depressions. As can be seen in figure 52, the free tin atoms were not evenly distributed within the viewing zones of the atomizer. This suggests that $H_2$ was not totally effective in removing all the entrained oxygen. The absorbance signals for the addition of two- and ten-fold excess $Na_2SO_4$ and two-fold excess $K_2SO_4$ were very small in the first zones and rapidly decayed to the baseline noise level within the first

# TIN

## PEAK HEIGHT

✳ = TIN
▣ = EQ. SODIUM SULFATE
✕ = 2X SODIUM SULFATE
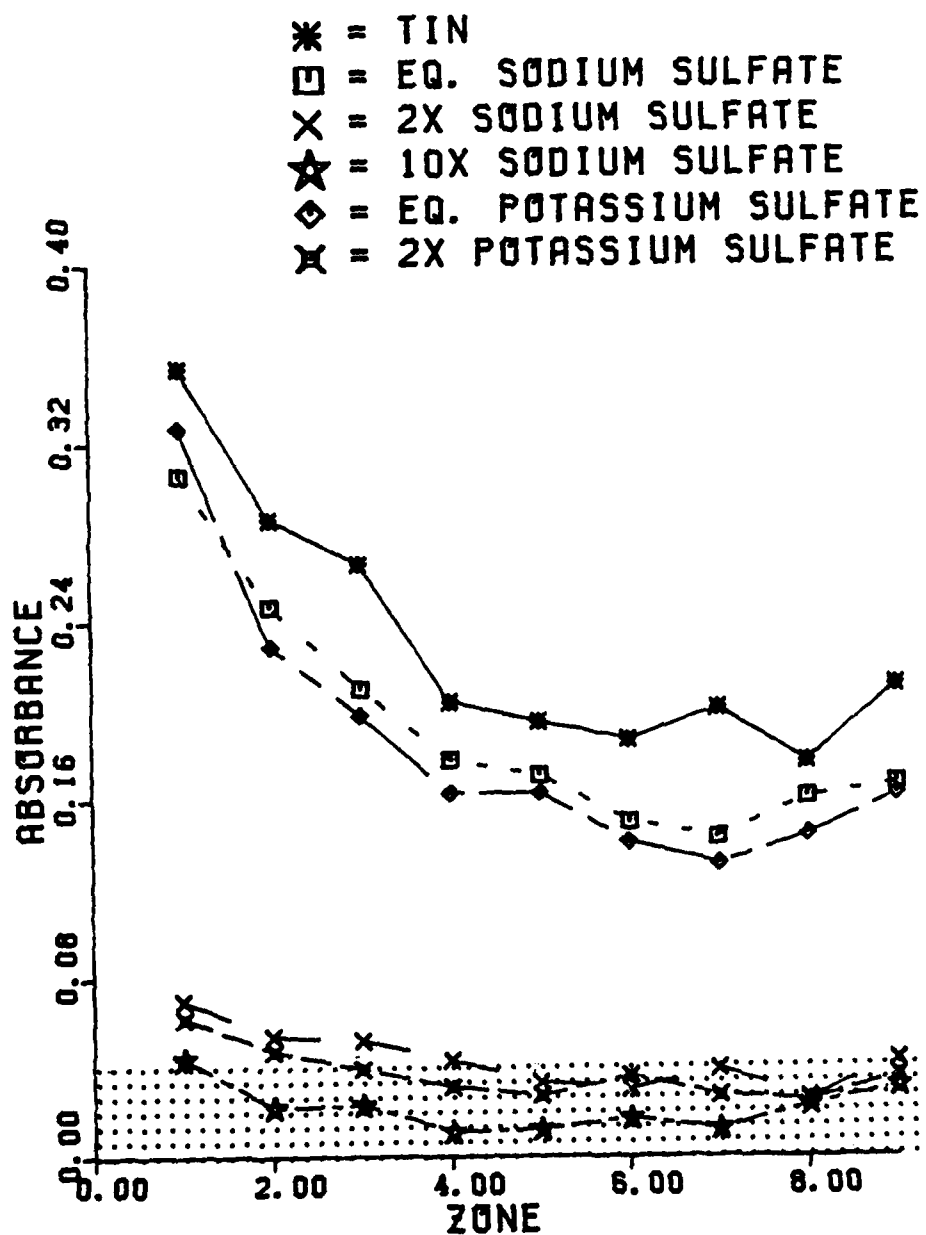✪ = 10X SODIUM SULFATE
◇ = EQ. POTASSIUM SULFATE
✖ = 2X POTASSIUM SULFATE



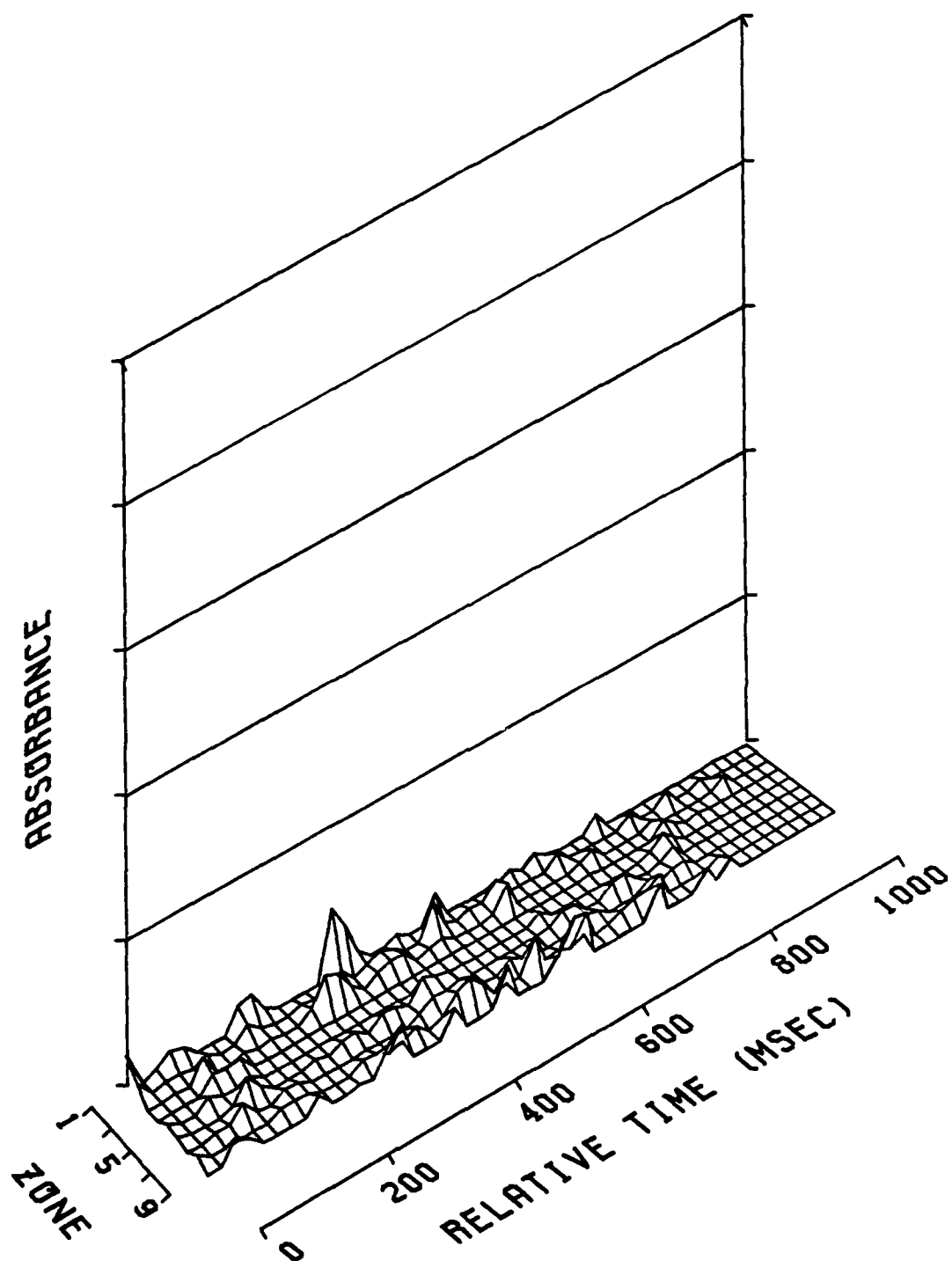Figure 52.   Spatially Resolved Furnace Results

four zones (figures 53 and 54).

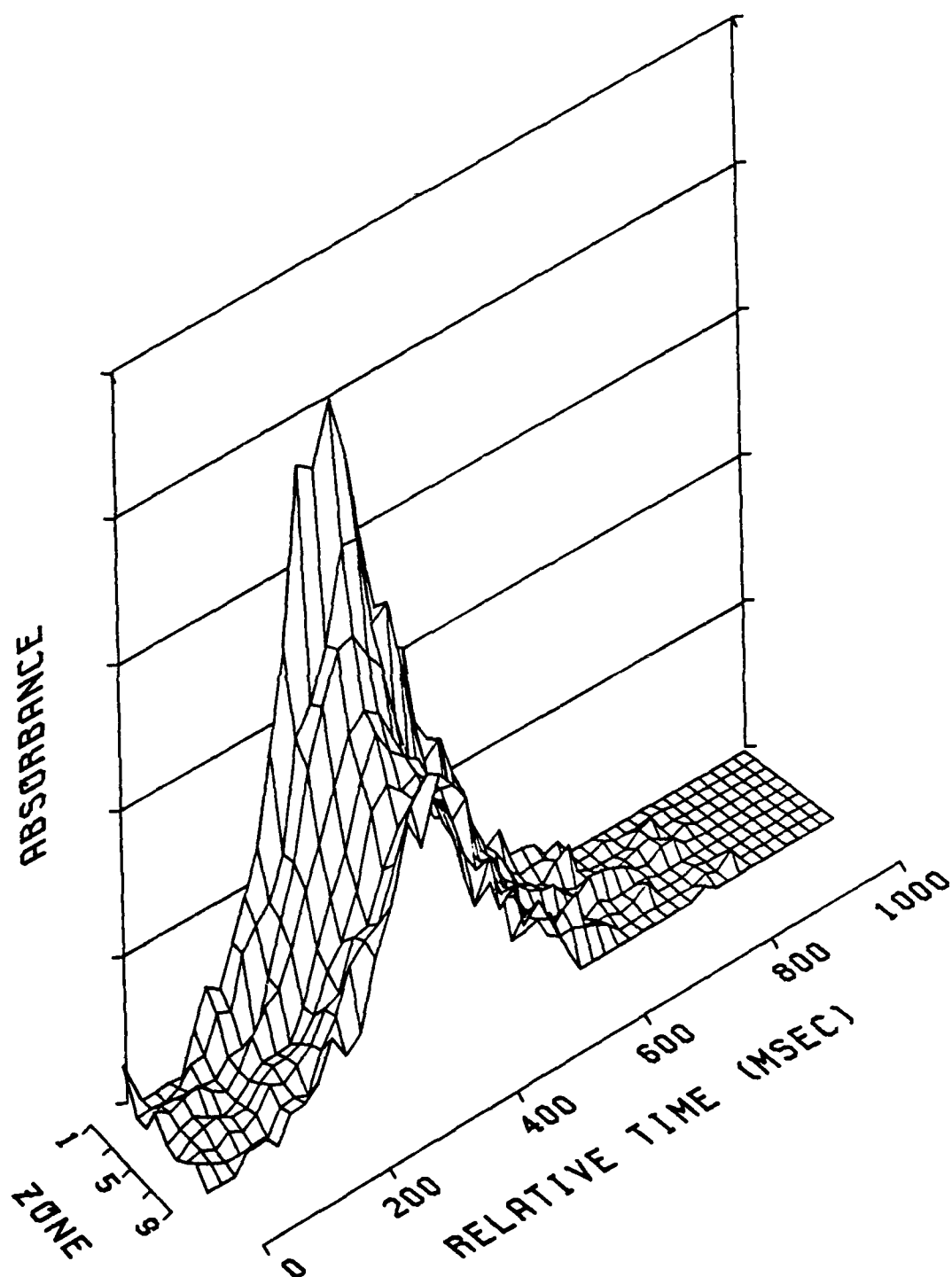Figure 53.   Absorbance Profile for Sn + $10 \times Na_2SO_4$

Figure 54.   Absorbance Profile for Sn + Eq $Na_2SO_4$

## 4.8 Silver

Silver exhibited the lowest appearance temperature of the elements studied. As shown in table I, the metal oxide bond strength of 33 kcal/mole is also the weakest and is indicative of the thermodynamic driving force of the silver oxygen reaction. The results of the thermodynamic studies are shown in figure 55. These calculations, which omit the role of graphite, illustrate that no analyte signal depressions would be expected from partial pressures of oxygen as great as $10^{-2}$ atm. Previous kinetic studies in this laboratory (Table I) indicate that the silver oxygen reaction kinetics are very slow in comparison to the other elements studied.

FILAMENT ATOMIZER: As illustrated in figure 56, the sulfate interferents produced no significant signal depression using the filament atomizer. Figure 57 shows only a slight depression with a hundred-fold excess of $KNO_3$. The three-dimensional profiles for the filament atomizer, as shown in figure 58, illustrate the rapid absorbance signal decay from the first viewing zone to zone nine.

# SILVER

FRACTION AS FREE METAL

PARTIAL PRESSURE OF OXYGEN
⊙ = 1.0E-2
△ = 1.0E-3
+ = 1.0E-4
✕ = 1.0E-5
PARTIAL PRESSURE OF METAL = 1.0E-5

TEMP (K) ✕10¹
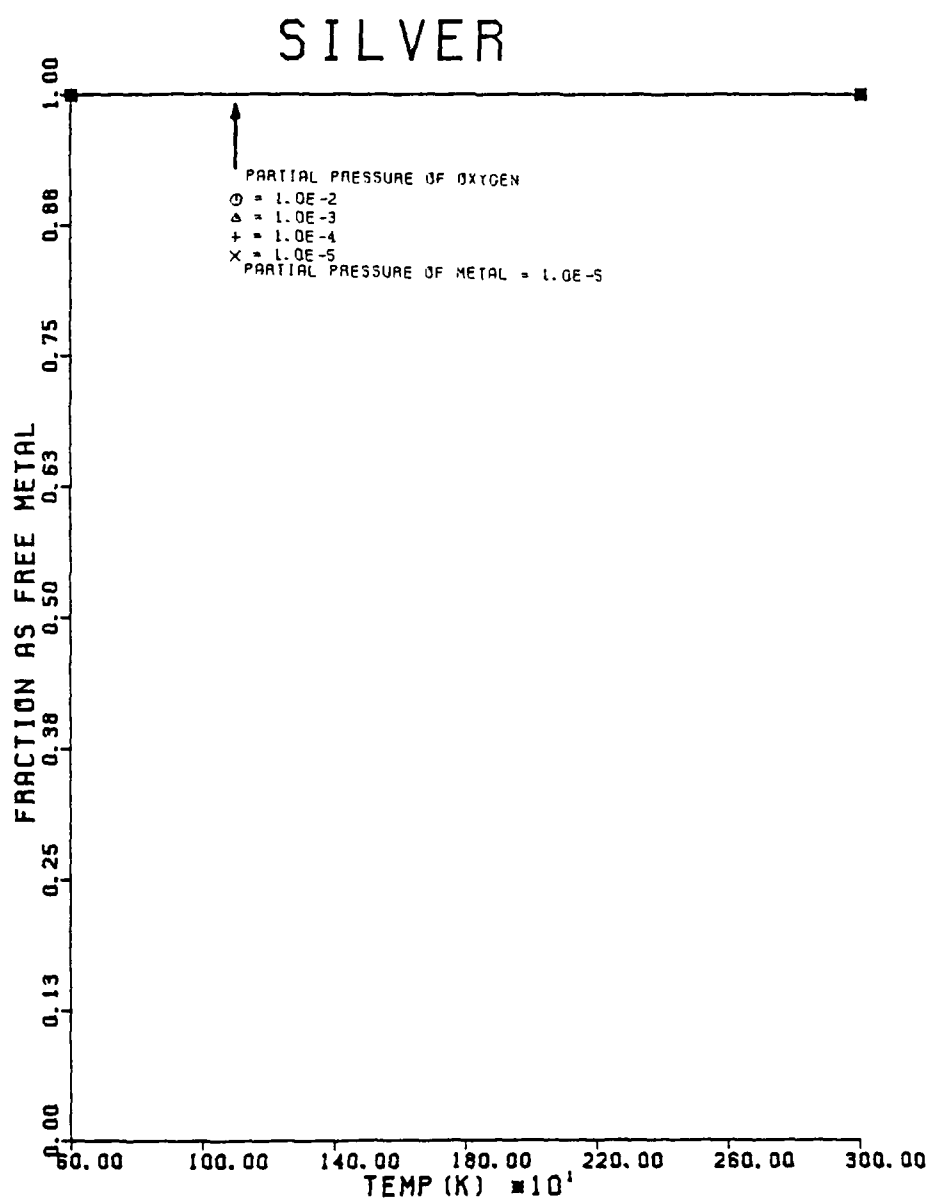
Figure 55.   Results of Thermodynamic

Calculations for Ag

# SILVER

## PEAK HEIGHT

✳ = ANALYTE +/- ONE STD. DEV.
⊡ = 10X SODIUM NITRATE
✕ = 100X SODIUM NITRATE
☆ = 10X POTASSIUM NITRATE
◈ = 100X POTASSIUM NITRATE
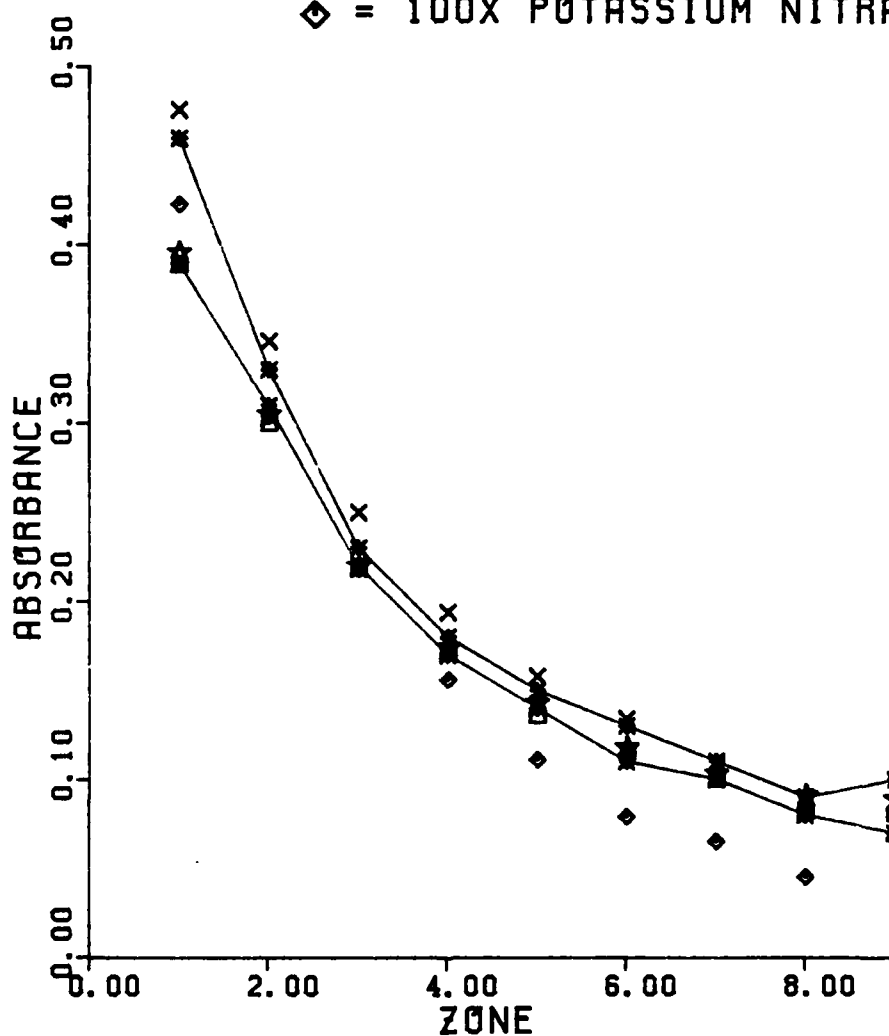


Figure 56.   Filament Atomizer Results

# SILVER

## PEAK HEIGHT

* = ANALYTE +/- ONE STD. DEV.
⊞ = 10X SODIUM SULFATE
✕ = 100X SODIUM SULFATE
☆ = 10X POTASSIUM SULFATE
◇ = 100X POTASSIUM SULFATE
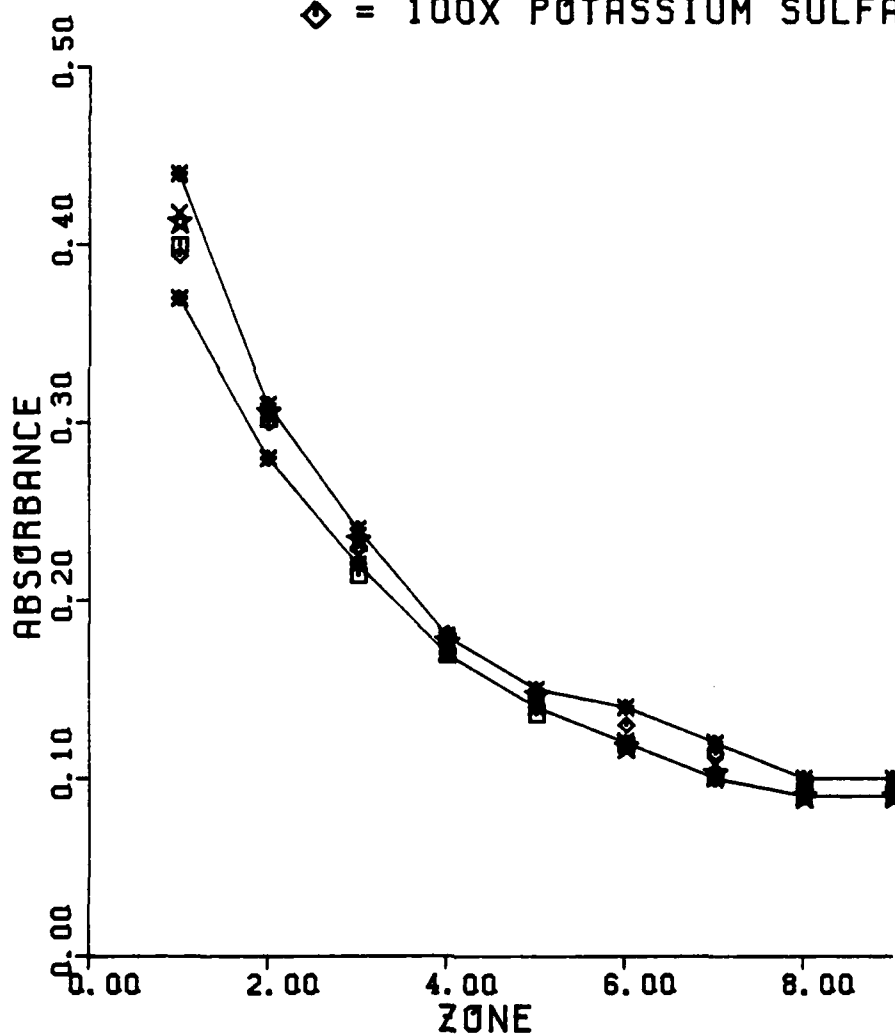
Figure 57.  Filament Atomizer Results
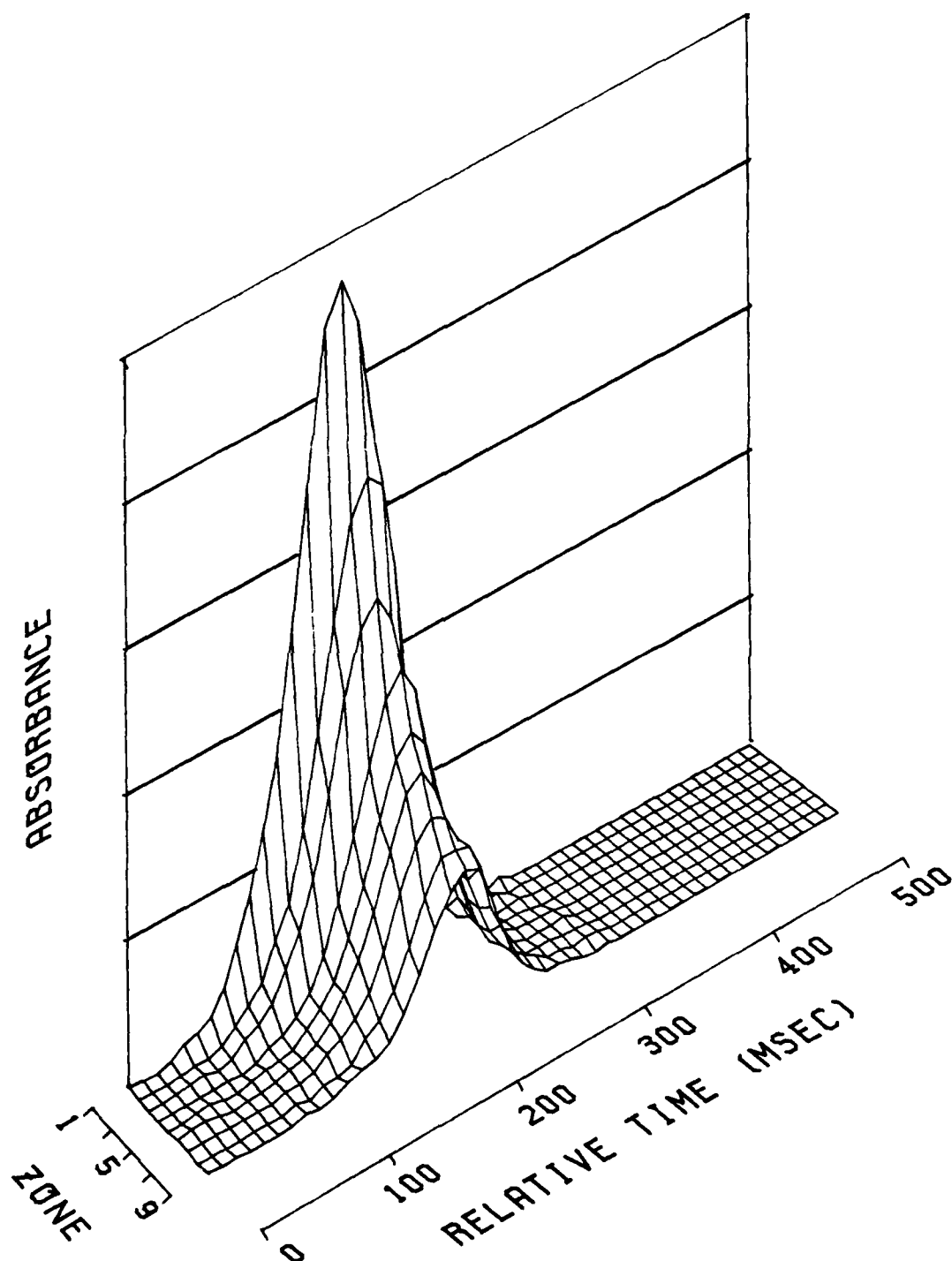
Figure 59.   Absorbance Profile for Ag

FURNACE ATOMIZER: There were no absorbance signal depressions observed with the commercial apparatus. This is consistent with the kinetic and equilibrium considerations which do not greatly favor the formation of the metal oxide.

SPATIALLY RESOLVED FURNACE ATOMIZER: As shown in figures 59 and 60, depressions were observed for the nitrate interferents, while no depressions were observed for the addition of sulfates to the analyte solution. This was consistent with the results of the filament atomizer study. The absorbance-time-height graph, figure 61, illustrates that the free Ag atoms are uniformly distributed across the vertical diameter of the furnace atomizer.

# SILVER

## PEAK HEIGHT

✳ = ANALYTE +/- ONE STD. DEV.
☐ = 10X SODIUM SULFATE
✕ = 100X SODIUM SULFATE
★ = 10X POTASSIUM SULFATE
◇ = 100X POTASSIUM SULFATE
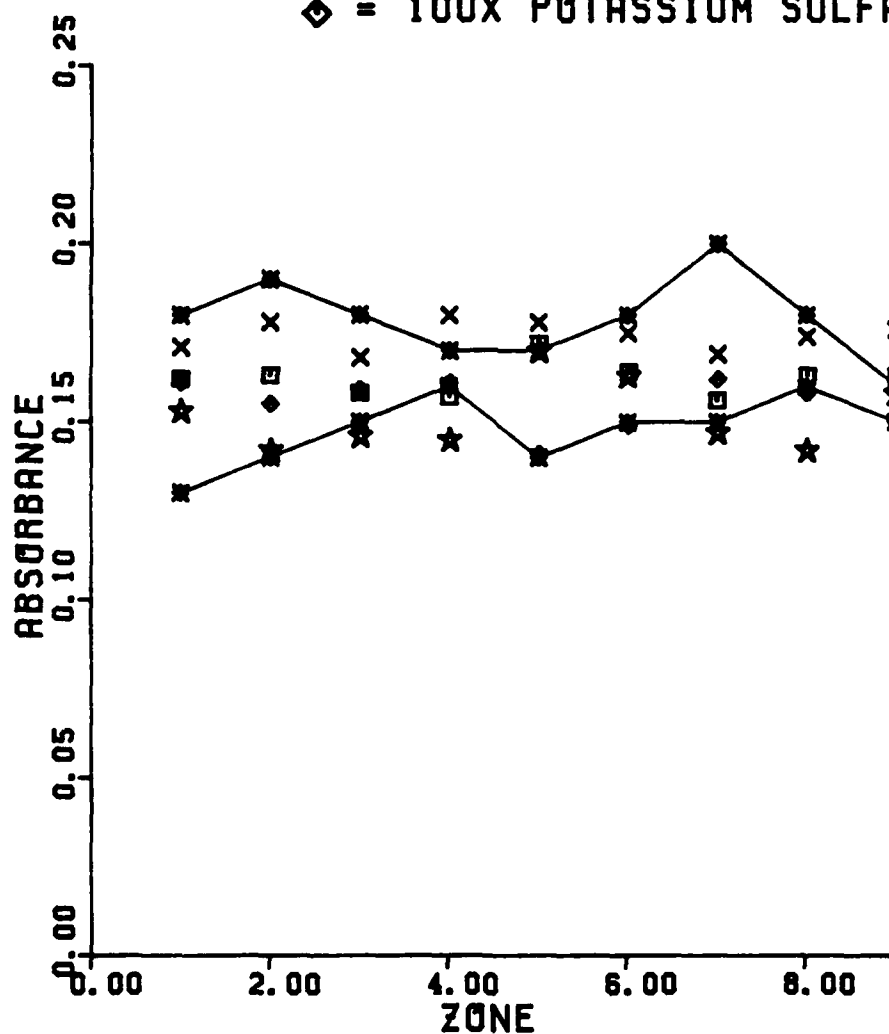


Figure 59.   Spatially Resolved Furnace Results

# SILVER

## PEAK HEIGHT

**✳ = ANALYTE +/- ONE STD. DEV.**
**⊡ = 10X SODIUM NITRATE**
**✕ = 100X SODIUM NITRATE**
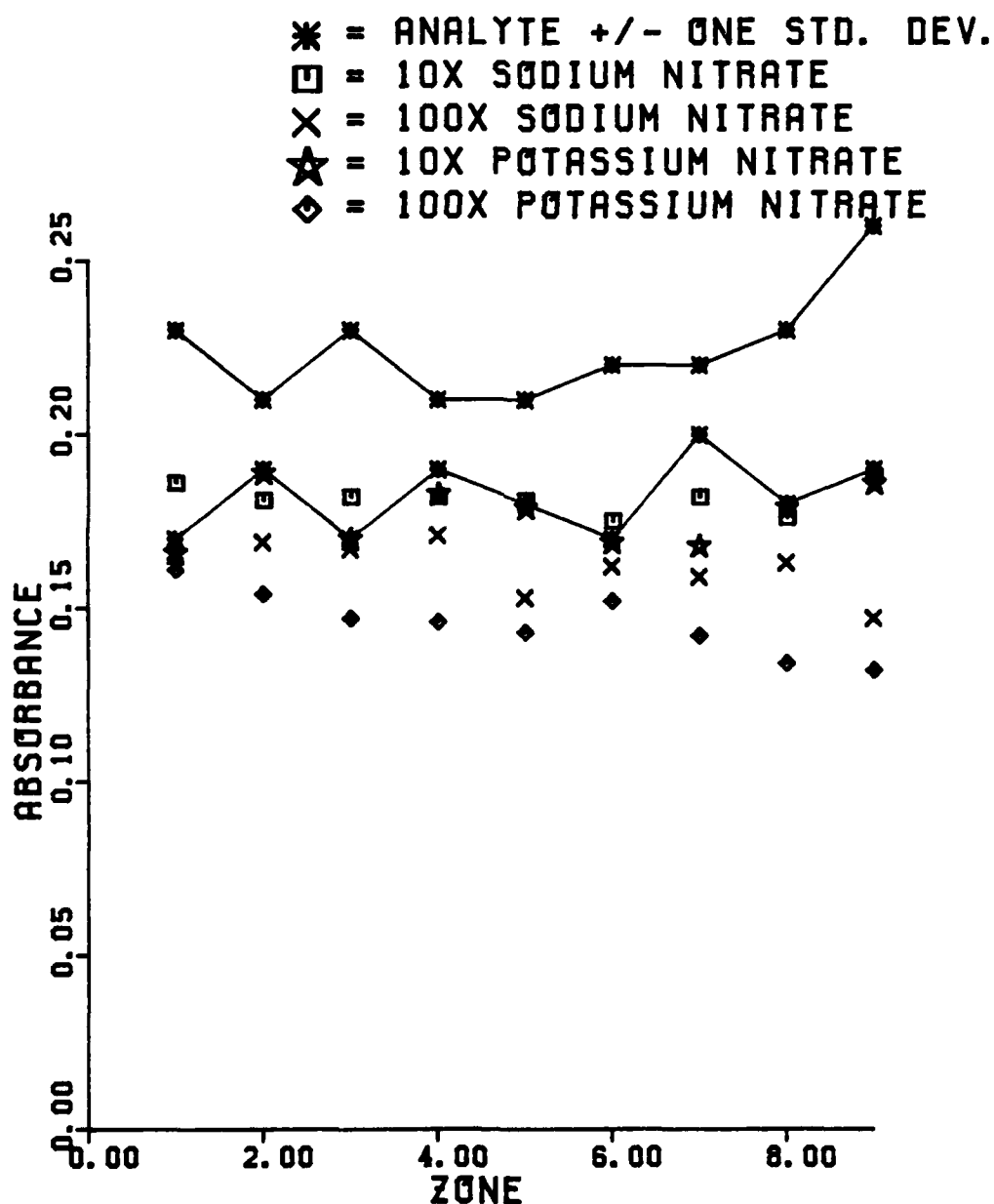**✪ = 10X POTASSIUM NITRATE**
**◇ = 100X POTASSIUM NITRATE**



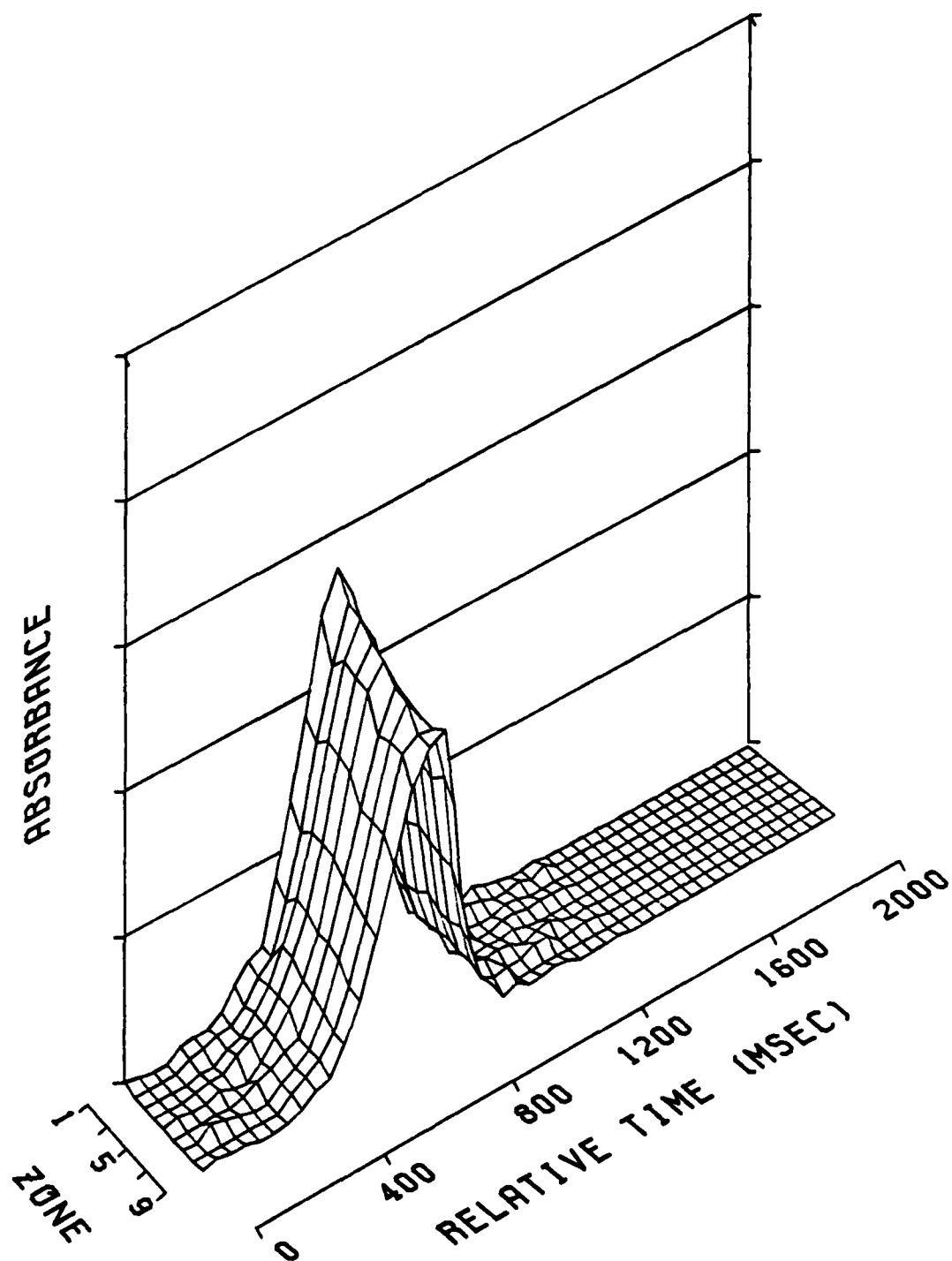Figure 60.   Spatially Resolved Furnace Results

Figure 61.   Absorbance Profile for Ag

4.9  Conclusions

   The extension of the unique optical system
for obtaining simultaneous time and spatial
resolution to the commercial furnace atomizer has
enabled a preliminary study of gas phase reactions
within the furnace atomizer.  As the experimental
results demonstrate, gas phase *coincidence of*
analyte and interferent appears imperative if
absorbance signal depressions from concomitant
salts are to occur.  Thus, those elements with
higher appearance temperatures, e.g. nickel and
chromium, probably did not encounter the inter-
ferent oxidant produced from the nitrate and
sulfate salts used in this study.

   Once the coincidence of analyte and
interferent has been established, kinetics may
limit the extent of the interference reaction.
In the filament atomizer the interaction time between
the metal and oxidant within the viewing zone is
approximately 20 msec.  Similarly, the thermodynamic
driving force for the formation of the metal oxide
is greater for the filament atomizer due to the
likelihood of reduced gas phase temperature at
elevated distances above the heated surface in
comparison to the enclosed analytical volume of the

furnace atomizer. Residence time within the furnace, as measured by the absorbance signal time profile is between 400 and 800 msec. These differences in temperature and time may be critical for elements such as Cu and Fe which exhibit interferences using the filament but not the furnace. However, with tin which forms a stable oxide and exhibits rapid kinetics, severe depressions are observed for both atomizer types. To effectively probe the reaction kinetics within the furnace atomizer, better time resolution may be required. With the present experimental arrangement, this simply requires increasing the SIW rotation velocity. However, to accommodate the increased sampling rate, the memory capacity of the sampling device needs to be expanded. Perhaps analog to digital conversion with direct data stored into the memory of the microcomputer could be utilized. In either instance it should be recognized that the photomultiplier tube/hollow cathode lamp noise may be a limiting factor in the success of this approach. The incorporation of new lamp designs with higher intensity and better stability would make this approach more tractable. To completely understand these reactions, a probe of the molecular species

is required.  Mass spectroscopy would allow more
complete monitoring of both reactants and products
of any reaction, as well as the determination of
the appearance temperature of interferent species
in gas phase.

The thermodynamic model, which was developed
to predict or explain the extent of analyte
absorbance signal depressions due to the formation
of the metal oxide, is handicapped by the
requirement to ignore or reduce the influence
of the graphite in the equilibrium calculations.
With the assumption of total chemical equilibrium
*including the graphite*, calculations indicate that
no signal depressions should occur for any of the
elements studied.  The fact that depressions were
observed indicates that graphite is only partially
effective in removing oxygen within the atomizer
and/or reducing the metal oxide bond.  Further
studies, perhaps utilizing such surface probes as
Auger spectroscopy, ESCA, or scanning electron
microscopy, aimed at elucidating the role of
graphite in the atomization process would enhance
this thermodynamic model.

The appearance time shifts, which were
observed for the addition of $H_2$ to the Ar sheath

gas in the Sn study, suggest that different
analyte release mechanisms from the graphite
surface were occurring. These shifts in appearance
time have not been observed for Sn prior to this
study, however timeshifts for the more volatile
elements, e.g. Pb and Zn, are well documented.[14]
The fundamental cause of these time-shifts is
presently under study in this laboratory. Another
interesting study would be to chemically modify
the graphite surface to delay volatilization of
the analyte until the furnace reaches a higher
temperature. This higher analyte appearance
temperature might serve to minimize some inter-
ference effects. Modification of the graphite by
forming refractory metal carbide surfaces have
been considered by a few investigators, although
the studies to date have been fairly pragmatic
and focus only on the analytical utility of these
surfaces with little emphasis on the chemical
basis for observed absorbance signal changes. These
metal carbide surfaces are fairly inert, which
deprives the chemical system of the reducing
ability of the graphite.

The importance of minimizing the entrain-
ment of air into the atomizer was demonstrated

in both the Cr and Sn studies. Other commercial furnace atomizers are available which completely enclose the atomizer in a pressurizable housing. These atomizers allow for stopping the Ar sheath gas during the atomization cycle. This design would better enable a study of the effects of reactive gases, such as $O_2$, and the role of graphite on the analyte absorbance signal. Due to the open design of the present atomizer, it is impossible to stop the gas flow during the atomization cycle. Thus additional variables, such as the effects of connective mass transport near the ends of the furnace, cannot be eliminated. Conversely, the totally enclosed atomizer would allow an initial assumption of diffusion-controlled mass transport to be made, as a first step in modeling this system.

In summary, this work has demonstrated that:

1) The simultaneous collection of time and spatial absorbance data within the 3 mm diameter commercial furnace atomizer is feasable. The information available from the time and spatial absorbance maps appears to augment the simple absorbance-time data that can be conventionally

obtained.

2)  Several gas phase interferent reactions observed previously in the filament atomizer also exist within the furnace atomizer.

3)  The elevated gas temperature and/or the presence of a second graphite collision surface within the furnace is effective in reducing the depressive effects of concomitant nitrate and sulfate salts which previously exhibited depressions with the filament.

4)  Total chemical equilibrium inclusive of the graphite is unlikely and reaction kinetics and/or mass transport of oxidants and metal oxides to the graphite surface may reduce the effectiveness of the graphite surface.

5)  Gas phase coincidence between the thermal decomposition products of the concomitant and the analyte appears to play a significant role in determining the extent of the interferences.

References for Chapter Four

1.  S. Yasuda and H. Kakigama, Bunseki Kagaku, 24, 377 (1975).

2.  R.H. Eklund and J.A. Holcombe, Anal. Chim. Acta, 109, 97 (1979).

3.  J.A. Holcombe, R.H. Eklund, and J.E. Smith, Anal. Chem., 51, 1205 (1979).

4.  D.R. Stull, H. Prophet, et al, JANAF Thermochemical Tables, Second Edition, U.S. Government Printing Office, Washington, D.C., (1971).

5.  G.M. Barrow, Physical Chemistry, 3rd edn., McGraw-Hill Book Co., New York, N.Y., p. 223.

6.  Ibid, p. 225.

7.  Ibid, p. 311.

8.  B.V. L'vov, Spectro. Chim. Acta, 33, 153 (1978).

9.  Light Sources for Atomic Absorption Spectroscopy, Varian Techtron Pty., Ltd, Mulgrave, Australia

10. R.C. Weast (Ed.), Handbook of Chemistry and Physics, 51st edn, Chemical Rubber Co., Cleveland, Ohio, 1970-71.

11. G. Guiochon, B. Hircq, and C. Tailland, Anal. Chim. Acta, 99, 125 (1978).

12. R.H. Eklund and J.A. Holcombe, Anal. Chim. Acta, 109, 97 (1979).

13.  A. Fontijn, S. Kurzius, and S. Houghton,
     "XV Symposium (International) on Combustion",
     Pittsburgh, Pa., 1973, p. 167.

14.  E.J. Czobik and J.P. Matousek, Talanta, <u>24</u>,
     573 (1977).

APPENDIX A:   CALCULATION OF SPATIAL RESOLUTION WITHIN

THE FURNACE ATOMIZER

With the center of the furnace in sharp focus, a wire grid of known dimensions was inserted into the atomizer workhead assembly in place of the atomizer.  The spatial isolation wheel (SIW) was rotated and the resulting output recorded by the Bio-mation and plotted on a strip chart recorder.  Strip chart recordings were also obtained for the images of the wire grid at either end of the furnace atomizer. The distance between the wire grid was measured by an optical micrometer as .0381 cm.  The distance between the two field stops immediately in front of the SIW was measured as .9335 cm.

The magnification was determined by the distance between adjacent grid peaks compared to the distance between the SIW peaks.  Therefore, at the center of the furnace the strip chart recording showed:

SIW peak-to-peak distance = 52.4 cm

Grid peak-to-peak distance = 8.1 cm

Half width of grid peak = 2.5 cm

The magnified distance, $d_m$, between the center of two adjacent grid wires was:

133

$$d_m = \frac{(8.1 \text{ cm})(0.9335 \text{ cm})}{52.4 \text{ cm}} = 0.144 \text{ cm}$$

The magnification, m, of the optical system was obtained by dividing the magnified grid spacing by the measured grid spacing:

$$m = \frac{.144 \text{ cm}}{.03810 \text{ cm}} = 3.78$$

The magnified resolution, $\Delta d$, was determined by the half width of the grid peak relative to the SIW peak-to-peak distance. Thus, at the center of the furnace:

$$\Delta d = \frac{(2.5 \text{cm})(0.9335 \text{cm})}{52.4 \text{ cm}} = 0.0445 \text{ cm}$$

Division of the magnified resolution by the magnification yields the optical resolution, $R_o$, within the center of the furnace:

$$R_o = \frac{0.0445 \text{ cm}}{3.78} = .0118 \text{ cm}$$

The optical resolution at the end of the furnace closest to the hollow cathode lamp was calculated at $211 \mu m$ with a magnification of 3.66, while the resolution at the end of the furnace closest to the SIW was $194 \mu m$ with a magnification of 3.72.

The data collection program divides the

distance between the SIW field stops into ten zones. Subsequent division by the magnification yields the sampling resolution, $R_s$, at the center of the furnace atomizer:

$$R_s = \frac{.09335 \text{ cm}}{3.71} = .0252 \text{ cm}$$

Thus, the worst optical resolution of 211μm is less than the sampling resolution of 252μm.

## VITA

Nils Akerlind, Jr. was born in Washington, D.C., on January 19, 1950, the son of Carrie F. Akerlind and Nils Akerlind. After graduating from Pompano Beach Senior High School, Pompano Beach, Florida, in 1968, he entered the University of Florida at Gainesville, Florida. He received a Bachelor of Science degree from the University of Florida in June, 1972. In June, 1972, he married Mary Loretta Fudge of Thonotosassa, Florida. Nils Akerlind entered military service in October, 1972, and upon graduation from Officers Training School in January, 1973, was commissioned a Second Lieutenant in the United States Air Force. He was promoted to Captain in January, 1977. Upon selection for advanced academic training, he was assigned to The University of Texas in August, 1978.


Permanent address:   341 S.E. 4 Street
                     Pompano Beach, Florida

This thesis was typed by Loretta Akerlind.

# VITA

Nils Akerlind, Jr. was born in Washington, D.C., on January 19, 1950, the son of Carrie F. Akerlind and Nils Akerlind. After graduating from Pompano Beach Senior High School, Pompano Beach, Florida, in 1968, he entered the University of Florida at Gainesville, Florida. He received a Bachelor of Science degree from the University of Florida in June, 1972. In June, 1972, he married Mary Loretta Fudge of Thonotosassa, Florida. Nils Akerlind entered military service in October, 1972, and upon graduation *from* Officers Training School in January, 1973, was commissioned a Second Lieutenant in the United States Air Force. He was promoted to Captain in January, 1977. Upon selection for advanced academic training, he was assigned to The University of Texas in August, 1978.


Permanent address:  341 S.E. 4 Street
                    Pompano Beach, Florida

This thesis was typed by Loretta Akerlind.